Design and Analysis of Reconfigurable Analog System

by

Payam Lajevardi

B.A.Sc. Electrical Engineering, University of British Columbia, 2003

and

S.M. Electrical Engineering, Massachusetts Institute of Technology, 2005

Submitted to the Department of Electrical Engineering and Computer Science

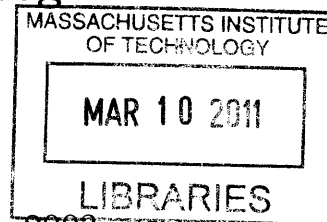in partial fulfillment of the requirements for the degrees of

Doctor of Philosophy

at the

MASSACHUSETTS INSTITUTE OF TECHNOLOGY

February 2011

Author . . . .
Department of Electrical Engineering and Computer Science
· · October 18, 2010

Certified by. . . . .
Anantha P. Chandrakasan
Joseph F. and Nancy P. Keithley Professor of Electrical Engineering
Thesis Supervisor

Certified by. . . . .
Hae-Seung Lee
Professor of Electrical Engineering
Thesis Supervisor

Accepted by . . . .
Terry P. Orlando
Chairman, Departmental Committee on Graduate Students

Report Documentation Page		

1. REPORT DATE **FEB 2011**	2. REPORT TYPE	3. DATES COVERED **00-00-2011 to 00-00-2011**
4. TITLE AND SUBTITLE **Design and Analysis of Reconfigurable Analog System**		5a. CONTRACT NUMBER
		5b. GRANT NUMBER
		5c. PROGRAM ELEMENT NUMBER
6. AUTHOR(S)		5d. PROJECT NUMBER
		5e. TASK NUMBER
		5f. WORK UNIT NUMBER
7. PERFORMING ORGANIZATION NAME(S) AND ADDRESS(ES) **Massachusetts Institute of Technology,77 Massachusetts Avenue,Cambridge,MA,02139**		8. PERFORMING ORGANIZATION REPORT NUMBER
9. SPONSORING/MONITORING AGENCY NAME(S) AND ADDRESS(ES)		10. SPONSOR/MONITOR'S ACRONYM(S)
		11. SPONSOR/MONITOR'S REPORT NUMBER(S)

12. DISTRIBUTION/AVAILABILITY STATEMENT
Approved for public release; distribution unlimited

13. SUPPLEMENTARY NOTES

14. ABSTRACT

A highly-configurable analog system is presented. A prototype chip is fabricated and an ADC and filter functionalities are demonstrated. The chip consists of eight identical programmable stages. In an ADC configuration, the first five stages are programmed to implement a 10- bit ADC. The ADC has ENOB of 8 bits at 50 MSPS. The ENOB improves to 8.5 bits if the sampling rate is lowered to 30MSPS. The ADC has an FOM of 150fJ/conversionstep which is very competitive with the state of the art ADCs. The first stage is responsible for 75% of the input-referred noise power. The sampling noise is responsible for 40% of the total noise power and the zero-crossing detector is responsible for 60%. The chip is tested in two different filter configurations. In one test, the first two stages of the chip are configured as a second order Butterworth filter and the third stage is configured as an amplifier. In another test, the first three stages of the chip are programmed as a third-order Butterworth filter. The desired filter functionalities are demonstrated in both configurations. It is shown that in a third order Butterworth filter, more than 90% of the noise is due to the zero-crossing detector of the last stage. This is mainly due to the fact that the noise of earlier stages is filtered with the filter transfer function, but the noise of the last stage is not filtered. The ZCBC architecture has been used to avoid the stability problems and scale power consumption with sampling frequency. A new technique is introduced to implement the terminating resistors in a ladder filter. This technique does not have any area or power overhead. An asymmetric differential signaling is also introduced. This method improves the dynamic range of the output signals, which is particularly important in new technology nodes with low supply voltage.

15. SUBJECT TERMS

16. SECURITY CLASSIFICATION OF:			17. LIMITATION OF ABSTRACT	18. NUMBER OF PAGES	19a. NAME OF RESPONSIBLE PERSON
a. REPORT **unclassified**	b. ABSTRACT **unclassified**	c. THIS PAGE **unclassified**	**Same as Report (SAR)**	**152**	

Design and Analysis of Reconfigurable Analog System

by

Payam Lajevardi

Submitted to the Department of Electrical Engineering and Computer Science
on August 29, 2010, in partial fulfillment of the
requirements for the degrees of
Doctor of Philosophy

Abstract

A highly-configurable analog system is presented. A prototype chip is fabricated
and an ADC and filter functionalities are demonstrated. The chip consists of eight
identical programmable stages.

In an ADC configuration, the first five stages are programmed to implement a 10-
bit ADC. The ADC has ENOB of 8 bits at 50 MSPS. The ENOB improves to 8.5 bits if
the sampling rate is lowered to 30MSPS. The ADC has an FOM of 150fJ/conversion-
step, which is very competitive with the state of the art ADCs. The first stage is
responsible for 75% of the input-referred noise power. The sampling noise is respon-
sible for 40% of the total noise power and the zero-crossing detector is responsible for
60%.

The chip is tested in two different filter configurations. In one test, the first two
stages of the chip are configured as a second order Butterworth filter and the third
stage is configured as an amplifier. In another test, the first three stages of the chip are
programmed as a third-order Butterworth filter. The desired filter functionalities are
demonstrated in both configurations. It is shown that in a third order Butterworth
filter, more than 90% of the noise is due to the zero-crossing detector of the last stage.
This is mainly due to the fact that the noise of earlier stages is filtered with the filter
transfer function, but the noise of the last stage is not filtered.

The ZCBC architecture has been used to avoid the stability problems and scale
power consumption with sampling frequency. A new technique is introduced to im-
plement the terminating resistors in a ladder filter. This technique does not have
any area or power overhead. An asymmetric differential signaling is also introduced.
This method improves the dynamic range of the output signals, which is particularly
important in new technology nodes with low supply voltage.

Thesis Supervisor: Anantha P. Chandrakasan
Title: Joseph F. and Nancy P. Keithley Professor of Electrical Engineering

Thesis Supervisor: Hae-Seung Lee
Title: Professor of Electrical Engineering

Acknowledgments

Contents

List of Figures

List of Tables

Chapter 1

Introduction

While digital FPGAs provide a fast and cost-efficient method to prototype digital circuits, the development of similar system for analog circuits is still limited because it is difficult to realize a programmable analog system that can be configured to wide variety of analog circuits. A highly programmable analog system that can be configured for an arbitrary analog functionality is very valuable. Many electronic devices use multiple communication standards. As the number of communication standards are growing rapidly, electronic devices tend to incorporate more communication standards, which increases the cost of the system. To integrate multiple standards on the same chip, a highly-programmable analog system can replace the analog blocks of all these systems. In addition, highly-programmable analog systems can be used as the analog core of software defined radios (SDR) to perform its required analog functionalities such as analog to digital conversion (ADC), filtering, and programmable gain amplification. Clearly, SDR requires programmable radio frequency circuits as well (such as programmable mixer, low-noise amplifier, oscillator). Highly programmable analog systems can also be used in fast prototyping of analog systems. They can also be used for educational purposes (similar to digital FPGAs that are used in educational implementation of digital systems).

Field programmable analog arrays (FPAA) have been previously proposed [1] . It uses continuous-time blocks whose gain is programmable by changing transconductance of amplifiers. Programmable connectivity between analog circuits is a major

challenge in reconfigurable analog systems. It uses permanent connection between adjacent blocks and sets the gain of adjacent blocks to zero to effectively disconnect them. Another implementation uses programmable transconductance and programmable capacitor to control the gain of stages [2]. A programmable ADC that can be configured as sigma-delta or pipeline employs programmable capacitors, programmable connectivity, and adjustable biasing [3]. This project demonstrates a highly-reconfigurable analog system that can be used to implement pipeline ADCs and switched-capacitor filters. Zero-crossing based circuits (ZCBC) are utilized for superior power efficiency and reconfigurability.

In the rest of this chapter, ADCs and switched-capacitor filters are reviewed. In Chapter 2, zero-crossing based circuits are described. Chapter 3 describes how the system is implemented. Chapter 4 analyzes the noise of the system and Chapter 5 reviews the sensitivity of the reconfigurable system to capacitor mismatch and to the offset of the zero-crossing detectors. Chapter 6 describes the measurement results of the fabricated chip and Chapter 7 concludes the thesis.

1.1 ADC Review

An analog to digital convertor (ADC) converts an analog signal to its corresponding digital code. Main ADC architectures include flash ADCs [4][5][6], successive-approximation-register ADCs [7][8], pipeline ADCs [9][10], sigma-delta ADCs [11], and time-interleaved ADCs [12][13]. As shown in Figure 1-1, each architecture is more suitable for a particular range of sampling rate and resolution [14]. Flash and time-interleaved ADCs are suitable for higher speeds than pipeline ADCs (which is not shown on Figure 1-1). There is an overlapping area where more than one architecture may be suitable. Pipeline ADCs are chosen for this research to cover medium to high speed and resolution range.
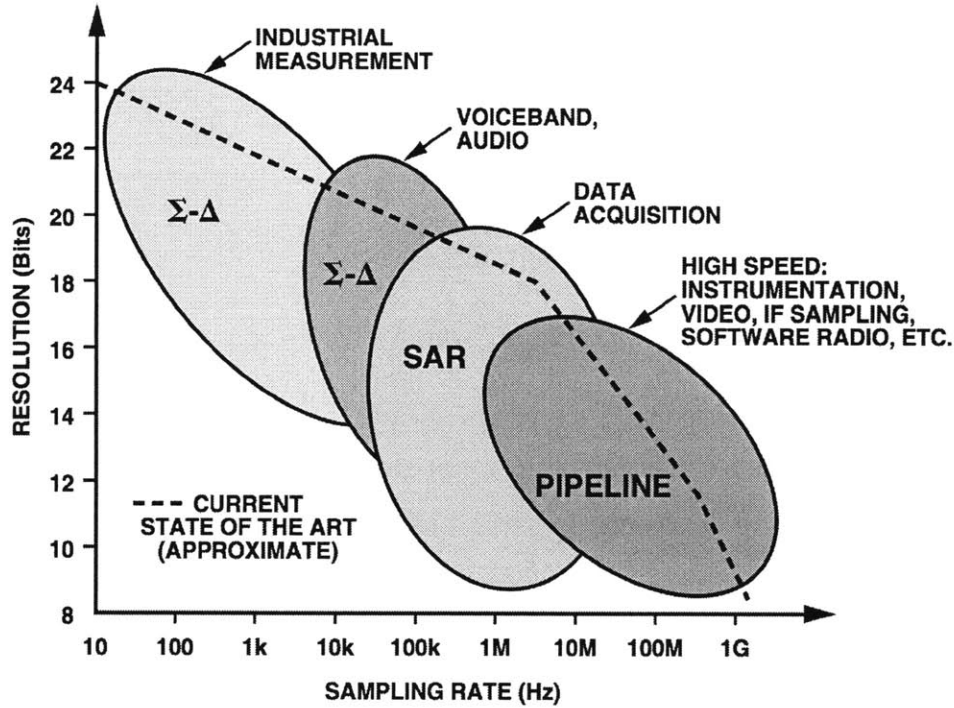
Figure 1-1: ADC Architecture for different sampling rates and resolution [14].

1.1.1 Pipeline ADC

Pipeline ADCs consist of several identical stages that are cascaded. The block diagram of each stage is shown in Figure 1-2. Each stage is composed of four components, a sub-ADC, a digital-to-analog convertor (DAC), an adder, and an amplifier. A sub-ADC is usually an ADC with limited number of quantization levels, n. For example, it may be a flash ADC with only one or two bits, while the overall pipeline ADC may have 10-14 bits.

When an analog signal is converted to a digital code, there is a difference between the amplitude of the analog signal and the amplitude of the digital code. The difference is due to the limited number of the bits in the digital code and is called quantization error. As the number of the digital bits increases, the quantization error reduces.

In pipeline ADCs, the sub-ADC has a limited resolution. To increase the overall resolution of a pipeline ADC, the quantization error of the sub-ADC is sent to the

21
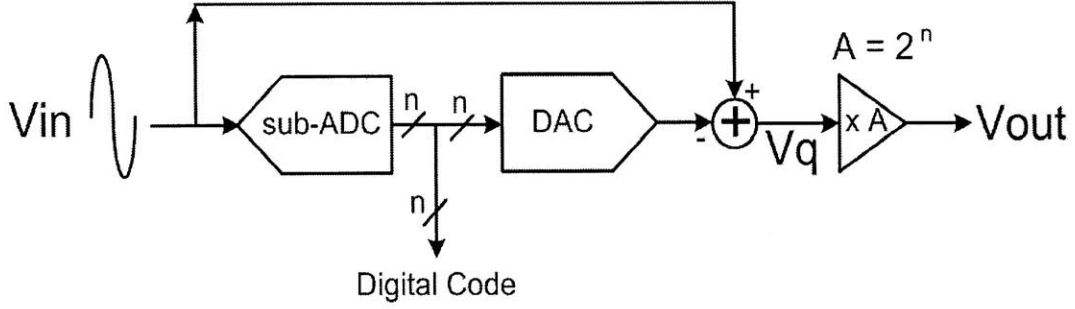
Figure 1-2: Block diagram of one stage of a pipeline ADC

subsequent stages. Subsequent stages convert the quantization error of earlier stages to the corresponding digital codes and add it to the overall digital output. As a result, each cascaded stage increases the resolution of the ADC. To find the quantization error of each stage, V_q, the output of the sub-ADC is sent to a DAC and subtracted from the input signal as shown in Figure 1-2. Since the amplitude of V_q is small, it is typically amplified. If n is the number of the bits of the sub-ADC, the range of V_q is smaller than the full-scale input range by a factor of $\frac{1}{2^n}$. If it is desired that V_{in} and V_{out} have the same range, the amplifier should have a gain of 2^n. This is usually the case for pipeline ADCs utilizing identical stages. Figure 1-3 shows the relationship between the input and output of each stage and the corresponding digital code if the sub-ADC has 2-bit resolution.

To construct the digital output code of a pipeline ADC, the output of each stage should be multiplied by the gain of earlier stages and added to the final digital code. If a pipeline ADC has k stages, and each stage has n quantization bits (Di for stage i), the digital output code of the ADC is given by:

$$ADC_{code} = D1 + D2 * 2^n + D3 * 2^{2n} + ... + Dk * 2^{(k-1)n} \qquad (1.1)$$

1.1.2   Over-Range Protection in Pipeline ADC

The sub-ADC may have an offset in its threshold voltages for different digital codes as shown in Figure 1-4. As a result, V_{out} may exceed the full scale input range (V_{ref}

22
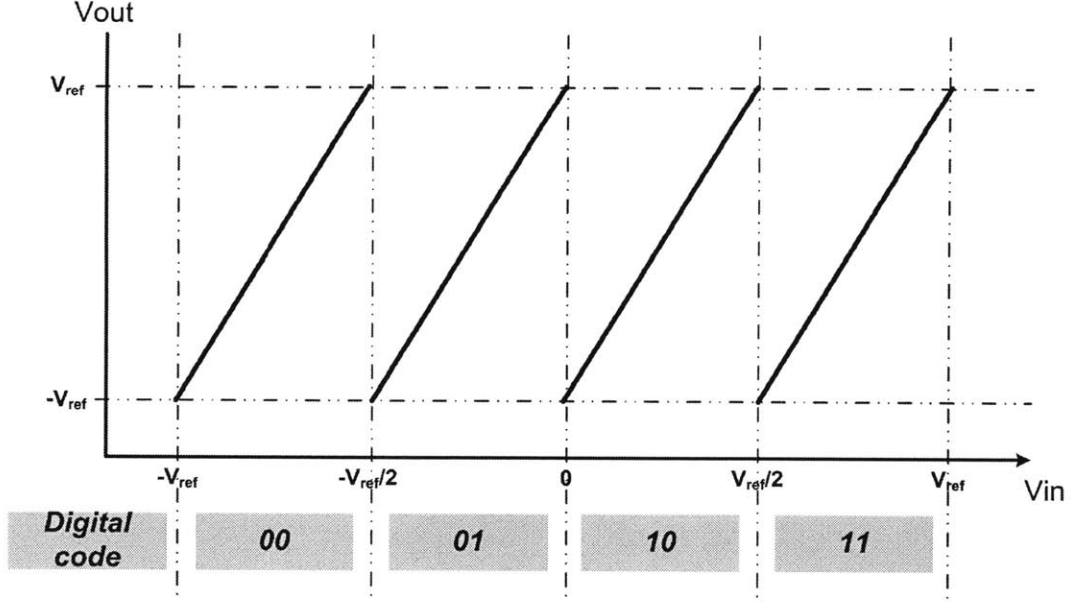
Figure 1-3: The relationship between the input and output signals for each stage of a pipeline ADC when the sub-ADC has 2-bit resolution (n=2).

or $-V_{ref}$) of subsequent stages for some values of V_{in}. In that case, the subsequent stages cannot resolve the input voltage in the region that saturates the subsequent stage. To avoid this problem, the threshold voltages of the sub-ADC are chosen so that the output does not exceed V_{ref} or $-V_{ref}$ as shown in Figure 1-5. If needed, the number of threshold levels can be increased. This method provides some margin of error for the threshold of the sub-ADC digital codes.

1.2 Filter Review

There are two main architectures to implement switched-capacitor filters, biquad filters [15] and ladder architecture [16]. Since this chip is intended to implement any arbitrary filter, the exact functionality of each stage is not known *a priori*. For example, the order of the filter and its cutoff frequency are programmable. Since biquad-based filters are sensitive to capacitor matching [16], ladder filter architecture is used in this research.
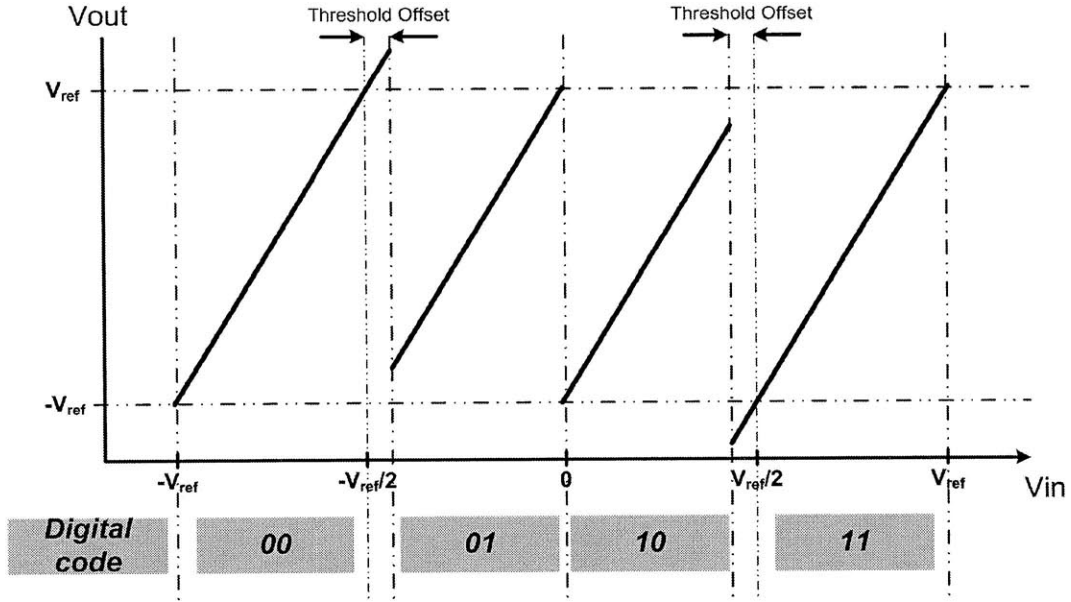
Figure 1-4: The effects of the offset of the sub-ADC threshold levels on the output voltage.

1.2.1 Passive Ladder Filter

Figure 1-6 shows a passive ladder filter. The number of storage components (capacitors, and inductors) determines the order of the filter and the type of the components determines the type of the filter. For example, Figure 1-6 shows a low-pass filter. If the capacitors are replaced with inductors, and the inductors are replaced with capacitors, a high-pass filter is obtained (Figure 1-7). Similarly, replacing capacitors in Figure 1-6 with a parallel combination of a capacitor and an inductor, and replacing the inductor with a series combination of a capacitor and an inductor results in a band-pass filter (Figure 1-8). The value of the capacitors, inductors, and the resistors determine the cut-off frequency of the filter and the shape of the filter (e.g. Butterworth, Chebyshev, and Elliptic). The design of ladder filters is researched extensively [17][18]. The value of each component in the ladder filters can be easily determined with software as well [19].

24
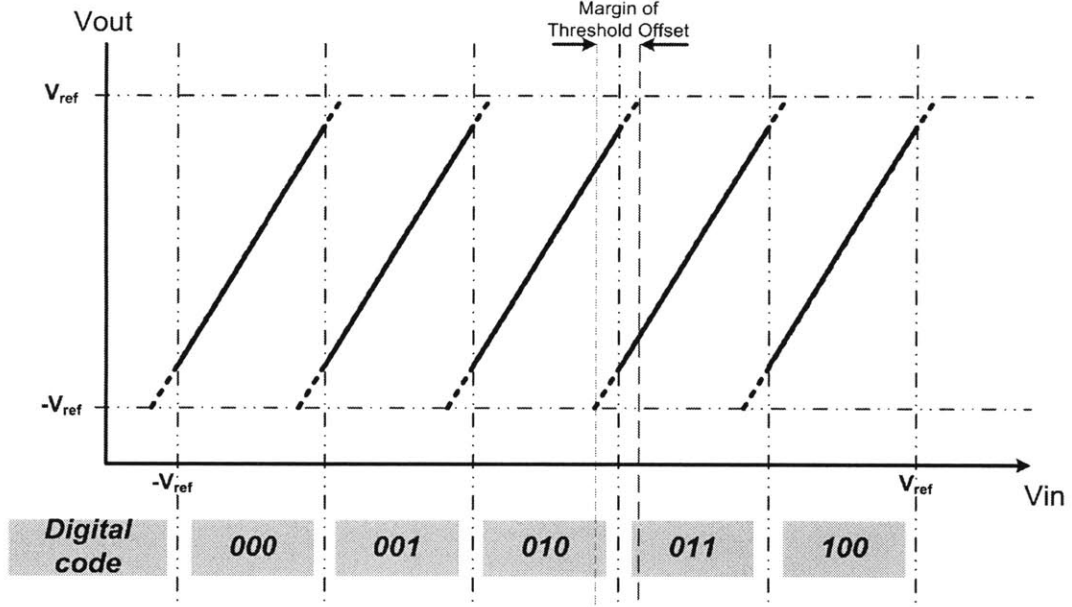
Figure 1-5: Over-range protection to provide margin for sub-ADC threshold levels.
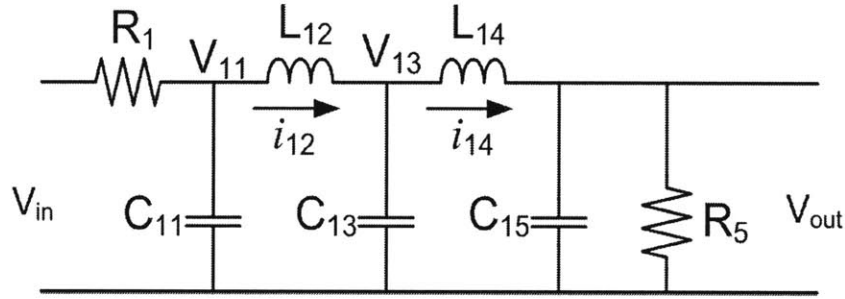
Figure 1-6: Passive implementation of a fifth-order low-pass ladder filter.

1.2.2 Active Ladder Filter

An opamp-based implementation of the low-pass ladder filter is shown in Figure 1-9 as proposed by [16]. This architecture is used to implement filters in this chip. In this section, first it is shown that the passive filter in Figure 1-6 and the active filter in Figure 1-9 are equivalent. Then, it is described how to determine the value of different components in the active filter, if the value of all components in the equivalent passive filter is known.

In Figure 1-6, the state variables are, V_{11}, i_{12}, V_{13}, i_{14}, and V_{out}. Each state variable can be written in terms of other state variables and the input. For example,
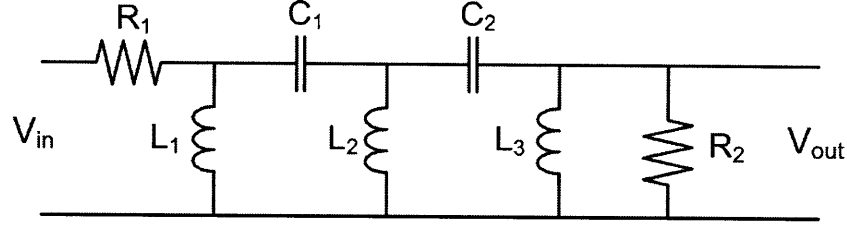
Figure 1-7: Passive implementation of a high-pass ladder filter.
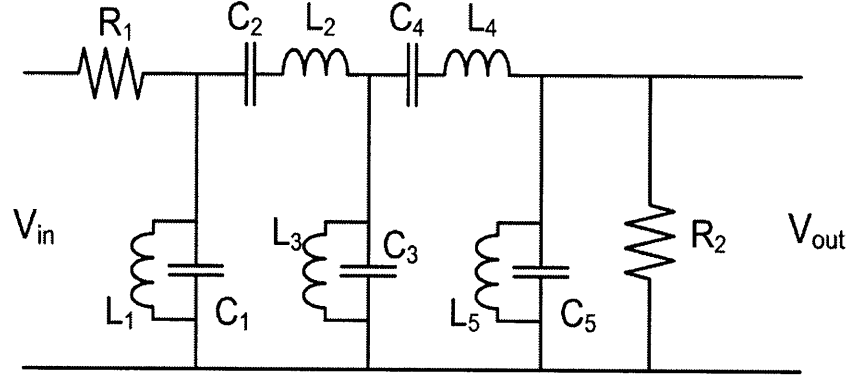
Figure 1-8: Passive implementation of a band-pass ladder filter.

V_{11} can be written as a function of other state variables as in Equation 1.2. For simplicity, it is assumed that $R_1 = 1$ and $R_5 = 1$.

$$\frac{dV_{11}}{dt} = \frac{\Delta V_{11}}{\Delta t} = \frac{1}{C_{11}}(V_{in} - V_{11} - i_{12}) \tag{1.2}$$

In Figure 1-9, the state variables are, V_{21}, V_{22}, V_{23}, V_{24}, and V_{out}. In the active filter, V_{21} is equivalent to V_{11} in the passive filter. V_{21} can be written as a function of other state variables as in Equation 1.3. For simplicity, it is assumed that all the sampling capacitors have a unit value.

$$\Delta V_{21} = \frac{1}{C_{21}}(V_{in} - V_{21} - V_{22}) \tag{1.3}$$

Table 1.1 shows the equivalent state variables in the two filters. In order to make Equation 1.2 and Equation 1.3 equivalent state equations in the two circuits, the relationship between C_{21} and C_{11} should be:

26

$$C_{21} = \frac{C_{11}}{\Delta t} = C_{11} \cdot f_{clk} \qquad (1.4)$$

where Δt in the passive filter is equivalent to the period of each clock cycle in the active implementation. Table 1.2 shows the equivalent state equations for the two circuits. Since the state equations are equivalent, the two circuits are equivalent as well. Table 1.3 shows the value of each component in the active filter based on the value of its corresponding compoent in the passive filter.
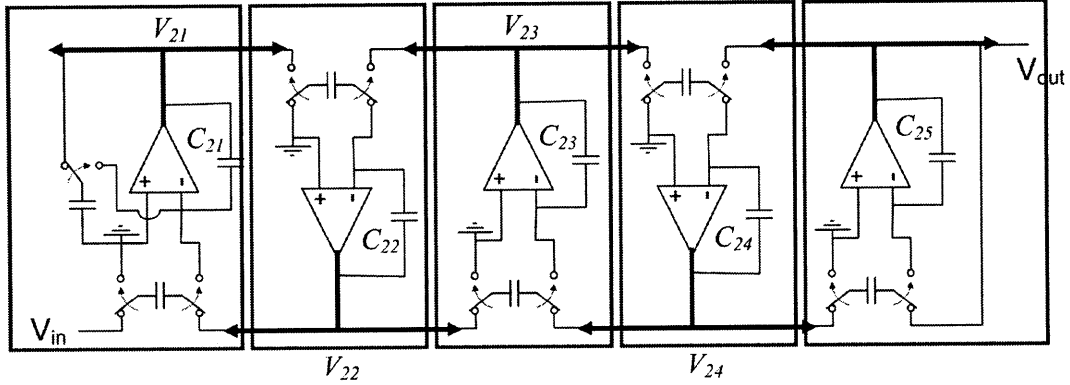
Figure 1-9: Passive implementation of a band-pass ladder filter.

Table 1.1: Equivalent state variables in the passive filter and the active filter.

Passive filter	Active filter
V_{11}	V_{21}
i_{12}	V_{22}
V_{13}	V_{23}
i_{14}	V_{24}
V_{out}	V_{out}

1.2.3 Thesis Contribution

In this research, a new architecture for a reconfigurable analog system is proposed. This architecture is suitable to implement an ADC and low-pass ladder filters. Zero-crossing based circuits are used for the first time to implement a reconfigurable system. It is also the first time that filter functionality is achieved with zero-crossed

Table 1.2: Equivalent equations in the passive filter and the active filter.

Passive filter	Active filter
$\frac{dV_{11}}{dt} = \frac{\Delta V_{11}}{\Delta t} = \frac{1}{C_{11}}(V_{in} - V_{11} - i_{12})$	$\Delta V_{21} = \frac{1}{C_{21}}(V_{in} - V_{21} - V_{22})$
$\frac{di_{12}}{dt} = \frac{\Delta i_{12}}{\Delta t} = \frac{1}{L_{12}}(V_{11} - V_{13})$	$\Delta V_{22} = \frac{1}{C_{22}}(V_{21} - V_{23})$
$\frac{dV_{13}}{dt} = \frac{\Delta V_{13}}{\Delta t} = \frac{1}{C_{13}}(i_{12} - i_{14})$	$\Delta V_{23} = \frac{1}{C_{23}}(V_{22} - V_{24})$
$\frac{di_{14}}{dt} = \frac{\Delta i_{14}}{\Delta t} = \frac{1}{L_{14}}(V_{13} - V_{out})$	$\Delta V_{24} = \frac{1}{C_{24}}(V_{23} - V_{out})$
$\frac{dV_{out}}{dt} = \frac{\Delta V_{out}}{\Delta t} = \frac{1}{C_{15}}(i_{14} - V_{out})$	$\Delta V_{out} = \frac{1}{C_{25}}(V_{24} - V_{out})$

based circuits. One unique characteristic of the proposed system is that the power consumption scales linearly with the sampling rate.

Asymmetric signaling is introduced for the first time to increase the dynamic range of ZCBCs. In addition, a new technique is introduced to implement the terminating resistors of a ladder filter. This technique improves the programmability of the system and reduces the complexity and area overhead of each stage.

The noise of the system is analyzed in both ADC and filter configurations. The dominant sources of noise are identified and their noise contributions are quantified. In addition, the sensitivity of the system to capacitor mismatch and the offset of zero-crossing detector is analyzed.

Finally, a chip is fabricated to show the ADC and filter functionality. Many measurements are performed to characterize the chip. The cost of reconfigurability is also estimated for the fabricated chip.

Table 1.3: The value of the components in the active filter based on the value of their corresponding components in the equivalent passive filter.

Value of components in the active filter
$C_{21} = C_{11}.fclk$
$C_{22} = L_{12}.fclk$
$C_{23} = C_{13}.fclk$
$C_{24} = L_{14}.fclk$
$C_{25} = C_{15}.fclk$

Chapter 2

Zero-Crossing-Based Circuits (ZCBC)

Figure 2-1 shows an opamp-based circuit that amplifies its input. The analog input signal is sampled across C_1 and C_2 in phase 1. The opamp-based circuit transfers the charge on capacitor C_2 to capacitor C_1 in phase 2. As a result, the output voltage is equal to the amplified input signal. In a negative feedback configuration, the value of differential input voltage of an opamp is close to zero. If the positive input of the opamp is connected to the ground instead of V_{cm}, the voltage at node V_x is nearly the same as the ground without direct connection to the ground. Therefore, it is referred to as a virtual ground. The terminology is used even when the positive input of the opamp is not connected to the ground. In general, the condition in which the differential input of an opamp has zero value is referred to as virtual ground condition.

The same functionality can be implemented using zero-crossing-based circuits (ZCBC) as shown in Figure 2-2 and proposed by [20],[21],[23],[24]. The opamp is replaced by a combination of a current source and a zero-crossing detector. Unlike an opamp that continuously forces virtual ground condition, ZCBCs detect the virtual ground condition. To do this, the output starts from one extreme voltage (V_{dd} or ground) and swings toward the other extreme voltage. The zero-crossing detector continuously monitors its differential inputs. When the virtual ground condition is detected, it stops the output swing. If the detector has no delay, the shape of the

output voltage waveform does not affect the accuracy of the circuit. If the zero-crossing detector has a constant delay, the overshoot of the output voltage depends on the delay and the slope of the output voltage when virtual ground condition is detected. In this case, a linear output waveform yields the best performance because with a constant delay and a constant slope at the output, the overshoot is always constant. Many analog circuits including ADCs and filters tolerate a constant offset at the output voltage as long as the output does not saturate.

In Figure 2-2, an analog input is sampled across C_1 and C_2 in a sampling phase (phase 1). In the charge-transfer phase (phase 2), the input is amplified. To do so, the output is preset first. Then, the current source turns on. Since the current source provides a constant current and the load is capacitive, the output voltage is a linear ramp. The zero-crossing detector opens the sampling switch of the next stage when virtual ground condition is detected.

One difference between ZCBCs and opamp-based circuit is the way the output can be sampled. While the output of opamp-based circuits is ready for sampling during phase 2 of the current clock cycle and phase 1 of the next clock cycle, the output of ZCBCs can be only sampled during phase 2 of the current clock cycle.
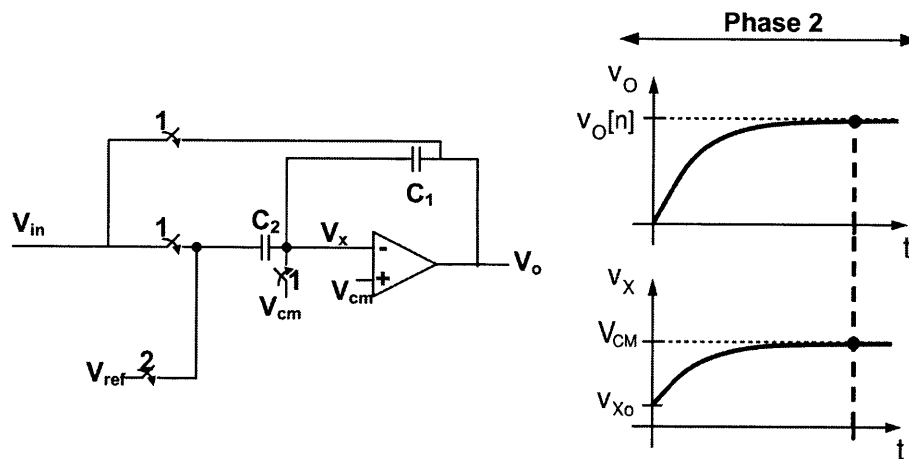
Figure 2-1: Basic opamp-based amplifier.
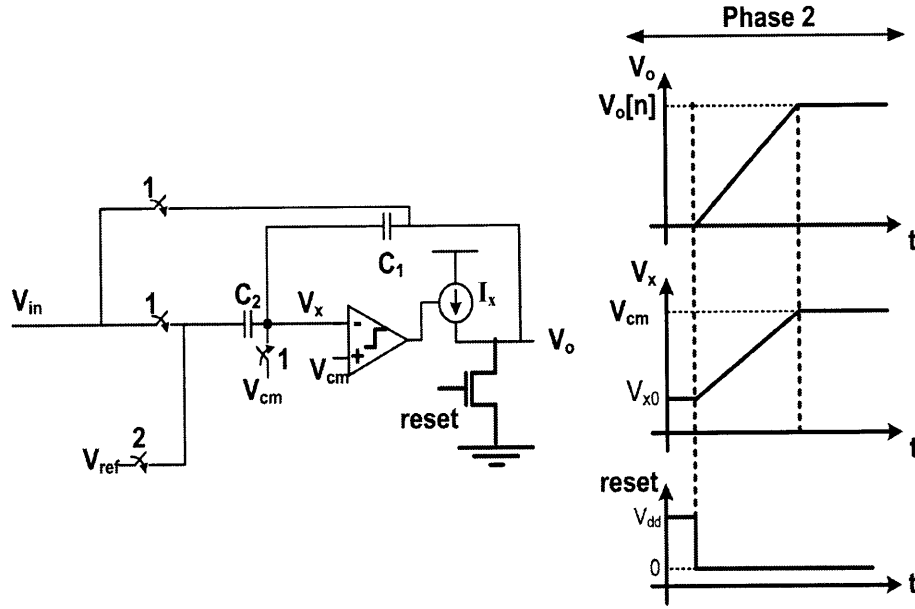
Figure 2-2: Basic zero-crossing based amplifier.

2.1 Advantages of ZCBCs

ZCBCs have several advantages. One important advantage is its lack of explicit feedback. Since opamp-based circuits have negative feedback and more than one pole, the stability of the circuit is an important issue, and often requires large power consumption. If the load or the feedback ratio of the circuit is variable, the frequency compensation should be designed for the worst case situation. In ZCBCs, since there is no explicit feedback, there is no stability concern even with widely varying load and feedback condition.

While the speed of transistors improves in the new technology nodes, the intrinsic gain of transistors degrades. Since large open-loop gain is desired for opamps, the design of opamps is more challenging in new technology nodes. One method to increase the gain is by cascading several gain stages which deteriorates the stability of the system because of more poles. Another method to increase the gain of an opamp is cascoding which is challenging with low supply voltage in new technology nodes. As a result, opamp-based circuits are harder to design in new technology nodes. ZCBC is more suitable for new technology nodes since the current source and

33

the zero-crossing detector can be optimized independently. Zero-crossing detector can use cascaded stages for higher gain since stability is not a concern.

Finally, the power consumption of ZCBCs scale with the sampling frequency. This is due to the fact that once virtual ground condition is detected, all parts of the analog circuit including the current sources and zero-crossing detector turn off and the circuits do not consume static power any longer. As a result, if the circuit operates at a much lower speed, the power consumption scales accordingly. The power consumption of opamp-based circuits can also scale by adjusting its bias currents. However, the power consumption of ZCBCs can be adjusted for a very wide range of sampling frequencies.

2.2   Sources of Nonlinearity

There are several sources of nonlinearity in ZCBCs [23]. The first source of nonlinearity is the delay of the zero-crossing detector. The delay causes an overshoot at the output. If the output is a linear ramp, a constant delay of zero-crossing detector generates a constant overshoot and can be treated as a constant offset. However, delay variation of zero-crossing detector from one clock cycle to another (for example, due to common-mode variation) causes overshoot variation, which causes an error at the output.

In new technology nodes, the output resistance of current sources are low. As a result, when the output voltage changes, the current of the current source does not stay constant and the slope of the output voltage does not stay constant either. The nonlinearity of current sources causes signal-dependant overshoot variation. This gives a similar effect to that of finite gain in opamps. In addition, voltage-dependent capacitive load introduces nonlinearity at the output ramp, which causes overshoot variation. In this chip, the size of the linear capacitive load is much larger than the nonlinear parasitic capacitors. The delay of the zero-crossing detector is also sensitive to the common mode voltage variation and the ramp rate at its input.

In opamp-based circuits, the current that passes through the sampling switches

34

approaches to zero with time. As a result, the voltage drop on the sampling switches is negligible. In ZCBCs, the current that passes through the sampling switches stays constant during the sampling period. As a result, there is a voltage drop across the switches during the sampling time. If the output current source provides a constant current and the switch has a constant resistance, the voltage drop is constant and causes an offset. However, current sources have a limited output resistance (especially in new technology nodes). In addition, the resistance of switches changes widely with the input voltage; as a result, there is a variation on the voltage drop of the sampling switches, which causes an error at the output and the corresponding nonlinearity.

2.3 Solution to some Challenges

There are several techniques to improve the linearity of ZCBCs. One technique is to use multiple ramps as opposed to one [23]. The first ramp is a coarse search for virtual ground, and the next ramp(s) is (are) fine search. Since the ramp rate decreases after the first ramp, there is less sensitivity to the delay variation of the zero-crossing detector. The overshoot is also smaller because of slower ramp rate, which corresponds to a smaller error at the output and a smaller offset.

Another technique to improve the linearity of ZCBCs is to split the output current source in three sections [24] as shown in Figure 2-3. The output current source of the first stage (I_0) should drive the capacitive load of the first stage (C_{11} in series with C_{12}) and the input capacitance of stage 2 (C_{21} in parallel with C_{22}). A large current that charges C_{21} and C_{22} passes through switch 1 and switch 2 and causes a large voltage drop on those switches. Two current sources (I_1 and I_2) are added after switch 1 and switch 2 to provide the current to capacitors C_{21} and C_{22} and I_0 is reduce to provide current only to the capacitors in stage 1. In case of mismatch between I_0, I_1, and I_2, the mismatch current between the current sources passes through switch 1 and switch 2. The mismatch current is much smaller than the total current. Note that I_1 and I_2 are controlled with the same signal that controls I_0. Since the current that passes through the switches reduce, the voltage drop and its variation reduce as

well.
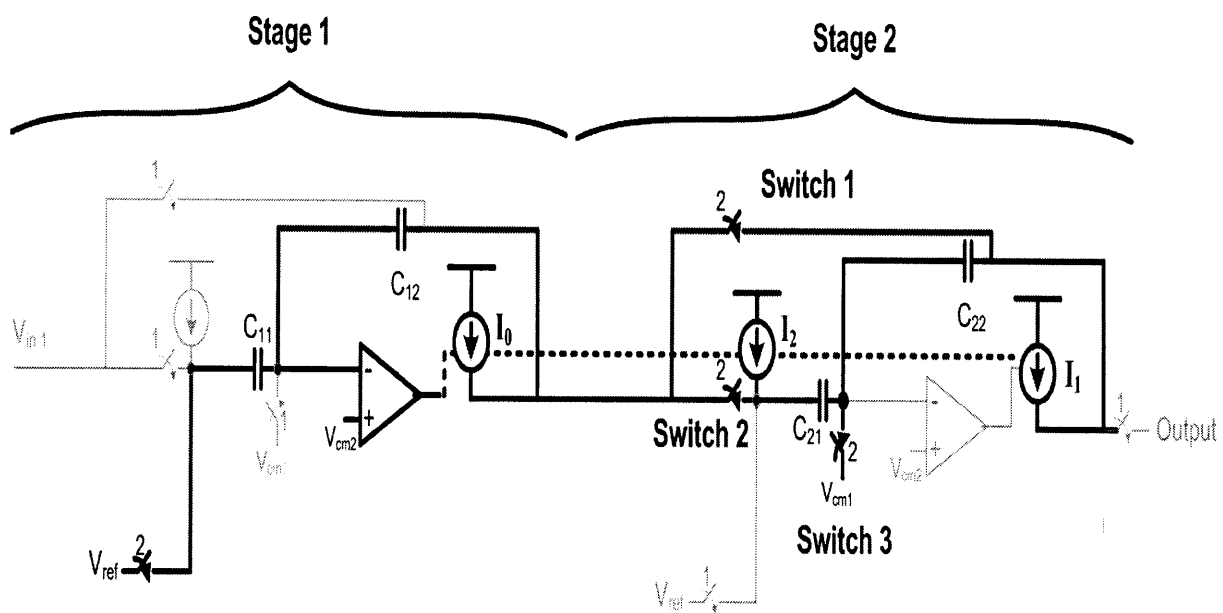
Figure 2-3: Spliting the output current source.

Chapter 3

System Architecture and Implementation

In this chapter, the architecture of the system is described and it is shown how different functionalities are implemented. Then, the implementation of individual circuit blocks is reviewed. A new technique is described to implement the termination resistor in the filter. In addition, asymmetric differential signaling is introduced which increases the dynamic range of the signal. Finally, full system simulation for a 10-bit ADC and a third-order Butterworth filter are presented.

3.1 System Description

Figure 3-1 shows the block diagram of the ideal system. It consists of configurable analog blocks, programmable switches, and the configuration block. Configurable analog blocks have both amplification and integration functionality. Unlike digital FPGAs, the required connectivity of analog blocks is limited (both in terms of number of connections and the distance between source and destination blocks). As a result, the switches are placed only between adjacent blocks.

Figure 3-2 shows how an opamp-based switched-capacitor circuit can either amplify or integrate the input signal. If the input signal is sampled on both capacitors
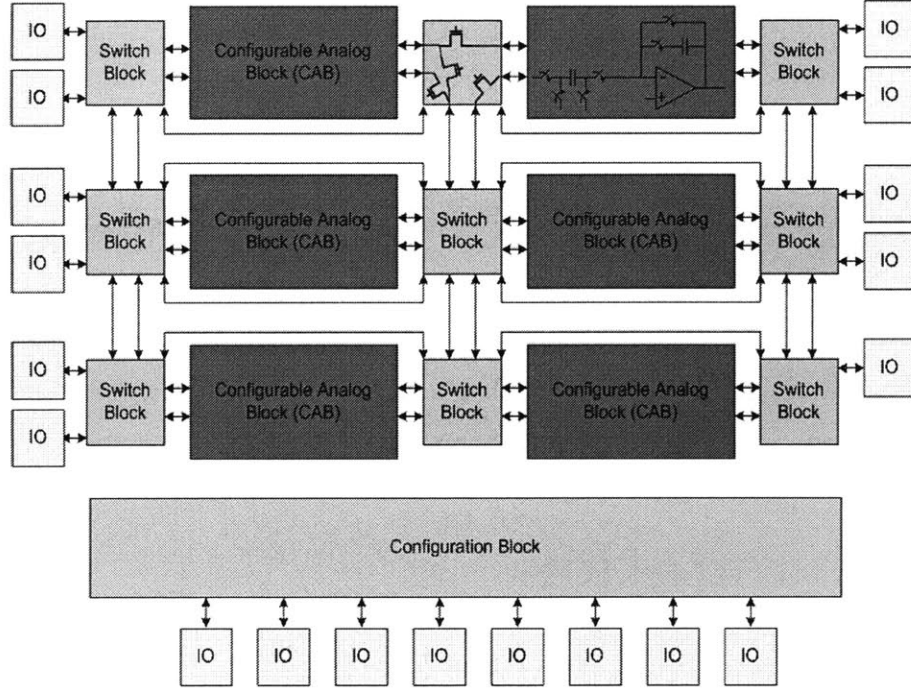
Figure 3-1: Block Diagram of an Ideal System.

during phase 1, the total charge across the capacitors in phase 1 is given by:

$$Q[n] = (C_1 + C_2)V_{in1}[n] \tag{3.1}$$

The charge on C_1 is transferred to C_2 in phase 2. The output at the end of phase 2 is:

$$V_{out}[n + 1/2] = \frac{C_1 + C_2}{C_2}V_{in1}[n] \tag{3.2}$$

Thus, the circuit performs amplification during phase 2.

If the input signal is only sampled on capacitor C_1 without resetting the integration capacitor (C_2), the charge on capacitors C_1 and C_2 are given by:

$$Q_{C1}[n] = C_1 V_{in1}[n] \tag{3.3}$$

$$Q_{C2}[n] = Q_{C2}[n - 1/2] \tag{3.4}$$

The charge on C_1 is transferred to C_2 in phase 2. The output at the end of phase 2

38

is:

$$V_{out}[n + 1/2] = \frac{C_1 V_{in1}[n] + Q_{C2}[n - 1/2]}{C_2} = \frac{C_1}{C_2} V_{in1}[n] + V_{out}[n - 1/2] \qquad (3.5)$$

Thus, the circuit performs integration.

Figure 3-3 shows the building block of a pipeline ADC. It has a set of bit-decision-comparators (BDC) and reference voltages in addition to the basic circuit of Figure 3-2. The circuit samples the input across both capacitors during phase 1. BDCs operate as the sub-ADC for each stage of a pipeline ADC. The sampled input voltage is amplified during phase 2. V_{ref1}, V_{ref2}, and V_{ref3} are related to the outputs of the DAC in each stage of a pipeline ADC which are controlled by the outputs of BDCs and added to the output. The output voltage is given by:

$$V_{out}[n + 1/2] = \frac{C_1 + C_2}{C_2} V_{in1}[n] - \frac{C_1}{C_2} V_{refx} = \frac{C_1 + C_2}{C_2} (V_{in1}[n] - V_{DAC}) \qquad (3.6)$$

where V_{DAC} is the desired voltage of the DAC in each stage of a pipeline ADC, and V_{refx} is one of V_{ref1}, V_{ref2}, and V_{ref3} depending on the outputs of the BDCs. The output of the BDCs are also used to generate the final digital code for the sampled input.

Similarly, Figure 3-4 shows the building block of a low-pass filter. It samples two inputs that are being added and integrated. With differential implementation of these blocks, inverting a signal can be easily performed by switching the polarity of the differential signal.

Figure 3-5 shows the connectivity of five integrating blocks that form a fifth-order low-pass filter. The exact transfer function of the filter depends on the integration coefficient of each block.

3.1.1 The Need for ZCBC Implementation

Implementing the system with opamps raises two concerns. One is that in a highly-programmable system, the output load of the opamp is not known *a priori*. As a
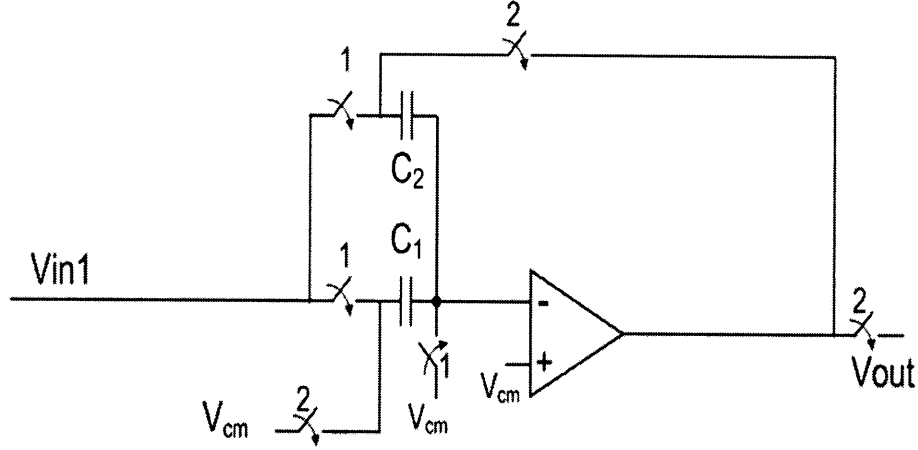
Figure 3-2: Amplification and integration using the same switched-capacitor circuit.
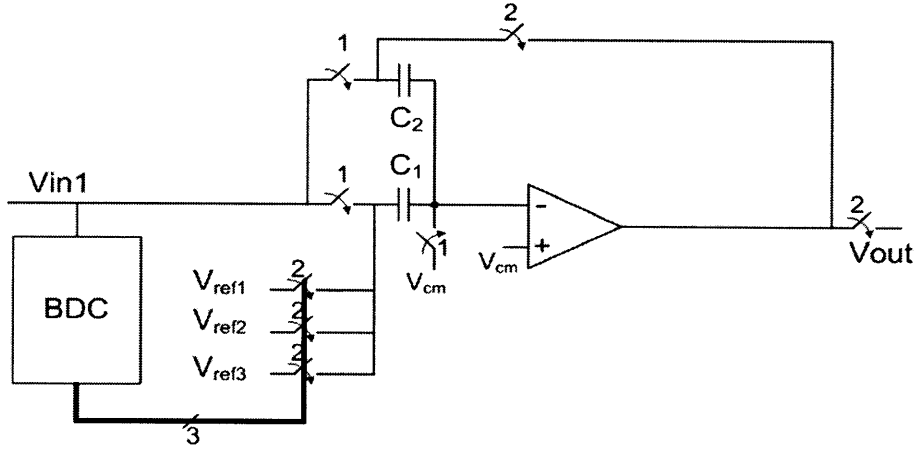
Figure 3-3: Building block of a pipeline ADC.

result, the frequency compensation must be designed for the worst-case load and feedback conditions. This greatly compromises speed and power consumption. Another concern with opamp-based circuits is the power consumption while the operating frequency changes. Opamps consume static power and are often optimized for a particular speed. In a reconfigurable system, the required sampling rate may change from one application to another. If the building blocks of the system use opamps, the power consumption of the system does not scale with sampling frequency for a wide range of sampling frequencies. To address both of these concerns with opamp-based circuits, zero-crossing based circuits (ZCBCs) have been used in the proposed system.
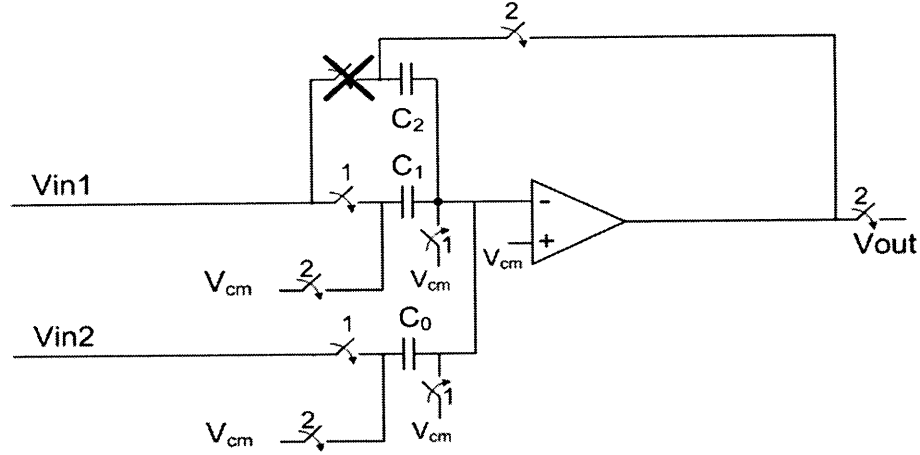
Figure 3-4: Building block of an active ladder filter.
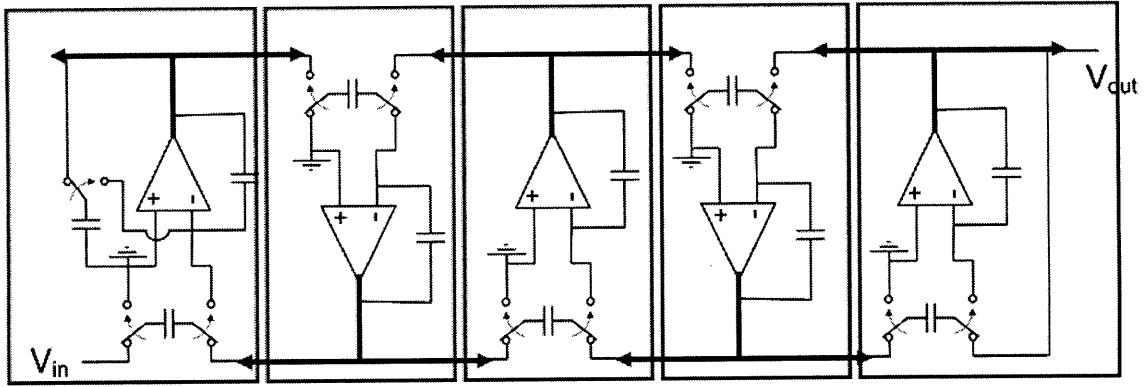
Figure 3-5: Schematic of an active ladder filter.

3.1.2 Implementation of a Reconfigurable Stage

Figure 3-6 shows the basic building blocks of each reconfigurable stage. It includes two sets of sampling capacitors (C_1 and C_0) as needed during the filter functionality. During the ADC functionality, only C_1 is active. A zero-crossing detector and its corresponding current sources are used instead of an opamp. BDCs that control reference voltages are active for ADC functionality. For simplicity 3 BDCs and reference voltages are shown, but the real implementation contains 5 BDCs and reference voltages. Seven programmable capacitors (C_{f1}-C_{f7}) are placed in the feedback, which provide a reconfigurable integration coefficient. Gate-boosting blocks are used to lower the resistance of the reconfigurable switches. The analog input of the gate-

boosting blocks is buffered to reduce the effects of its capacitive load on other blocks. All circuit components are reviewed in the next sections. The schematic is shown as single-ended for simplicity, but it is implemented differentially.
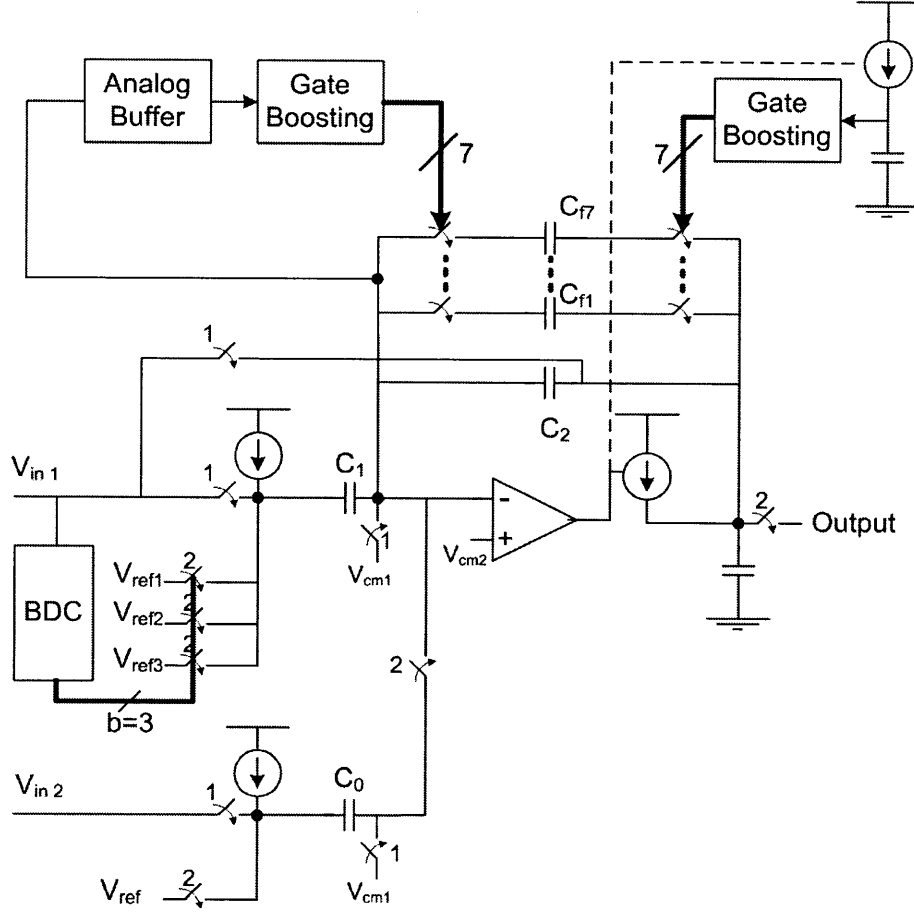
Figure 3-6: Basic building block of reconfigurable stage.

3.1.3 ADC Configuration

In the pipeline ADC configuration, 5 BDCs provide 2.6-bit quantization for each stage (which includes 0.6 bit over-range protection). For example, cascading five stages provides 10-bit resolution. Each stage has digitally-configurable feedback capacitors $(C_{f1}\text{-}C_{f7})$ which provide programmable integration-coefficients for filter functionality. While these capacitors are not active in an ADC configuration, their parasitic capacitors increase the capacitive load at the output. As a result, the power consumption

increases too. The programmable capacitors for the filter may be 10 to 20 times larger than the ADC capacitors, resulting in parasitic capacitors that are comparable in value to the ADC capacitors. Configurable switches are placed on both sides of the feedback capacitors to isolate their parasitics from the rest of the stage. Switches are bootstrapped to reduce their size and parasitic capacitance since bootstrapping reduces the ON resistance of the switch. To avoid any disturbance on the virtual-ground node, it is buffered by a source follower before feeding into the bootstrap block. While most circuits are shown as single-ended, the actual implementation is differential.

3.1.4 Filter Configuration

In the filter configuration, V_{in1} and V_{in2} are sampled across the sampling capacitors C_1 and C_0. The binary-weighted reconfigurable feedback capacitors are connected to configurable switches, which determine the integration ratio. Table 3.1 shows the ratio of the integration capacitor to the sampling capacitor for several different filters if the sampling frequency is 50MSPS and the cut-off frequency is at 1MHz. The BDCs are turned off and only one of the reference voltages is used during the operation.

Table 3.1: Ratio of feedback capacitor to the sampling capacitor for each stage of filter and different types of filters.

Filter Type	Stage 1	Stage 2	Stage 3	Stage 4	Stage 5
1st order Butterworth	15.9				
2nd order Butterworth	11.3	11.3			
3rd order Butterworth	7.9	15.9	7.9		
4th order Butterworth	6	14.7	14.7	6	
5th order Butterworth	4.9	12.9	15.9	12.9	4.9
5th order Chebyshev	16	8	23	8	16

3.2 System Components

In this section, the main building blocks of each stage are reviewed.

3.2.1 Sampling Circuit

The main criteria for designing a sampling circuit are sampling noise, input bandwidth, input voltage swing, and distortion. Bottom-plate sampling is used to reduce signal-dependent distortion [25] as shown in Figure 3-7. In Figure 3-6, these are the switches that are closed in phase 1.
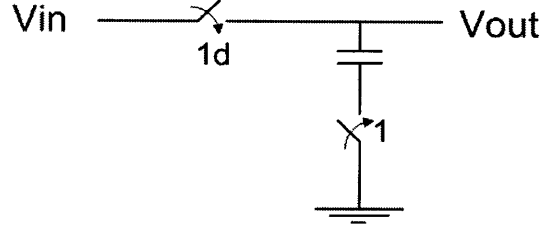
Figure 3-7: Single-ended bottom-plate sampling circuit.

The size of the sampling capacitor can be calculated based on the kT/C noise budget of sampling circuit (which is reviewed in more detail in Chapter 4). The 3dB cut-off frequency of the sampling circuit is a function of switch resistance and sampling capacitance as shown in Equation 3.7. The 3db frequency is set to be larger than the signal bandwidth.

$$f_{3dB} = \frac{1}{2\pi R_{switch} C} \tag{3.7}$$

Another concern is the input-dependant resistance of the sampling switch. Smaller input voltage swing causes less resistance variation at the cost of lower dynamic range. In opamp-based circuits, the current that passes through the switches approaches zero, but in ZCBCs, the current stays constant until the sampling moment. As a result, resistance variation of the two switches causes output voltage variation in ZCBCs. The resistance of the top-plate switch changes due to changes in V_{in}. The resistance of the bottom-plate switch changes due to changes on common-mode voltage (here shown as ground).

The top-plate and bottom-plate switches can be implemented in different ways, including regular NMOS, high-voltage NMOS, regular transmission gates, transmission

44

gate with high-voltage NMOS, and bootstrapped NMOS as shown in Figure 3-8.
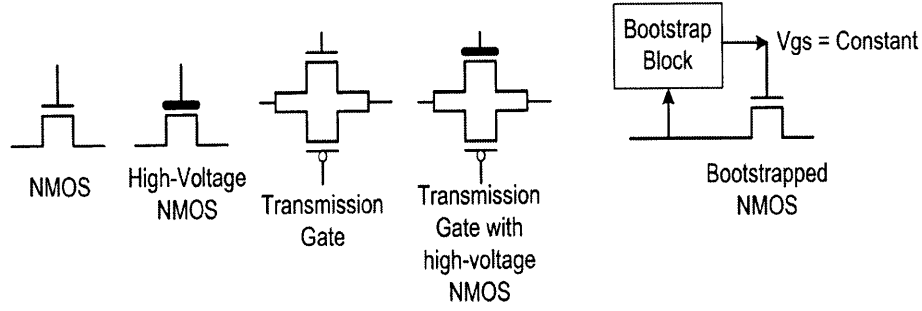
Figure 3-8: Possible switches for signal sampling.

The resistance of a switch is given by Equation 3.8 [26].

$$R_{on} = \frac{1}{\mu_n C_{ox} \frac{W}{L}(V_{GS} - V_{TH})}$$ (3.8)

where V_{TH} is given by Equation 3.9 [26].

$$V_{TH} = V_{TH0} + \gamma(\sqrt{|2\Phi_F + V_{SB}|} - \sqrt{|2\Phi_F|})$$ (3.9)

V_{TH0} is the threshold voltage when body-biasing is zero ($V_{SB} = 0$), γ is the body effect coefficient, $\Phi_F = (kT/q)\ln(N_{sub}/n_i)$, and V_{SB} is the source to bulk potential difference.

The resistance variation is mainly due to variation in V_{GS}, since V_{TH} variation is attenuated by the square root and γ in Equation 3.9. With regular NMOS, the gate voltage is 1V (V_{dd}=1V) when the transistor is on. If the input signal has a large swing (for example between 0.25V and 0.75V), the switch resistance increases as the source voltage increases. If high-voltage NMOS is used, the gate voltage is 2.5V (V_{dd}=2.5V for high-voltage NMOS) when the transistor is on. As a result, the changes in source voltage correspond to less variation in V_{GS} (percentage-wise). However, high-voltage devices require much larger area, have larger parasitic capacitance, and require a level converter so that a control signal in $V_{dd} = 1V$ domain is converted to $V_{dd} = 2.5V$ domain. The conversion itself increases the delay of the control signal and increases power consumption, which is not desired.

Transmission gate provides good conductivity for voltages close to ground or V_{dd}

where one of NMOS or PMOS are very conductive. However, for a signal near $V_{dd}/2$, the transmission gate has a large resistance variation.

Bootstrapping provides a nearly constant V_{GS} across the switch. This implies that when the source voltage is large (for example 0.7V), the gate voltage exceeds the supply voltage (for example 1.7V). Since V_{gs} and V_{gd} do not exceed V_{dd}, the large gate-voltage does not cause reliability problems. The switch resistance still varies due to changes in the threshold voltage due to the back-gate effect. In this system, bootstrapping is used. Figure 3-9 shows the resistance variation of different switches (the resistance of all switches are normalized). Figure 3-9 shows that the resistance of an NMOS switch changes by a factor of 1000. The resistance of a high-voltage NMOS changes by a factor of 2.8. A regular, and a high-voltage transmission gate have resistance variation by a factor of 18, and 1.8. Bootstrapped NMOS has resistance variation by a factor of 1.4.
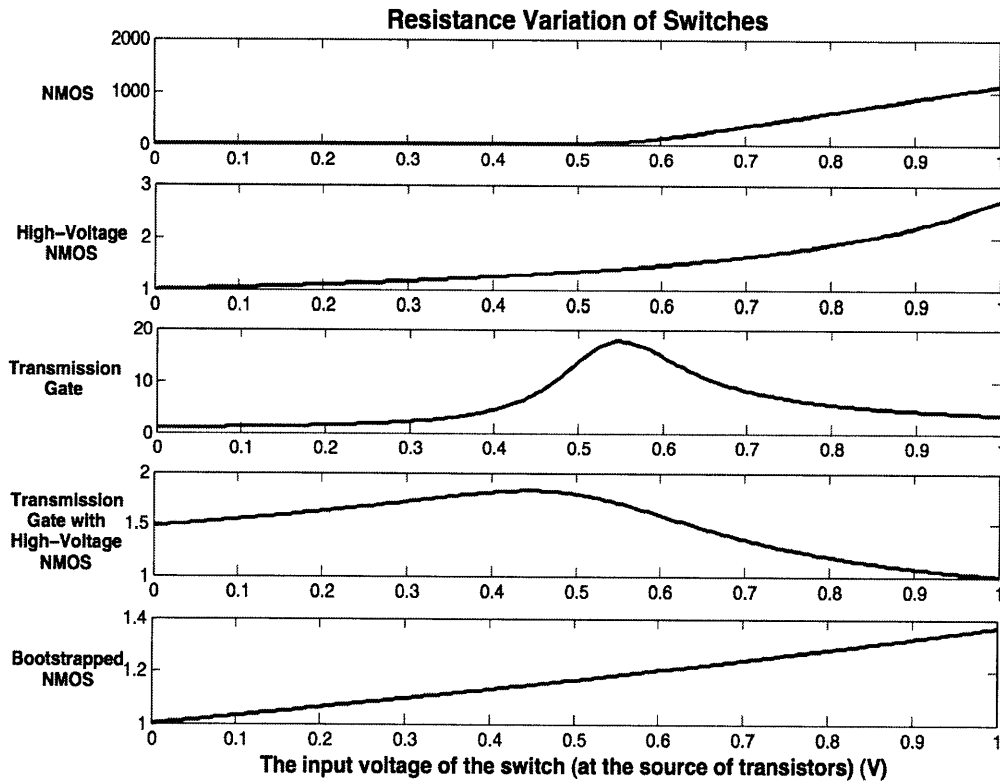
Figure 3-9: Resistance variation of different switches.

3.2.2 Bootstrapping

Figure 3-10 shows the bootstrap circuit [27] and Figure 3-11 shows the waveforms of some voltages (from simulation). It has two inputs, V_{in} and Clk. When Clk is high, transistor M1 is on and pulls down voltage V1 to zero. Transistor M9 and M8 are also on and pull down V_{out} to zero, which turns on transistor M2 and charges voltage V2 to V_{dd}. The capacitor is charged to V_{dd}. Transistor M4 is also on which keeps M7 off. Transistor M3, M5, and M6 are also off.

When Clk is low, Transistor M1, M9, and M8 are off. Transistor M3 turns on which turns on transistor M7. As a result V_{out} is connected to V_2. Since V2 was charged to V_{dd} when Clk was high, transistor M6 turns on and connects Vin to V1. Since V_{in} is connected to one side of the capacitor and V_{out} is connected to the other side, $V_{out} = V_{in} + V_{dd}$. If V_{out} is connected to a gate of a transistor and V_{in} is connected to the source (Figure 3-8), V_{GS} is held constant at V_{dd}.
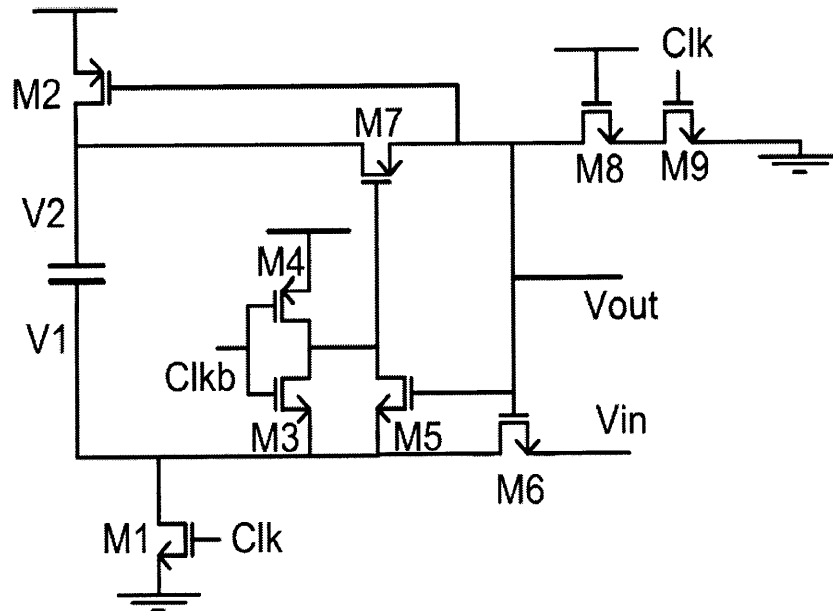
Figure 3-10: Schematic of bootstrap circuit.

Simulation of Bootstrapping Block
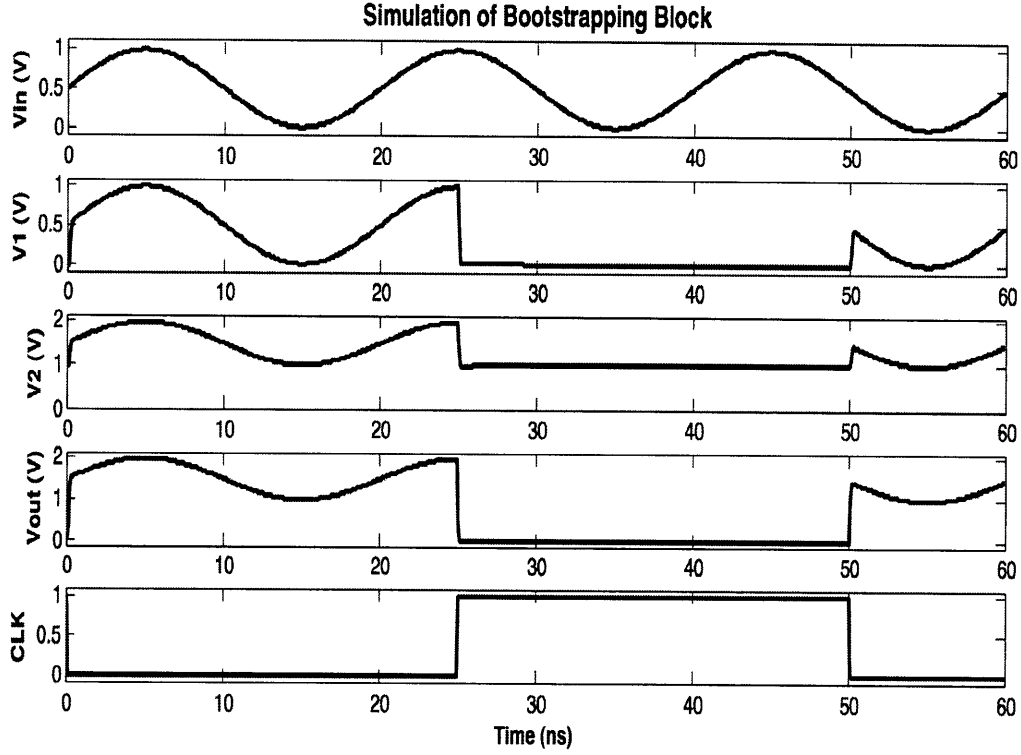
Figure 3-11: Simulation of the bootstrap circuit.

3.2.3 Zero-Crossing Detector

Zero-crossing detector replaces the opamp in opamp-based circuits to detect the virtual ground condition. When it detects, zero-crossing detector turns off the sampling switches of the next stage and the output current sources in its own stage. The schematic of zero-crossing detector is shown in Figure 3-12 [24]. The first stage consists of a differential amplifier and the second stage is a dynamic inverter [28]. Its operation is based on the fact that V_{inp} is pre-charged to a voltage larger than the virtual ground and ramps down linearly, and V_{inn} is pre-discharged to a voltage less than the virtual ground and ramps up linearly. When V_{inp} is high and V_{inn} is low, V_{o1} is high. As V_{inp} ramps down and V_{inn} ramps up, the voltage at V_{o1} starts to reduce. The second stage monitors V_{o1} and when it passes the threshold voltage of transistor M21, it pulls up V_{o2} and pulls down V_{cont}. The signal Enb is used to preset V_{o2} before

48

the detection starts. When V_{cont} is low, the current source of the first stage turns off to save power. It turns on before the next detection starts. In the first stage, the active load is binary-weighted and programmable to adjust the offset of the detector. Offset of the zero-crossing detector is mainly due to the mismatch of the transistors in its first stage. Process variation also affects the threshold voltage of the second stage of the zero-crossing detector. The offset of the zero-crossing detector causes an overshoot at the output voltage. In other words, the offset of the zero-crossing detector causes an offset at the output voltage. Table 3.2 shows some of the possible offset adjustments. When a binary-weighted load is connected, it is shown by code 1, and when it is disconnected, it is shown by code 0.
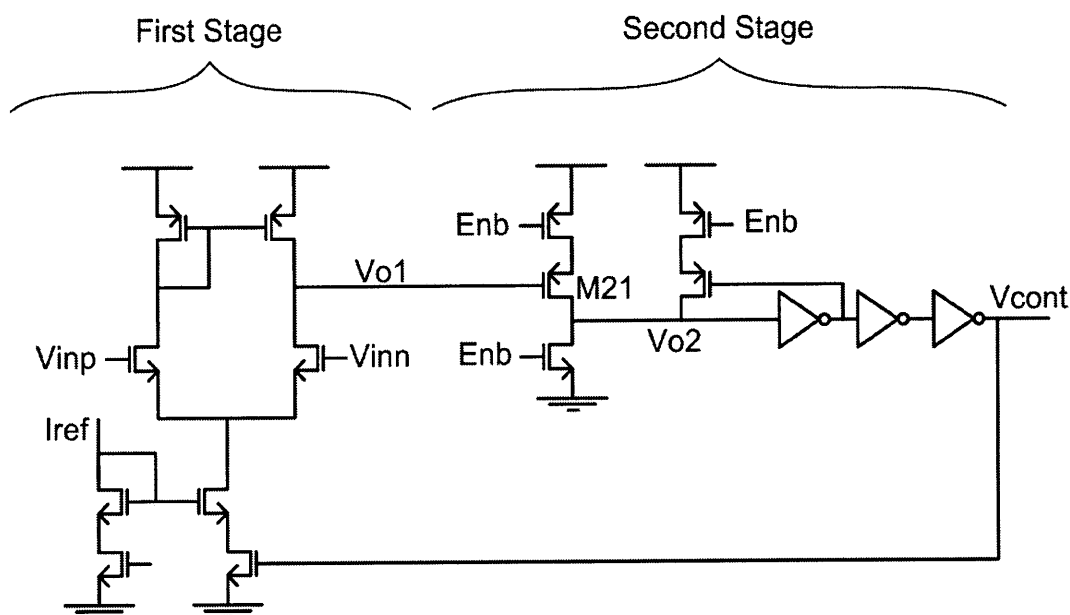
Figure 3-12: Schematic of zero-crossing detector.

3.2.4 Current Sources

In an ADC configuration, the output voltage is sampled by the sampling switches. After the output of a stage is sampled, the voltage on its sampling capacitors and feedback capacitors are not needed any longer. In comparison, in a filter configuration, since each stage is integrating its inputs, the current voltage of the integrating

49

Table 3.2: Offset adjustment of ZCBC detector based on the programmable load of the first stage.

Load on the positive leg	Load on the negative leg	Input Referred Offset
101	101	0mV
111	111	3mV
011	011	-10mV
101	011	-60mV
101	010	-100mV
101	111	+40mV

capacitor is needed in the subsequent clock cycles. As a result, the output current sources should turn off quickly when the zero-crossing is detected. Figure 3-13 shows the schematic of the current source. The current source is required to turn on and off very quickly, which can be done either by controlling the gate of transistor M1 or M2. Since the output current of the current source is mainly determined by transistor M1, the control signal is applied to the gate of transistor M2 so that the settling time of the gate voltage is less important. The linearity of the current source affects the linearity of the system [23]. Transistors with long channel length and cascoded architecture are used to improve the linearity.
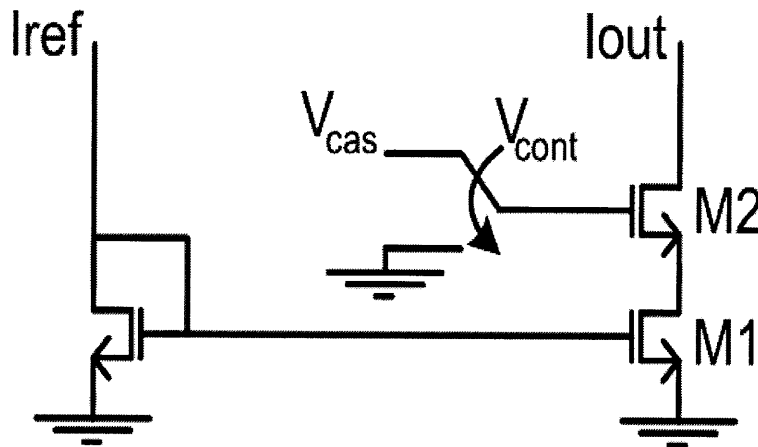
Figure 3-13: Schematic of a basic current source.

3.2.5 The first Stage

The level of the input voltage in the first stage is 0.25V-0.75V for both inputs of the differential signals. The input level of all other stages is 0.4V-0.91V on the positive input and 0.09V-0.6V on the negative input. As a result, the threshold voltage of BDCs and the reference voltages are adjusted accordingly for the first stage (it is shown in the residue plots in Figure 3-16 and Figure 3-17).

Since the output of all stages are linear ramps, the sampling switches conduct a relatively constant current to the sampling capacitor. As shown in Figure 3-14 and proposed in [24], an additional current source is added after each switch to provide a large portion of the current to the sampling capacitor. This technique reduces the current that passes through the sampling switch and reduces the corresponding voltage variation across the switch. Since the first stage samples its input from a regular voltage source (without ZCBC operation), the corresponding current sources are not needed.

3.2.6 Bit-Decision-Comparators (BDC)

Wide range of latched comparators have been developed [15],[29],[30]. Figure 3-15 shows the schematic of the bit-decision-comparator in this system (which is proposed by [31]). The differential input is sampled across the sampling capacitors in phase 1 (Clk = 0), while all internal nodes are pre-charged to V_{dd}. In phase 2, the sampling capacitors are connected to the reference voltages. Transistor M1 and M2 start to discharge V_{out} and V_{outb}. If one of the output voltages is discharged more quickly (for example V_{outb}), it disconnects the other output voltage (V_{out}) from the lower transistors (M2). A regenerative action helps both V_{out} and V_{outb} to reach their final voltage quickly. The mismatch of transistors and capacitors causes an offset in the BDC. Two binary-weighted capacitors are added as the load to adjust the offset. Table 3.3 shows the offset for different load connection when the common-mode voltage is 500mV. The offset adjustment is to be used when the offset is larger than the over-range protection. In this design, the BDC offset is adjusted manually for each stage.
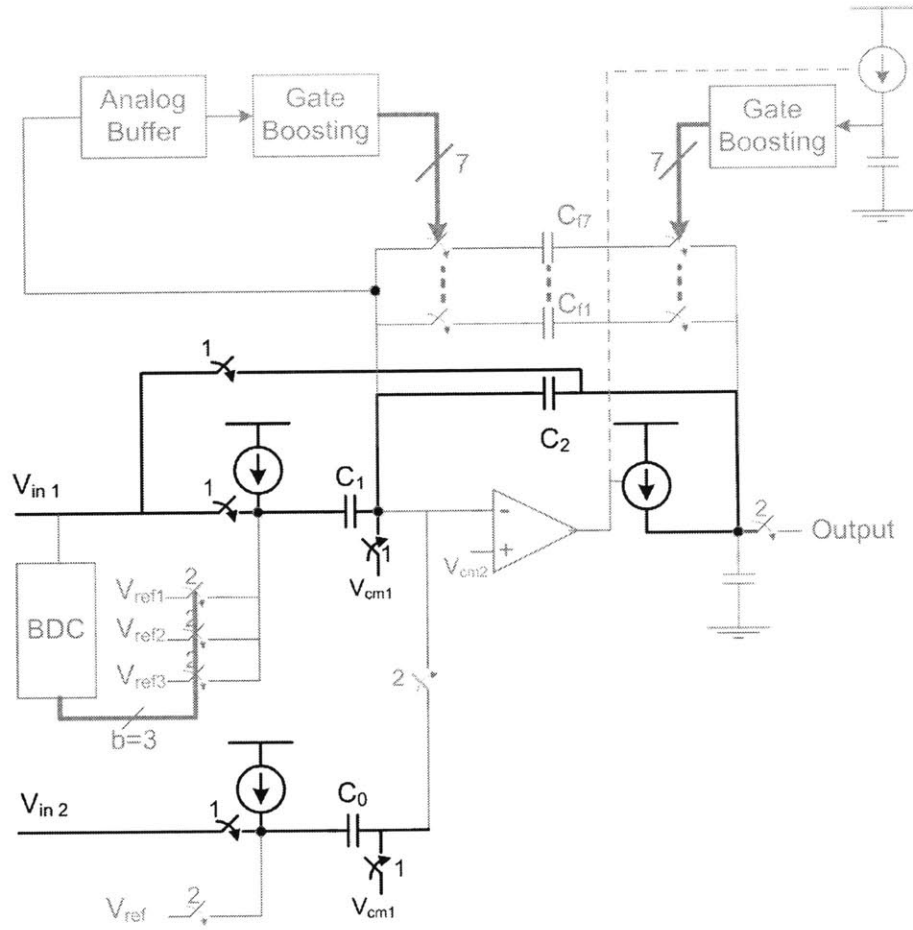
Figure 3-14: Basic building block of reconfigurable stage.

3.2.7 Residue Plot

Figure 3-16 shows the input-output relationship of each stage in ADC configuration (residue plot) for the positive input of the differential signal. The expected range of the input is from 0.5V to 0.833V. Two extra bit-decision-comparators are added (with threshold voltage of 0.5V and 0.833V) to increase the input-range to 0.4V-0.92V. The added margin is the over-range protection at the input. The output is expected to swing between 0.5V and 0.833V and stays linear from 0.4V to 0.92V. Based on the residue plot, five bit-decision-comparators are needed for each stage. The offset of BDCs should be less than 27mV otherwise the output may saturate.
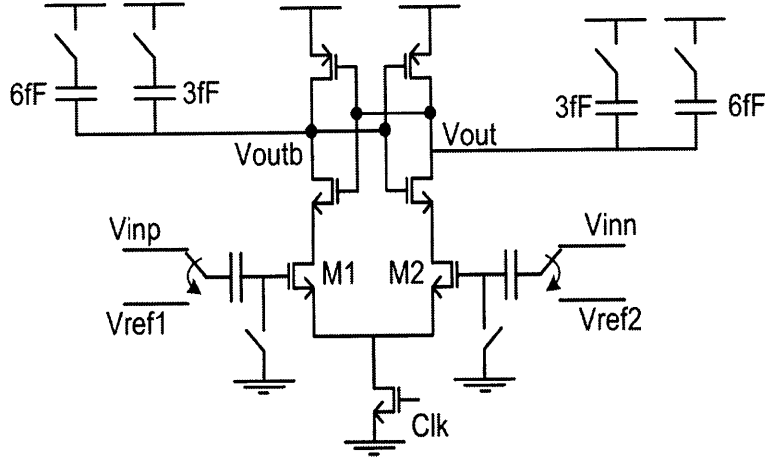
Figure 3-15: Schematic of a bit-decision-comparator.

Table 3.3: Offset adjustment of bit-decision-comparator.

Load on the positive leg	Load on the negative leg	Input Referred Offset
0fF	0fF	0mV
3fF	0fF	-14mV
6fF	0fF	-27mV
9fF	0fF	-36mV
9fF	3fF	-22mV

3.2.8 The Analog Buffer

The schematic of the analog buffer is shown in Figure 3-18. If a regular source follower is used, the voltage drop of the source follower reduces the level of the output voltage. The output of the analog buffer drives a bootstrapping block. If the analog buffer has a voltage drop, the same voltage drop appears at the output of the bootstrapping block, which drives the gate of a reconfigurable switch. As a result, the voltage drop of the source follower in Figure 3-6 causes lower overdrive voltage for the corresponding reconfigurable switch. A large capacitor is included in series at the output of the analog buffer to adjust its output level. In phase 1, when each stage is sampling its input, the input of the analog buffer is connected to V_{cm} (Figure 3-6). During this phase, V_{cm} is also connected to the output capacitor of the analog buffer and samples the voltage drop of the source follower across the capacitor. In phase 2, when the

53
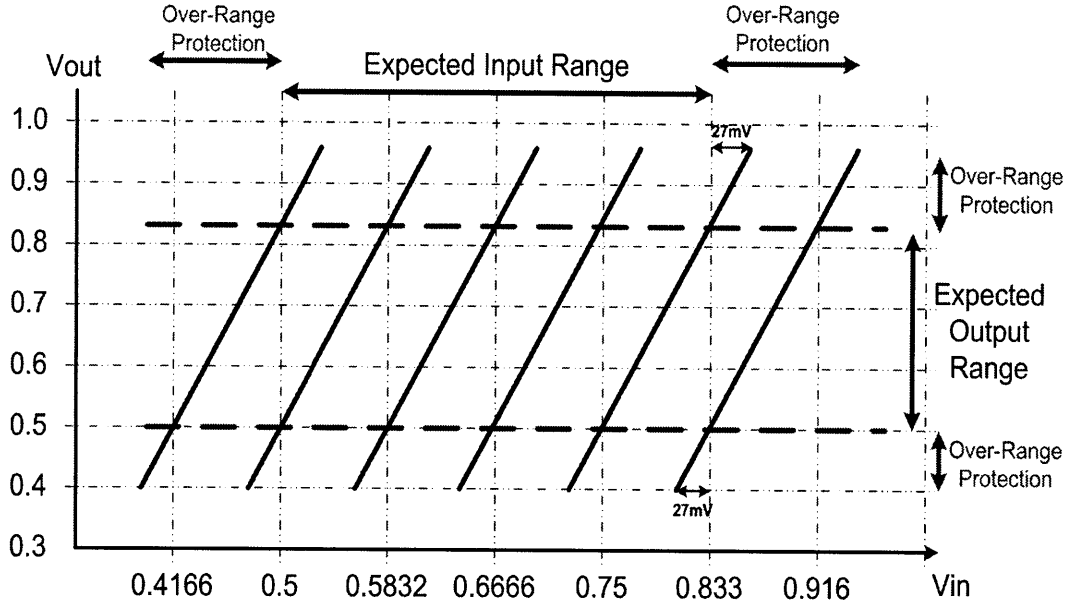
Figure 3-16: Residue plot in ADC configuration.

sampled signal is being amplified or integrated, V_{out} of the analog buffer tracks its V_{in} without any voltage drop because the voltage drop of the source follower is added back by the output capacitor.

3.2.9 Terminating Resistors

In a filter configuration, the terminating resistors at the input and output stages are implemented by adding an additional local feedback, which samples the output of the stage and subtracts it from the input in the next clock cycle (as shown in Figure 3-5). This implementation requires an additional set of sampling capacitors (C_{s2} in Figure 3-19a) when implemented in opamp-based system. In ZCBC implementation, the local capacitor must sample the output at the same time as it is connected to the input for integration. This timing conflict requires a second set of capacitors, so that one set samples the output while the other set is connected to the input for integration. A highly-programmable system requires such a block in every configurable stage. However, the implementation of the block is expensive in terms of required area, additional parasitics, and more complex control signals. A new technique is shown

54
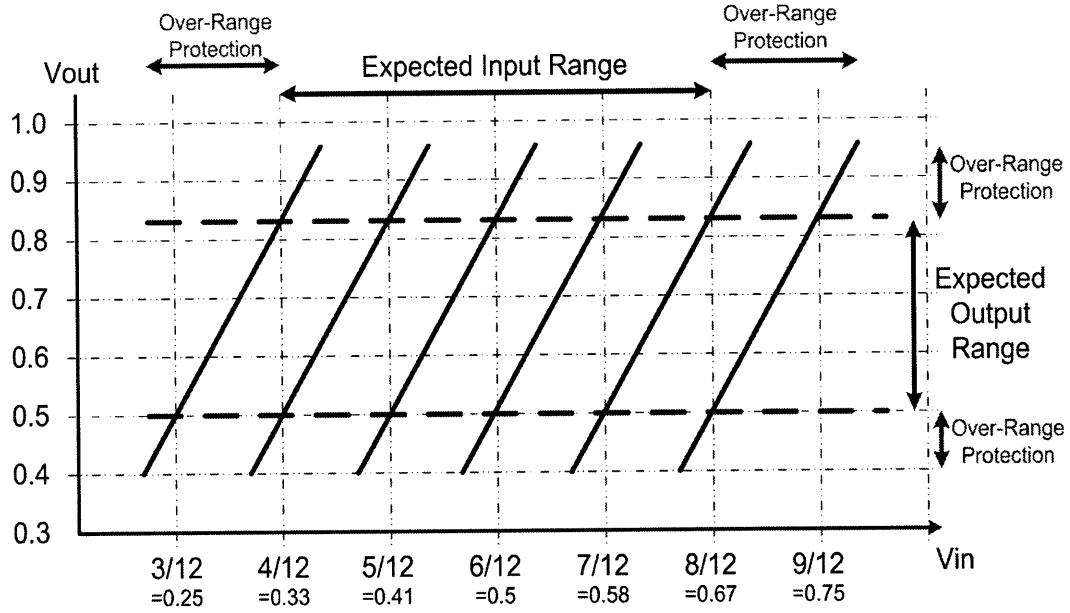
Figure 3-17: Residue plot of the first stage in ADC configuration.

in Figure 3-19. Figure 3-19a shows the original opamp-based implementation, where the output voltage is sampled across a unit-size capacitor and then subtracted from the input in the next cycle. The same output voltage is also sampled on the feedback capacitor. The input-output relation of the stage is shown by Equation 3.10.

$$V_{out}[n+1] = V_{out}[n] + \frac{1}{A}(V_{in}[n] - V_{in2}[n] - V_{out}[n]) \qquad (3.10)$$

Figure 3-19b shows the new circuit which performs the same functionality by splitting the feedback capacitor into two capacitors, one of which has a unit size. Instead of subtracting the output of the stage from the input in the next cycle, the unit-size capacitor in the feedback is discharged. The charge across both feedback capacitors before discharging the unit capacitor is:

$$Q[n] = (A-1)V_{out}[n] + V_{out}[n] = AV_{out}[n] \qquad (3.11)$$

If the unit size capacitor is discharged right before the integration, the total charge
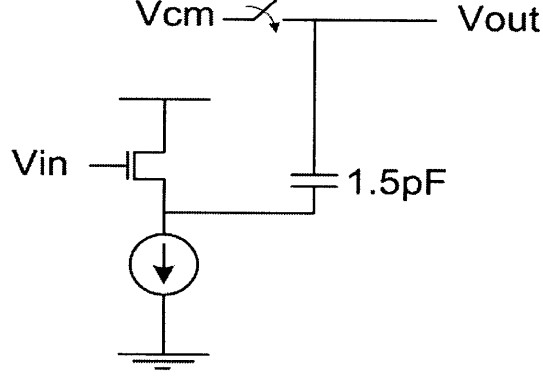
Figure 3-18: The schematic of the analog buffer.

on the feedback capacitor is:

$$Q[n] = (A - 1)V_{out}[n] + 0 = (A - 1)V_{out}[n] \qquad (3.12)$$

After the unit size capacitor is discharged, it is connected back to other feedback capacitors. The new output voltage is:

$$V_{out-new}[n] = \frac{A - 1}{A} V_{out}[n] \qquad (3.13)$$

The output voltage after integration is given by Equation 3.14 which is the same as Equation 3.10.

$$V_{out}[n + 1] = \frac{A - 1}{A} V_{out}[n] + \frac{1}{A}(V_{in}[n] - V_{in2}[n]) \qquad (3.14)$$

Since there are already binary-weighted capacitors in the feedback with the corresponding switches, this technique does not require any additional capacitors or switches to implement terminating resistors. The only additional component is the switch to discharge the unit-size capacitor (which is very small). Using this technique, all stages can implement the terminating resistors without any penalty.

a) Traditional opamp-based
implementation

b) The new method to implement
the terminating resistors
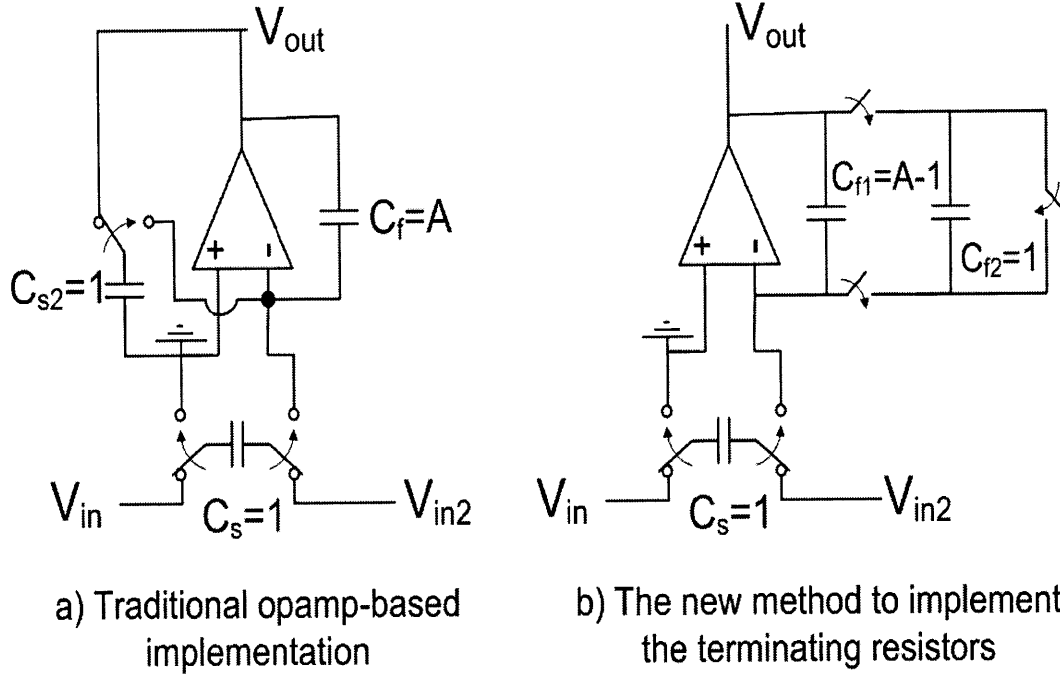
Figure 3-19: Implementation of terminating resistors in ladder filters.

3.3 Asymmetric Differential Signaling

Traditionally, differential signals have the same swing on the positive and negative direction. Figure 3-20 shows the signal swing at the output of each ZCBC block. If the output current source stays on, the output ramps linearly till it reaches the saturation region. ZCBCs are linear only if the output stays within the linear ramp region [23]. In Figure 3-20, V_{outn} is linear when it ramps up from 0V to 0.7V and V_{outp} is linear when it ramps down from 1V to 0.3V. With symmetric differential signaling, each of V_{outp} and V_{outn} can only swing between 0.3V and 0.7V. This indicates that the linear output range where V_{outp} ramps from 1V to 0.7 and V_{outn} ramps from 0V to 0.3V is not utilized. With supply voltage as low as 1V, the unutilized linear region makes up 42% of the total linear region. Asymmetric output swing is employed to utilize the full linear range of the output. Reference voltages are chosen from the residue plots (Figure 3-16 and Figure 3-17) so that they support the asymmetric signal range.
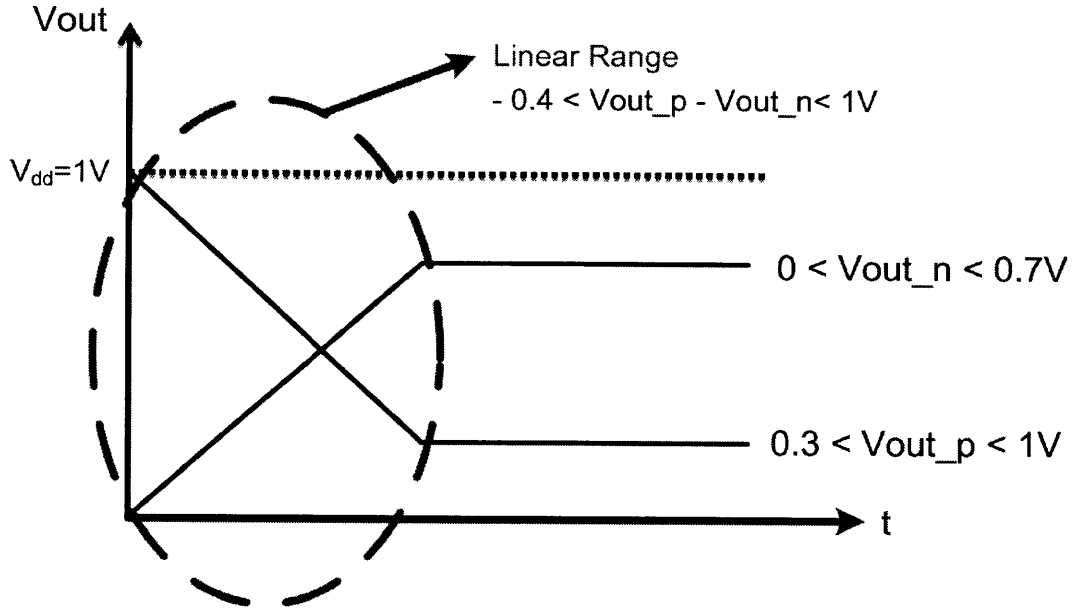
Figure 3-20: Signal swing in zero-crossing based circuits.

3.4 Programmability

The programmability of the system falls in three categories, functionality, calibration, and power optimization.

3.4.1 Programmability for functionality

Each stage can be programmed to perform either integration or amplification. The integration coefficient is determined by the ratio of the integrating capacitor to the sampling capacitor. Programmable binary-weighted integration capacitors provide the desired integration coefficient. In filter configuration, an additional local feedback loop is required in the first and the last stage to implement the terminating resistor. The terminating resistor can be programmed to be active or inactive as needed.

Similarly, BDCs can be turned off if not needed (for filters). Each stage has two sets of sampling capacitors. Depending on the functionality, one or both sampling capacitor is activated.

58

3.4.2 Programmability for Calibration

If the ramp rates at the output of one stage matches the ramp rate at the input of the next stage, smaller current passes through the top-plate switches and the distortion is reduced. The ramp rate depends on the ratio of current sources and load capacitors. The ramp rate can be adjusted by programmable binary-weighted current sources to compensate for changes in capacitive load in different configurations. In addition, the offset of BDC and zero-crossing detector can be adjusted.

Figure 3-21 shows the timing of phase 1 and phase 2 of the clock and the pulses at the beginning of each phase. Non-overlapping clocks are used in this system. At the same operating speed, a large non-overlap period results in smaller period for phase 1 and phase 2. Hence, a very small non-overlap period would be ideal. However, since the clock tree has skew and jitter, the non-overlapping period increases the skew and jitter tolerance of the system. In this system, the non-overlapping period is programmable to compensate for clock skew without introducing excessive margin. The non-overlap period can be adjusted from 100ns to 400ns (in 100ns steps).
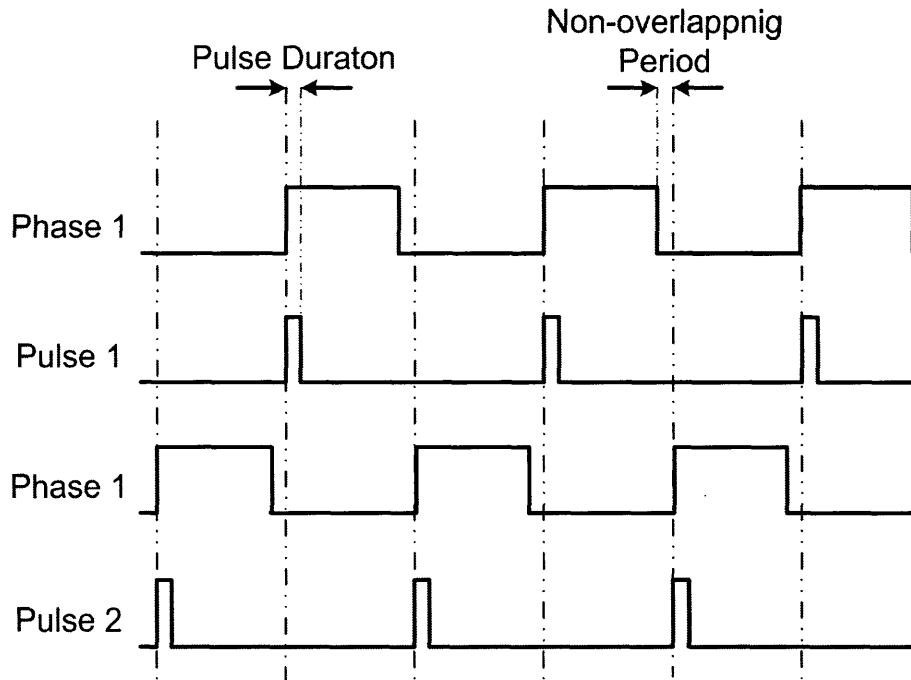
Figure 3-21: Timing of different phases of clock and pulses.

ZCBC architectures use short clock pulses at the beginning of both phase 1 and phase 2 to initialize the operation. The strength of the switches that perform pre-charging or pre-discharging may vary due to process variation. Similarly, the capacitive load of such nodes may vary. As a result, a programmable pulse period is implemented to compensate for such variation. Each pulse can be programmed to be from 100ns to 800ns (in 100ns steps).

The bias voltage for NMOS and PMOS transistors in cascode and the common-mode voltage can be either generated on-chip or provided off-chip. It is more desirable to generate these voltages on-chip to avoid the effects of bond-wire inductance. A 7-bit digital-to-analog convertor (DAC) generates each voltage.

3.4.3 Programmability for Power Optimization

If analog connectivity between some stages is not needed, the corresponding switches can be programmed to stay off. In addition, the clock and reference currents of unused stages can turn off to save power. The current source of any circuit block in each stage can turn off if the block is not needed. For example, in the ADC configuration, the zero-crossing detector of the last stage of pipeline ADC can turn off during the whole operation. Finally, digital output of each stage can be turned off if not needed.

3.5 System Simulation

The system is simulated with Spectre and the output is sent to Matlab for more analysis. In an ADC configuration, near Nyquist-rate sinusoid is applied to the input of the system and transient simulation is performed. The output of the transient simulation is sent to Matlab to analyze the frequency response.

To ensure that the simulation setup is appropriate, the system was first implemented with ideal elements using VerilogA models. Simulation settings such as an absolute and relative tolerance of voltages and currents and maximum time step are adjusted in this phase for 13-bit accuracy. Then, different components are replaced with the real implementation one at a time to evaluate the performance of each block.

Some voltages, such as supply voltages and reference voltages, are expected to stay constant. However, high-frequency activities in the system disturb these voltages when the voltages are provided off-chip due to the inductance of the bond-wires. The bond-wire model is added to the simulation so that the disturbance of these voltages and its effects on system performance can be estimated. The power supply model is shown in Figure 3-22 where R is 50ohm and L is 2nH. The disturbance can be mitigated by adding on-chip decoupling capacitors. The required size of the decoupling capacitors is estimated from the simulation.
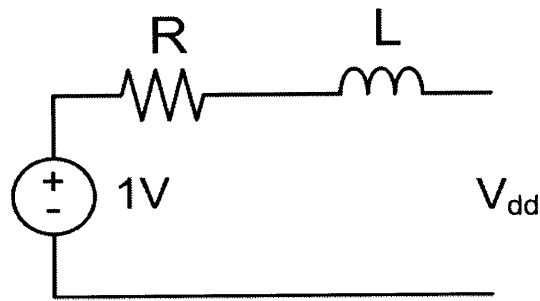
Figure 3-22: The power supply model.

The performance of pipeline ADC can be estimated from the performance of the first stage by measuring the distortion of its analog output voltage. This approach reduces the simulation time and is suitable for early simulations. Including all stages in simulation slows down the simulation significantly, but has several advantages. One advantage is that it confirms that the stages work properly together. In addition, all stages show their disturbance contribution to the reference voltages and the performance of the system can be measured more accurately.

Figure 3-23 shows the simulated performance of the ADC when a near Nyquist-rate sinusoid is applied. For this simulation, the ADC consists of five stages, each with 2.6-bit quantization level. The system has 10.6-bit quantization levels. The simulation includes the real implementation of all stages (as opposed to analyzing the overall performance based on the performance of the first stage). The simulation also includes the bond-wire model to account for transients on constant voltages, but it does not include device noise and capacitor mismatch. The simulation results in

effective number of bits (ENOB) to be 9.8-bit (which shows the linearity of each stage in this configuration). Adding the device noise, ENOB degrades further to 9.03bits. The transient simulation contains 64 clock cycles. Repeating the simulation with 256 clock cycles resulted in similar results suggesting the low number of the clock cycles does not cause inaccuracy.
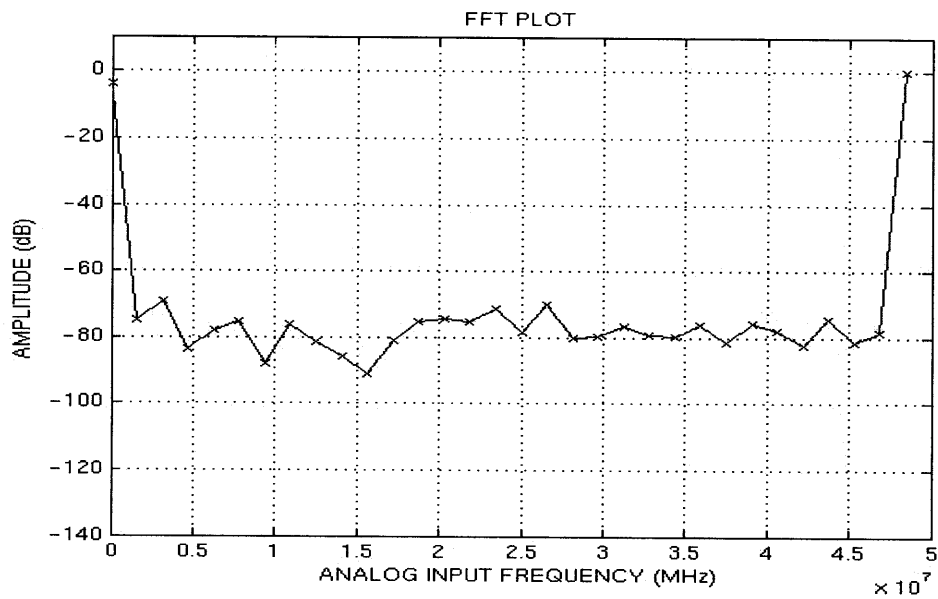
Figure 3-23: Simulated ADC performance when a near Nyquist-rate input is applied.

Integral nonlinearity (INL) is the deviation of the actual output from the ideal output. The proper method of measuring INL is by applying a low-frequency sinusoid to the ADC, gathering the outputs over a large number of clock cycles, and performing statistical analysis [33]. However the system simulation for such purpose takes a prohibitively long time. In addition, during the simulation, the exact value of the input signal is known which can be used to better estimate the INL. The INL of the system is estimated based on the transient simulation with 64 clock cycles and shown in Figure 3-24. This simulation provides a rough estimate of the INL based on very limited sampling points.

To evaluate filter functionality of the system, it is programmed as a 3rd order Butterworth filter. Separate transient simulations are performed at different input frequencies. The frequency response of the filter is shown in Figure 3-25.

62
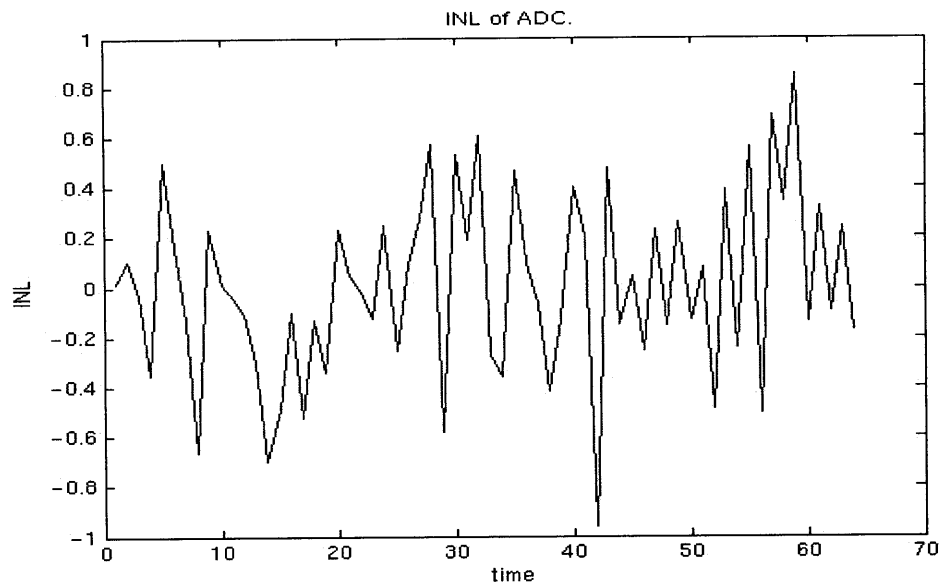
Figure 3-24: Estimated INL of ADC from simulation.
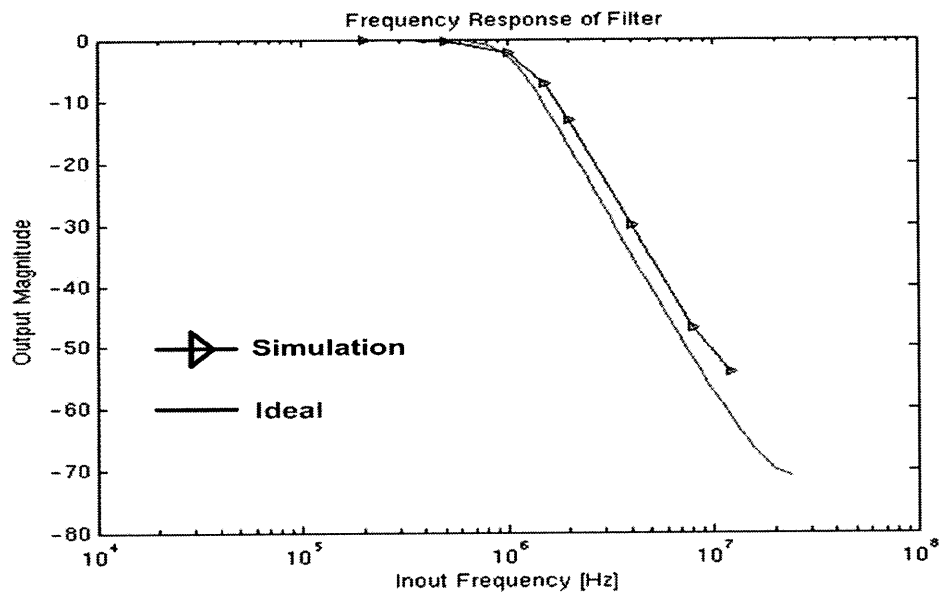
Figure 3-25: Third order Butterworth filter frequency response.

63

Chapter 4

Noise Analysis

During the design, the noise of the system should be estimated to ensure it is within the noise budget. The goal of this chapter is to estimate the noise when the chip is configured as an ADC and as a filter. In this chapter, the noise is reviewed briefly. Then the noise of a 10-bit ADC is estimated. After that, the noise of a third-order Butterworth filter is calculated. In each of the ADC and filter configurations, the main sources of noise are determined, and their contribution to the overall noise is calculated.

4.1   Noise Review

The noise of comparator-based switched-capacitor (CBSC) circuits has been analyzed in detail [21][22]. [22] shows that the main two sources of noise are the sampling noise (kT/C), and the noise of the preamplifier in a CBSC comparator. The noise of other circuit blocks such as current sources and switches has been also analyzed and shown to have significantly lower noise contribution. [22] also shows that the noise of the comparator-based system is non-stationary (meaning at least one of the mean and the standard deviation is time-dependant). The noise of different circuit blocks has been calculated twice, once when the circuit is in steady-state, and another time when the circuit it is not in steady-state. It has been shown that while the assumption of steady-state condition is more accurate. In out system, since the zero-crossing

detector is using a wide-band pre-amplifier, steady-state analysis is accurate.

Since the purpose of this chapter is a first-order estimate of noise in the system, the noise is assumed to be stationary. In addition, only the dominant sources of noise are taken into account.

4.1.1   Sampling Noise (kT/C Noise)

Figure 4-1 shows a basic sampling circuit where an NMOS transistor is used as a switch. When the transistor is on, the voltage across the capacitor tracks the input voltage. The resistance of the transistor creates thermal noise which can be expressed by Equation 4.1 [15].

$$S_{n,R}(f) = V_{n,R}^2(f) = 4kTR \qquad (4.1)$$

where k is Boltzmann constant (1.38×10^{-23} J/K), R is the ON resistance of the transistor when it is on, and T is temperature in degrees Kelvin. The thermal noise is a white noise and can be modeled as a voltage source of $V_{n,R}(f)$ in series with a noiseless resistor as shown in Figure 4-2. The total mean-square noise is the integral of $S_{n,R}(f)$ over all frequencies as shown in Equation 4.2. Note that the integral is infinite if the noise is not filtered. In practice, the noise is always filtered either by capacitive load at the output or by parasitic capacitances.
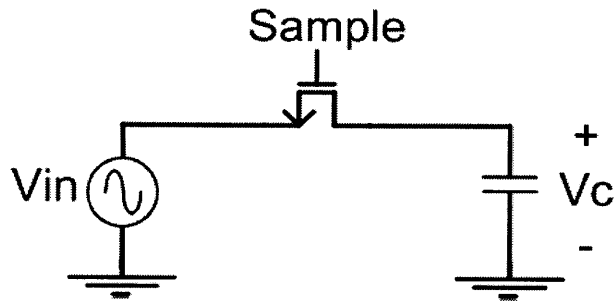
Figure 4-1: A basic sampling circuit.

$$\overline{V_o^2} = \int_0^\infty S_{n,R}(f)df \qquad (4.2)$$
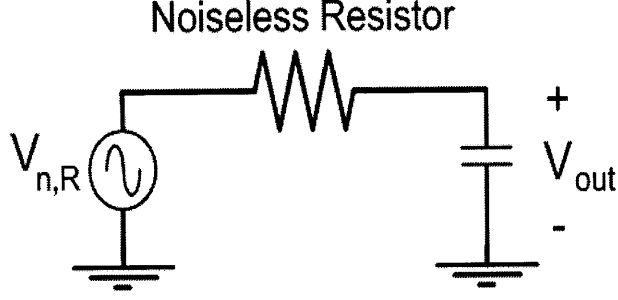
Figure 4-2: Circuit model of the noise of a sampling circuit.

The input signal is suppressed in Figure 4-2 to calculate only the noise contribution at the output. The noise of the resistor, $V_{n,R}$, is filtered by the low-pass RC circuit. The transfer function from $V_{n,R}$ to V_{out} is given by Equation 4.3.

$$\frac{V_{out}}{V_{n,R}}(s) = \frac{1}{RCs + 1} \tag{4.3}$$

The noise power spectral density is shaped by the transfer function. The output noise spectral density can be written as Equation 4.4 [26].

$$S_{out}(f) = S_{n,R}(f)|\frac{V_{out}}{V_{n,R}}(j2\pi f)|^2 = 4kTR\frac{1}{(2\pi fRC)^2 + 1} \tag{4.4}$$

The total mean-square noise is the integral of the output noise density over all frequencies as shown in Equation 4.5.

$$S_{n,out} = \int_0^\infty 4kTR\frac{1}{(2\pi fRC)^2 + 1}df = \frac{kT}{C} \tag{4.5}$$

While the noise is generated by the resistor, the overall noise is only a function of the sampling capacitance. This is due to the fact that the noise spectral density is proportional to the resistance value, but the cut-off frequency of the filter is inversely proportional to the resistance value. It is important to note that while the total mean-square noise only depends on the capacitance, the power spectral density (PSD) still depends on the resistance of the switch. This is important if thermal noise is further filtered by a subsequent circuit. In such cases, the total mean-square noise depends

67

on the power spectral density of the noise and the bandwidth of the whole circuit.

When the switch is still closed in Figure 4-1, kT/C noise appears across the capacitor. When the switch is opened, the noise is sampled across the capacitor. The sampling noise (kT/C) can be reduced either by lowering the temperature (which is not typically a design option) or increasing the size of the sampling capacitor.

4.1.2 Effective Number of Bits (ENOB) and Figure of Merit (FOM)

When an analog signal is quantized, a quantization error is introduced which is the difference between the analog input signal and the digital output signal. For an ideal ADC, the mean square quantization error is given by Equation 4.6 [34].

$$\overline{V_q^2} = \frac{(A/2^N)^2}{12} \tag{4.6}$$

where A is the full-scale range of the ADC and N is the number of quantization bits. The quantization error is one of the factors that limits the signal-to-noise ratio (SNR) of an ADC. It is shown that for an ADC with large number of bits (for example 10 bits or higher), quantization error can be treated as white noise if sampling is non-coherent [35]. If a sinusoidal signal with an amplitude of A/2 is applied to an ideal ADC with N-bit quantization, the signal-to-noise ratio is shown by Equation 4.7 [34].

$$SNR = N * 6.02dB + 1.76dB \tag{4.7}$$

Signal to noise and distortion ratio (SNDR) is the ratio of the signal power to the total power of quantization error, noise, and harmonics. The effective number of bits (ENOB) of an ADC is defined by Equation 4.8.

$$ENOB = \frac{SNDR - 1.76dB}{6.02dB/bit} \tag{4.8}$$

To compare different ADCs with different bit-resolution, different sampling frequency, and different power consumption, a figure of merit (FOM) is defined. The

FOM normalizes the power consumption with respect to the bandwidth of the input signal and ENOB as shown in Equation 4.9 [36][37].

$$FOM = \frac{PowerConsumption}{2 f_{InputBandwidth} * 2^{ENOB}} \tag{4.9}$$

4.1.3 Noise Gain

Figure 4-3 shows a simple block diagram of a system with transfer function of H(s) where $V_{in}(s)$ is the input and $V_{out}(s)$ is the output of the block. The input-output relation is given by Equation 4.10.

$$\frac{V_{out}(s)}{V_{in}(s)} = H(s) \tag{4.10}$$
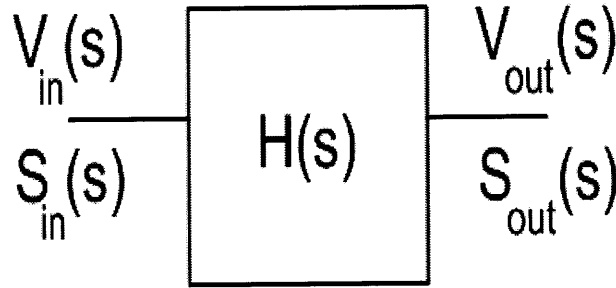
Figure 4-3: General block diagram of a system with transfer function of H(s).

Similarly, if $S_{in}(s) = |V_{n,in}(s)|^2$ is the noise power spectral density (PSD) at the input and $S_{out}(s) = |V_{n,out}(s)|^2$ is the noise PSD at the output, the relation of the input and output noise is given by Equation 4.11.

$$\frac{S_{out}(s)}{S_{in}(s)} = \frac{|V_{n,out}(s)|^2}{|V_{n,in}(s)|^2} = |H(s)|^2 \tag{4.11}$$

If the transfer function from an internal node to the output is known, this equation can be used to calculate the noise at the output due to the noise at the internal node. Signal gain is the value of the transfer function for the in-band signal. If Equation 4.11 is used to refer the output noise to the input of the system, the signal gain should be used so that the signal-to-noise ratio can be correctly calculated at the input.

4.1.4 Noise Bandwidth (NBW)

If a system has low-pass characteristics, noise bandwidth can be defined as follows:

$$NBW = \frac{1}{|H(0)|^2} \int_0^\infty |H(f)|^2 df \qquad (4.12)$$

where H(f)=H(s) for s=j2πf.

The noise bandwidth can be used to calculate the output noise of a low-pass circuit when a white noise is applied (by multiplying $S_{in}(0)$ with the noise bandwidth). For a first-order low-pass filter, noise bandwidth is given by Equation 4.13 [15],[26].

$$NBW = \frac{\pi}{2} f_{3dB} \qquad (4.13)$$

Equation 4.12 can be evaluated numerically with Mathematica (as shown in Appendix B). Table 4.1 summarizes the NBW for low-pass filters of different orders if all poles are located at the same frequency. The noise bandwidth in Table 4.1 can be used to estimate the noise of the chip when it is configured as a filter.

Table 4.1: Noise bandwidth of low-pass filters when all poles are located at the same frequency.

Order of the filter	Noise Bandwidth
First order	$1.57 f_{pole}$
Second order	$0.78 f_{pole}$
Third order	$0.58 f_{pole}$
Fourth order	$0.49 f_{pole}$
Fifth order	$0.43 f_{pole}$

4.1.5 Noise of an amplifier

Thermal noise of a MOSFET can either be modeled with current noise at the output as shown in Figure 4-4a or with a voltage noise at the gate as shown in Figure 4-4b [26]. For a long-channel transistor in saturation, the noise spectral density is:

$$\overline{I_n^2} = 4kT\gamma g_m = \frac{8}{3} kT g_m \qquad (4.14)$$

70

$$\overline{V_n^2} = \frac{4kT\gamma}{g_m} = \frac{8}{3}\frac{kT}{g_m} \qquad (4.15)$$

where γ is 2/3 for long-channel transistors. Equation 4.14 suggests that an increase in g_m increases the current noise at the output and Equation 4.15 suggests that an increase in g_m decreases the voltage noise at the input. In many cases, since the amplitude of the input signal is fixed, the signal-to-noise ratio is calculated by referring the noise to the input. In these cases, an increase in g_m improves signal-to-noise ratio.
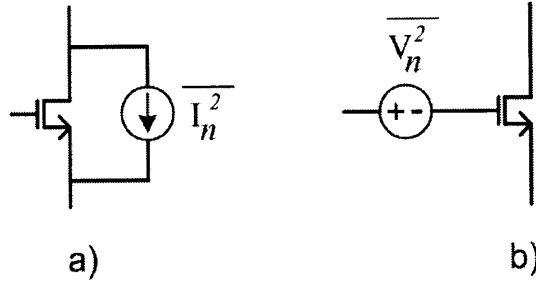
Figure 4-4: Thermal Noise of a MOSFET.

A basic differential amplifier is shown in Figure 4-5, which includes the transistor noise. Transistors M3, M4, and M5 are biased with constant voltages and are used as current sources. Since the output is fully differential, the noise of transistor M5 appears similarly at both V_{outp} and V_{outn}, and cancels out if the output is differential. The input referred noise density of the amplifier is given by Equation 4.16, assuming perfect matching between transistor M1 and M2, and between transistor M3 and M4.

$$\overline{V_n^2}(f) = 4kT\gamma\left(\frac{2}{g_{m1}} + \frac{2g_{m3}}{g_{m1}^2}\right) \qquad (4.16)$$

This is white noise and if the bandwidth is not limited, the mean-square noise is infinite. In practice, the capacitive load at the output limits the bandwidth.

4.1.6 Noise Aliasing

The block diagram of a sampling system is shown in Figure 4-6, where x(t) is the input signal which is sampled by p(t), a train of impulses. The time-domain and
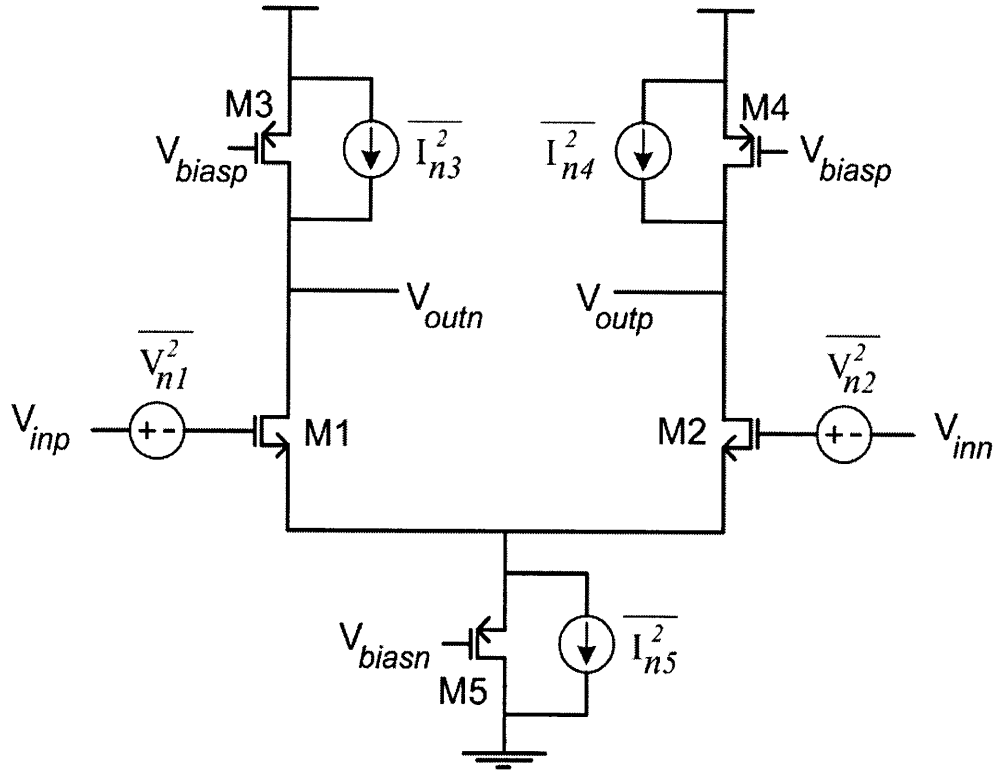
Figure 4-5: Basic differential amplifier and its sources of noise.

frequency domain representation of p(t) are shown in Figure 4-7 and Figure 4-8 [38].
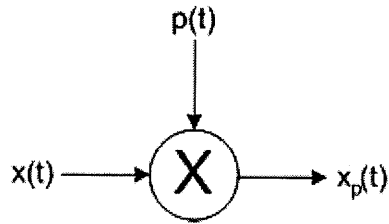
Figure 4-6: The block diagram of signal sampling.

If the input signal bandwidth is larger than half the sampling frequency, the high-frequency components of the signal are aliased to the lower frequencies [39] [40] as shown in Figure 4-9. In particular, since many sources of noise have a wide bandwidth, their high-frequency noise may alias into lower frequencies due to sampling. This is referred to as noise aliasing or noise folding. The total mean-square noise does not change due to sampling, however the power spectral density (PSD) changes. If white

72
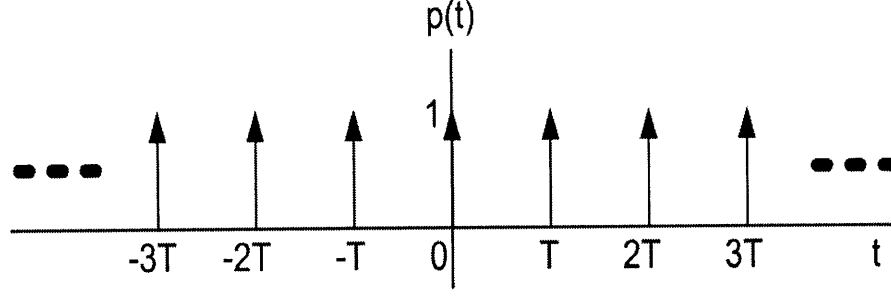
Figure 4-7: Time domain representation of the sampling signal.
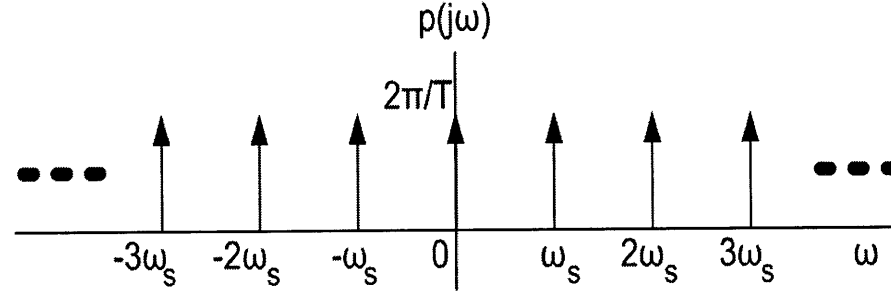
Figure 4-8: Frequency domain representation of the sampling signal.

noise is not filtered, it has infinite power. In continuous-time circuits, white noise may be filtered by subsequent circuits. However, if white noise is sampled before being filtered, its PSD is infinite. As a result, any filtering in the subsequent stages does not lower the noise which is aliased into the signal band.

4.2   Noise of the ADC

This section estimates the noise of the ADC for the designed chip. The dominant sources of noise in an ADC are the sampling noise and the noise of the zero-crossing detector. The input signal of the chip is differential and each differential input has a peak-to-peak value of 0.5V. As a result, the mean-square input signal is given by Equation 4.17.

$$\overline{V_{sin}^2} = \frac{A^2}{8} = \frac{1}{8}V^2 \qquad (4.17)$$

73
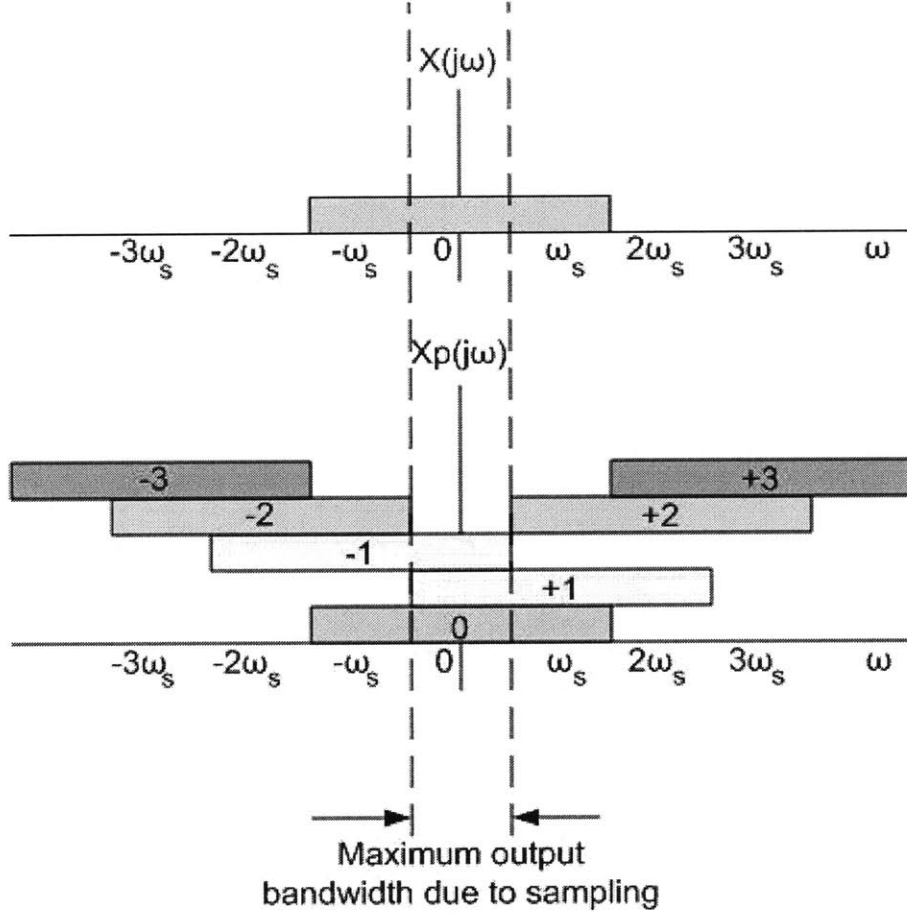
Figure 4-9: Frequency domain presentation of the sampling signal.

where A is the peak-to-peak amplitude of the sinusoidal input. The mean-square quantization error is calculated in Equation 4.18 for a 10-bit ADC.

$$\overline{V_q^2} = \frac{(A/2^N)^2}{12} = 79nV^2 \qquad (4.18)$$

The size of sampling capacitors is 180fF on each differential input. Since the sampling capacitors of the differential inputs are in series, the total sampling capacitance is 90fF. Equation 4.19 shows the total sampling noise.

$$S_{sampling} = \frac{kT}{C} = 46nV^2 \qquad (4.19)$$

Since the pre-amplifier in the implemented zero-crossing detector has a gain of 10, the noise of the threshold detector is attenuated by a factor of 10^2 (according

to Equation 4.11) and can be ignored compared to the noise of pre-amplifier. The input-referred noise of the pre-amplifier can be calculated similar to Equation 4.16 or obtained from simulation. The noise as found through simulation is:

$$S_{pre-amplifier} = 120nV^2 \qquad (4.20)$$

The noise gain from the input of the pre-amplifier to the output is 3 and the gain of the input signal to the output is 4 (Appendix D). As a result, the noise of the pre-amplifier is multiplied by $(\frac{3}{4})^2$ if it is referred to the input. The input-referred noise of one stage consists of the noise of all components when referred to the input. Since the sources of noise are uncorrelated, the total mean-square noise is the sum of individual mean-square noise referred to the input [15] as shown by Equation 4.21.

$$S_{one-stage} = 46nV^2 + 120nV^2 * (\frac{3}{4})^2 = 114nV^2 \qquad (4.21)$$

The total noise of the ADC can be calculated by referring the noise contribution of all stages to the input of the ADC and adding them up. Since the noise of different blocks are uncorrelated, their mean-square values are added. Since the gain of each stage is 4, the mean-square noise is scaled by a factor of $\frac{1}{4^2}$ when it is referred from the output of each stage to its input. The total noise of an ADC is calculated in Equation 4.22.

$$S_{ADC} = (1 + \frac{1}{4^2} + (\frac{1}{4^2})^2 + (\frac{1}{4^2})^3 + (\frac{1}{4^2})^4) * 114nV^2 = 1.33 * 114nV^2 = 152nV^2 \quad (4.22)$$

The mean-square noise can be added to the quantization error to calculate the ENOB of the ADC only due to its thermal noise and quantization error (ignoring harmonic distortion).

$$S_{ADC} = 79nV^2 + 1.33 * 114nV^2 = 227nV^2 \qquad (4.23)$$

According to Equation 4.8, this corresponds to an ENOB of 9.24bits (with the

harmonic distortion being ignored). This can be compared with the measurement results when the input is grounded. With grounded inputs, no harmonic distortion is present and the measured mean-square noise is only due to noise and quantization error. In Chapter 6, it is shown that the noise of the system with grounded inputs corresponds to an ENOB of 9.26bits.

Note that in an ADC configuration, the sampling noise and the noise of the pre-amplifier are aliased back to lower frequencies due to sampling. Noise aliasing does not change the total noise, but changes the power spectral density of the noise. Since the subsequent stages do not filter the noise, only the total mean-square noise is important. As a result, noise aliasing can be ignored when calculating the total noise.

4.3 Filter Noise

In this section, the noise of a filter is estimated. First, the noise model of an integrator is provided. Then, the sampling noise and the noise of the amplifier are aliased into the low frequencies due to sampling. The filter transfer function is used to filter different noise components. The total noise is calculated by adding the contribution of different components.

4.3.1 Noise of an Integrator

Figure 4-10 shows the schematic of a switched-capacitor integrator. Although an opamp model is used for simplicity, all the following equations apply to ZCBCs as well. The noise of an opamp (or zero-crossing detector) is represented by V_n. The dominant component of V_n is the noise of the differential pair at the first stage of an opamp (or the first stage of zero-crossing detector). This noise is estimated by Equation 4.20 for the implemented zero-crossing detector. The relation of input and output voltages is shown in Equation 4.24.

$$V_{out}[n+1] = V_{out}[n] + \frac{C_1}{C_2} V_{in}[n] \tag{4.24}$$

V_n can be added to the equation as following:

$$V_{out}[n+1] = \frac{Q_{out}[n+1]}{C_2} + V_n \tag{4.25}$$

where $Q_{out}[n+1]$ is given by:

$$Q_{out}[n+1] = Q_{out}[n] + C_1(V_{in}[n] + V_n) \tag{4.26}$$

Q_{out} is the charge on capacitor C_2. V_n appears both in Equation 4.25 and Equation 4.26. In Equation 4.25, V_n is added to the output voltage, but it is not integrated on the feedback capacitor. However, in Equation 4.26, V_n is also integrated across the capacitor.
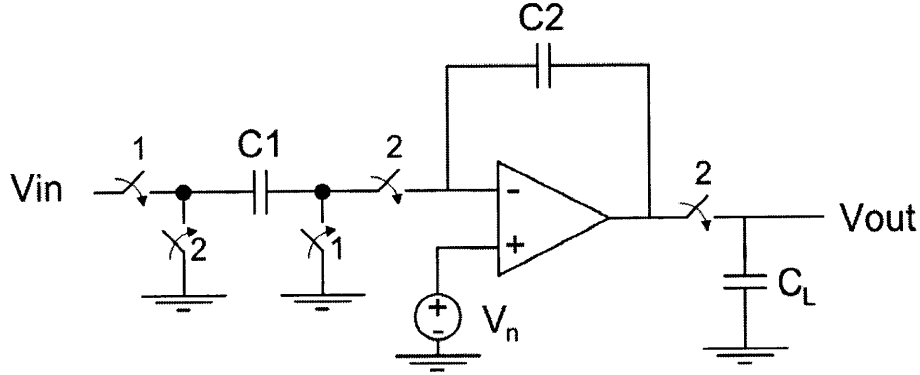
Figure 4-10: Schematic of a switched-capacitor integrator.

The noise directly adds both to the input voltage and to the output voltage. In other words, the noise can be modeled with two components, one which is at the input and one at the output as shown in Figure 4-11. Note that the two noise components are correlated. Therefore, their noise voltage should be added (as opposed to adding the mean-square noise). However, they experience different transfer functions to the output. It is shown that only one of them is dominant for each stage. As a result, adding the mean-square noise instead of noise voltages causes only a small

error. In the rest of the analysis, the two sources of noise are treated as uncorrelated acknowledging that the total noise is underestimated. The sampling noise can also be added to the input noise. As a results, $V_{n,in}$ and $V_{n,out}$ are shown by Equation 4.27 and Equation 4.28.

$$\overline{V_{n,in}^2} = kT/C + S_{pre-amplifier} = (46 + 120)nV^2 = 166nV^2 \qquad (4.27)$$

$$\overline{V_{n,out}^2} = S_{pre-amplifier} = 120nV^2 \qquad (4.28)$$
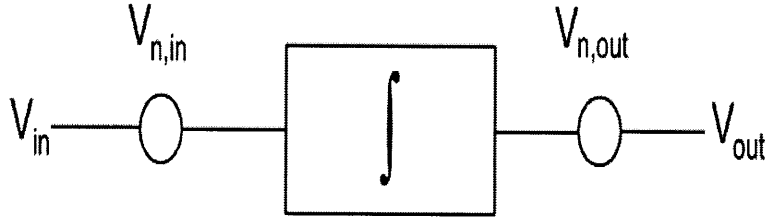
Figure 4-11: Noise model of the integrator.

The 3dB frequency of the sampling circuit is at 60 MHz. With a sampling rate of 50 MSPS, high-frequency noise is aliased to the low frequencies. It can be assumed that the total noise is uniform over the sampling bandwidth (0-25 MHz). Similarly, the noise of the opamp (or zero-crossing detector) can be assumed to be uniform over the sampling bandwidth (0-25 MHz).

4.3.2 Noise Transfer Function

The block diagram of a third-order low-pass ladder filter is shown in Figure 4-12. As shown earlier, the noise of an integrator can be modeled with two sources of noise, one at the input and one at the output. Figure 4-13 shows the block diagram of the same filter when the sources of noise are added to each block.

The values of $C_1 = 159nF$, $L_2 = 318nH$, and $C_3 = 159nF$ are chosen that correspond to a third-order Butterworth filter with a cut-off frequency of 1 MHz. For each source of noise, the noise transfer function can be calculated (as shown in
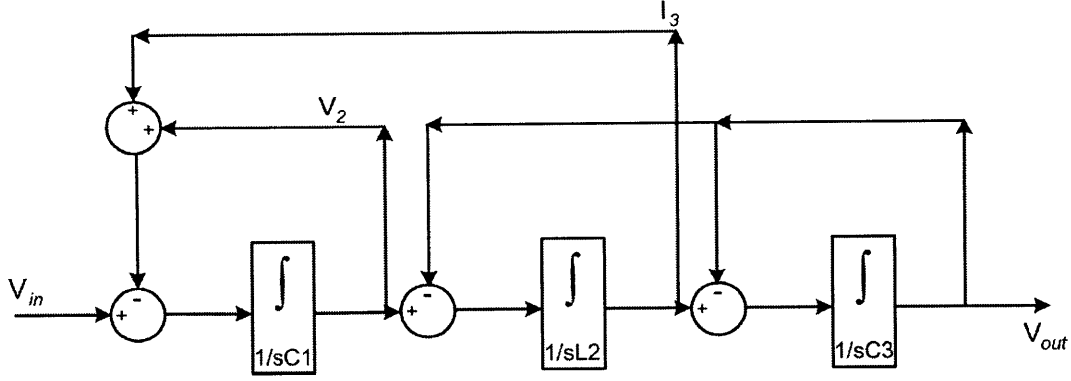
Figure 4-12: Block diagram of a third order low-pass filter.
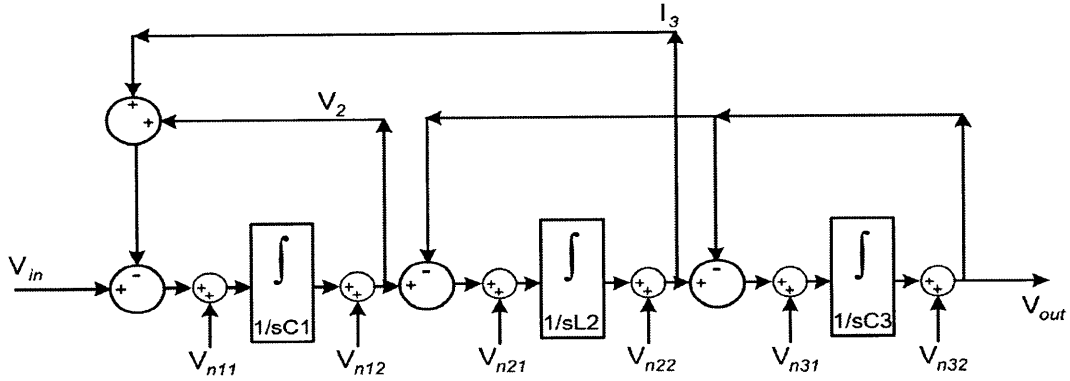
Figure 4-13: Block diagram of a third order low-pass filter with sources of noise.

Appendix C). For example, the transfer function from $Vn11$ to the output is:

$$H_{Vn11}(s) = \frac{V_{out}}{V_{n11}} = \frac{1}{(C1 + C3 + L2) * S + (C1 * L2 + C3 * L2) * S^2 + C1 * C3 * L2 * S^3 + 2} \tag{4.29}$$

Figure 4-14 shows the transfer function between the input-noise of the integrators (V_{n11}, V_{n21}, and V_{n31}) and the output. It is important to note that the three transfer functions are low-pass filters at 1 MHz. In addition, both the input signal and the noise are attenuated by a factor of two in low frequencies. This can be explained easily based on the passive implementation of the ladder filter where the terminating resistors at the input and the output determine the low-frequency gain. The mean-square noise of $\overline{V_{n31}^2}$ is $166 nV^2$. After sampling at 50 MSPS, the noise is aliased into the sampling bandwidth (0-25 MHz). The power-spectral-density of V_{n31} in the

79

sampling bandwidth is:

$$S_{n31}(f) = \frac{166nV^2}{25MHz} \qquad (4.30)$$

Since the noise is filtered at 1 MHz with a first order filter and attenuated by a factor of two, the output referred noise of V_{n31} is:

$$S_{n31,output} = \frac{166nV^2}{25MHz} * 1.57MHz * \frac{1}{2^2} \qquad (4.31)$$

and the input referred noise of V_{n31} is:

$$S_{n31,output} = \frac{166nV^2}{25MHz} * 1.57MHz \qquad (4.32)$$

The input-referred noise contribution of V_{n11}, V_{n21}, and V_{n31} can be estimated as:

$$S_{n1,input} = \frac{166nV^2}{25MHz} * (1.57MHz + 0.78MHz + 0.58MHz) = 19.5nV^2 \qquad (4.33)$$

The noise could be overestimated by assuming that all sources of noise are filtered by a first-order low-pass filter. For a more accurate estimation, the results of Table 4.1 are used. However, the total noise contribution of these sources is not significant.

Figure 4-15 shows the transfer functions between the output-noise of the integrators (V_{n12}, V_{n22}, and V_{n32}) and the output of the filter. V_{n12} and V_{n22} are band-pass filtered at 1 MHz. The output-noise of the integrator in the last stage, V_{n32}, is high-pass filtered. The noise contribution of V_{n21} and V_{n22} is negligible since they are band-pass filtered and their noise is even less than V_{n11}, V_{n12}, and V_{n31}. The noise of V_{n32} is not filtered from 1 MHz to 25 MHz (which is 96% of the frequency range after aliasing) and is partially filtered from 0-1 MHz. Since the output mean-square noise contains more than 96% of the noise, it is approximated that the noise is not filtered at all.

$$S_{n32-output} = 120nV^2 \qquad (4.34)$$

The main noise contributor in the ladder low-pass filter is the zero-crossing detector noise in the last stage. The noise can be referred to the input of the filter as shown in Equation 4.35.

$$S_{n32-input} = 120nV^2 * 2^2 = 480nV^2 \qquad (4.35)$$
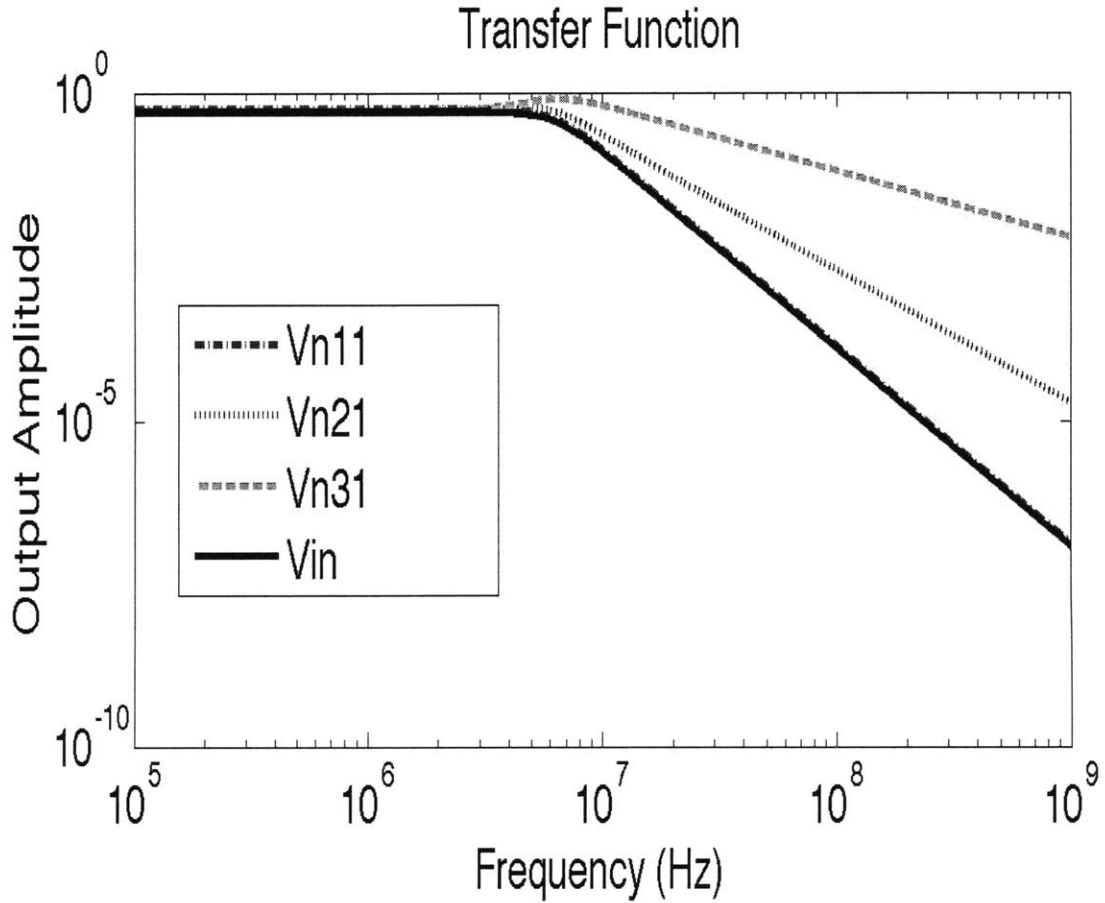
Figure 4-14: Noise transfer function of integrators input noise in a third order Butterworth filter.
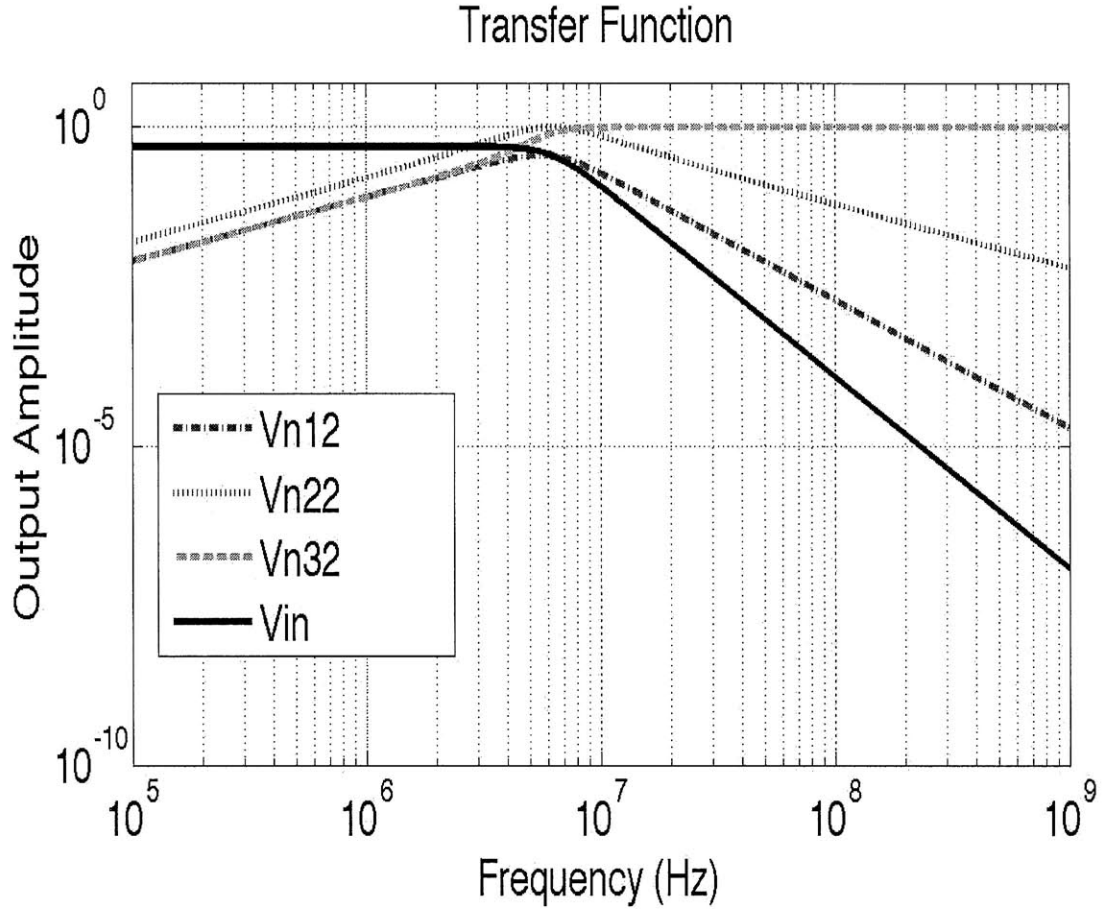
Figure 4-15: Noise transfer function of integrator output noise in a third order Butterworth filter.

4.4 Coupling Noise

A signal coupling to other signals, reference voltages, and supply voltages is referred to as coupling noise because of its similarities to noise when it is viewed in the time domain. However, it is correlated with the activity of the blocks that generate it. It is also not feasible to predict the exact shape of the signal, which is another reason to treat it as a random noise. In this section, the coupling noise on some important voltages are reviewed.

4.4.1 Noise on Reference Voltages

Ripples on the reference voltage(s) can reduce the signal to noise ratio. In an ADC, the reference voltage is connected to the capacitor that holds the input signal. Any noise or ripple on the reference voltage in the first stage of a pipeline ADC is directly added to the noise or ripple on the sampled signal. Therefore, even if the ADC is designed with reasonably low noise and distortion, a poor reference voltage lowers its SNDR significantly. In a pipeline ADC, only the first block is very sensitive to the noise on the reference voltage, but in a filter, the noise couples directly to the input signal in all stages. Depending on where the noise is injected, it is filtered with the corresponding transfer function to the output. Therefore, low-frequency and high-frequency ripples have different effects on the filter performance.

While reference voltages provide a constant voltage, their current flowing through them contains high-frequency components. The high-frequency components is due to the activity of all stages. In this chip, the reference voltage is provided externally. When high-frequency current passes through the bond-wire inductance, a voltage drop appears across the bond-wire. An on-chip decoupling capacitor is used to reduce the voltage ripples.

Figure 4-16 shows the simulated noise on reference voltages if the bond wire has a resistance of 20Ω, inductance of 2nH, and is decoupled on-chip with a 4nF capacitor. The reference voltage is provided differentially. The top signal in Figure 4-16 is the differential signal and the next two signals are the negative and the positive sides of the differential signal. The differential signal has a transient response at the beginning where it drops from 1V to 991mV. This portion of the response can be ignored since it happens during the power up. Each side of the differential signal has peaks on the order of 70mV, which is large compared to 1LSB of the ADC (1LSB is on the order of 1mV). However, the differential reference voltage has a peak-to-peak ripple of 253uV.

The noise on the power supply also couples to the output and may decrease the signal-to-noise ratio of the system. Simulation shows that the zero-crossing detector has 40dB supply noise rejection. The supply noise is analyzed in detail in [24]. The
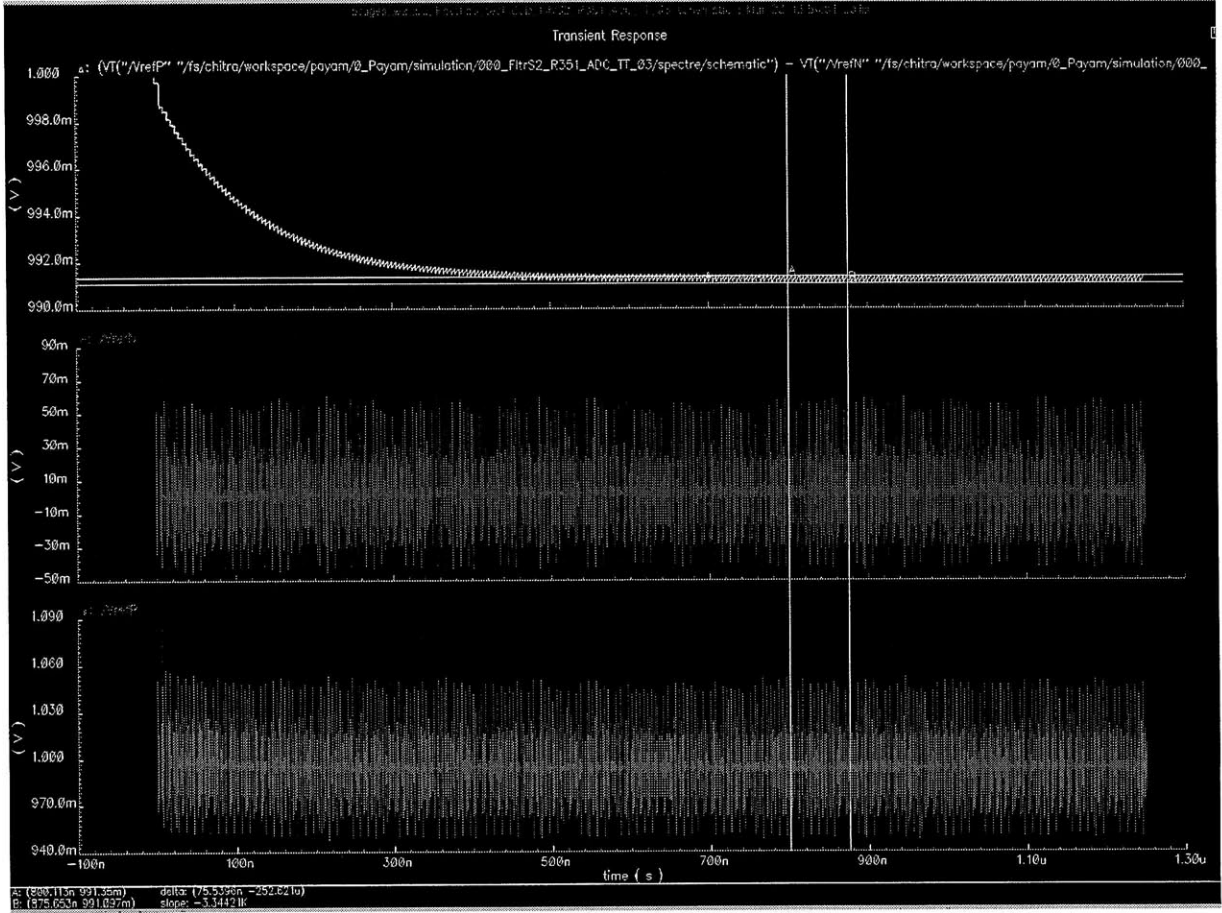
Figure 4-16: Noise of reference voltage based on simulation.

supply noise is attenuated by an on-chip decoupling capacitor. A more appropriate method is to use an on-chip voltage regulator (as opposed to an off-chip regulator).

Common-mode voltage may also experience high-frequency current that creates high-frequency ripples on it as shown in Figure 4-17. The ripple on the common mode voltage tends to be much smaller because in differential circuits, since the positive and negative sides of the circuit (I_p and I_n) inject opposite currents to the common-mode voltage that cancel out if the circuit is perfectly matched. In addition, the common-mode rejection of the zero-crossing detector also attenuates the effects of common-mode ripples at the output.

84
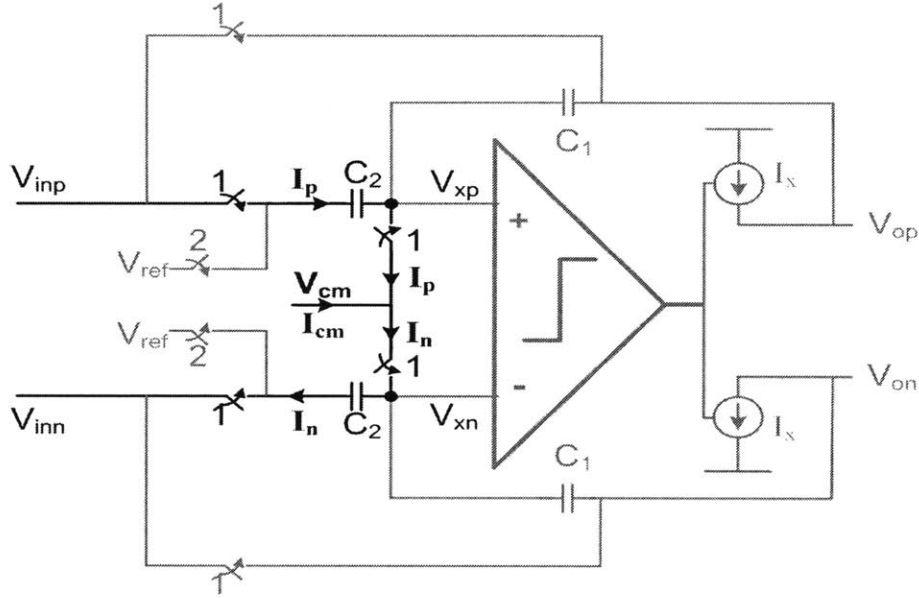
Figure 4-17: The currents that passes through Vcm in a fully differential circuit.

4.5 Conclusion

In this chapter, the noise of an ADC and a filter were estimated. In an ADC configuration, the noise is mainly due to the first stage. The noise contribution of the sampling circuit and the zero-crossing detector is estimated. The total noise is dominated by the noise of the zero-crossing detector. In a filter configuration, the noise is a function of the filter order and is shaped by the filter. The sampling noise of each stage is filtered by the filter transfer function and its effect is very small on the total noise of the system. It was shown that the noise of the zero-crossing detector in the last stage is the dominant source of the noise since it is not filtered and directly adds to the output. In an ADC configuration, the gain of the first stage attenuate the noise of the next stages when it is referred to the input. In a filter configuration, the in-band signal is not amplified when it goes to the next stage. As a result, each stage contributes similarly to the total noise (except that its noise is being filtered).

Chapter 5

Sensitivity of the System

In this chapter, the sensitivity of the system is analyzed to the mismatch of capacitors, and the offset of zero-crossing detector when configured as an ADC or as a filter.

5.1 Sensitivy to Capacitance Values

Manufacturing tolerances causes mismatch in capacitor ratios. This section reviews how the mismatch affects the ADC and filter functionality.

5.1.1 ADC Configuration

In an ADC configuration, the residue is amplified before being sent to the next stage. The gain of the amplifier is given by $1 + \frac{C1}{C2}$. The mismatch between the feedback capacitor and the sampling capacitor changes the gain of the amplifier from the desired value. Figure 5-1 shows the residue plot of one stage of a pipelined ADC with no gain error. A gain error changes the residue to that of Figure 5-2. Figure 5-3 and Figure 5-4 show the ADC transfer function when the gain of the first stage is larger or smaller than the ideal gain (respectively). As shown, a larger gain causes a wide code and a smaller gain causes missing codes.

Capacitor mismatch also affects the BDCs since its sampling capacitors may have mismatch. The threshold voltage is adjusted with the assumption that the sampling

87

capacitors have the same value. Capacitor mismatch changes the effective threshold voltage of BDCs. For small changes in threshold voltage of BDCs, the over-range protection avoids the subsequent stage to be saturated. However, a large deviation in threshold voltage of BDCs saturates the subsequent stages.
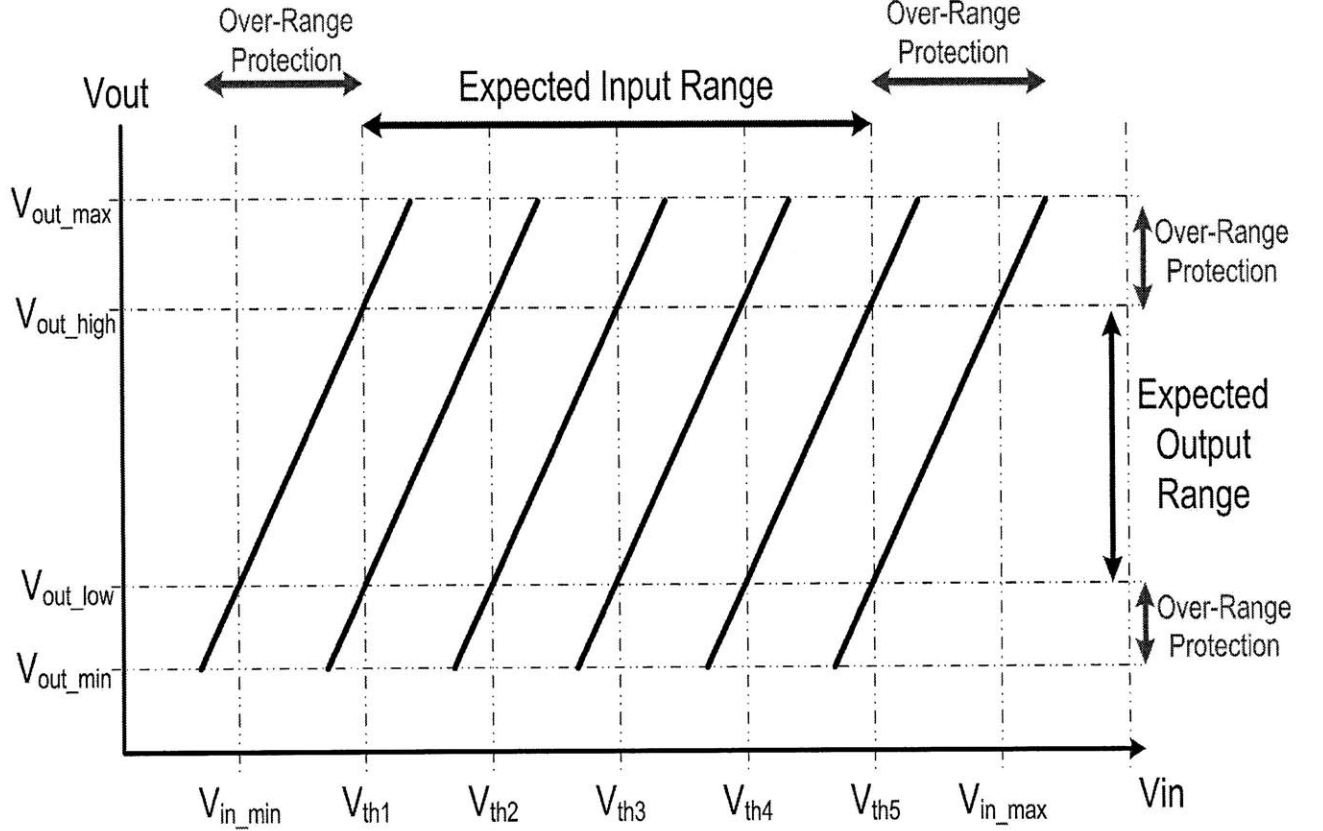
Figure 5-1: Residue plot of a stage with no gain error.

5.1.2 Filter Configuration

In a filter configuration, the mismatch between the feedback capacitor and the sampling capacitor changes the integration coefficient. Since the integration capacitors are large, the capacitor mismatch is smaller in the filter configuration. However, since the feedback capacitors are reconfigurable, the desired capacitor may not be available. In such cases, the closest capacitor value is used and the integration capacitor experiences up to 10% error. Figure 5-5 shows the filter characteristics for an ideal
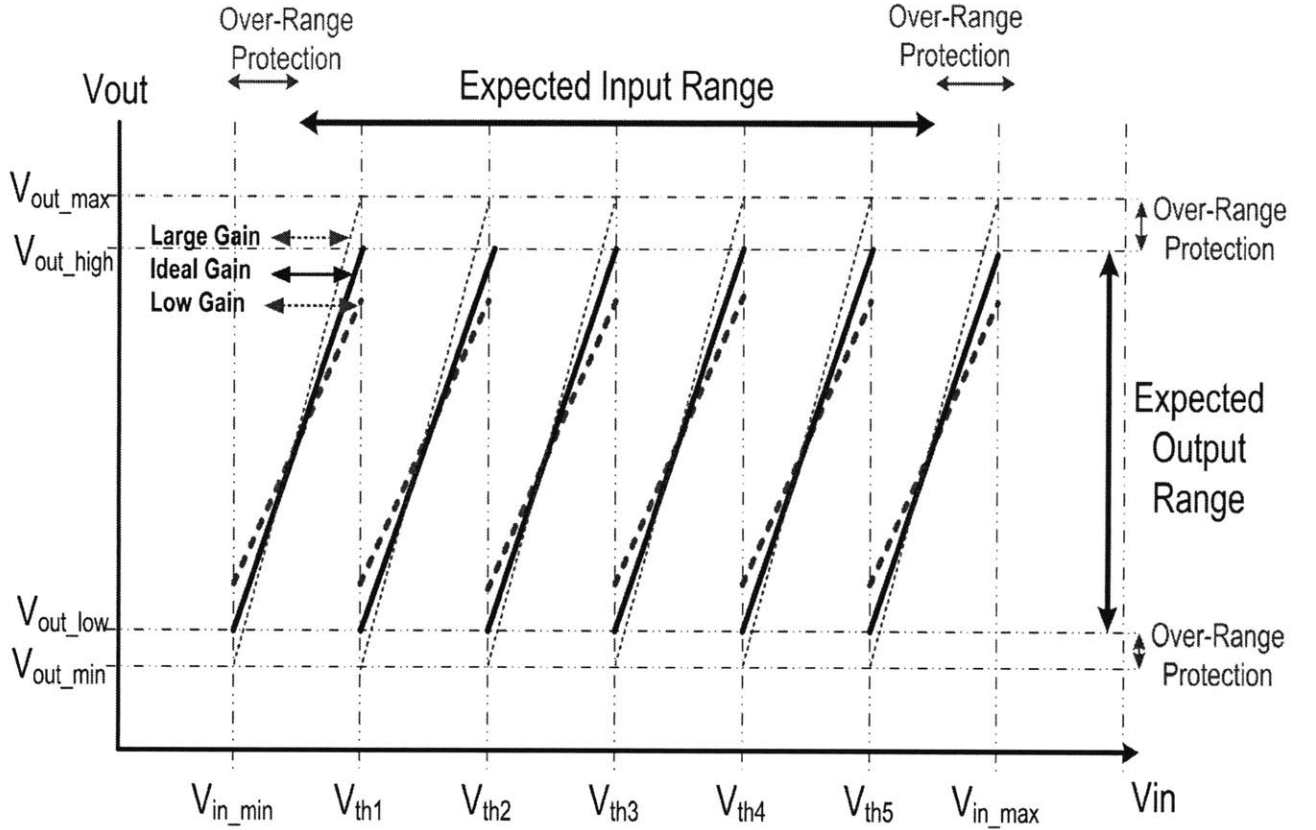
Figure 5-2: Residue plot of a stage with gain error.

third-order Butterworth filter with cutoff frequency of 1MHz. It also shows the characteristic of the same filter if the integration coefficient of only one stage experiences 20% mismatch (20% mismatch is used so that the effect of the mismatch is better observed). In Figure 5-5, Cap1, Cap2, and Cap3 are the integration capacitor of the first stage, the second stage, and the third stage respectively. It is shown that the integrator gain error changes the cutoff frequency and the overall shape of the filter. However, the filter characteristic does not deviate significantly from the ideal one.

In the first stage and the last stage of a filter, the capacitance mismatch may also affect the value of the terminating resistors. Figure 5-5 shows the effects of the mismatch of the capacitors used as a terminating resistors on the overall filter characteristic (20% mismatch is used only to signify the effects of the mismatch). In this design, since the terminating resistors do not have a reconfigurable value, the mismatch is only limited to the mismatch of the capacitors.
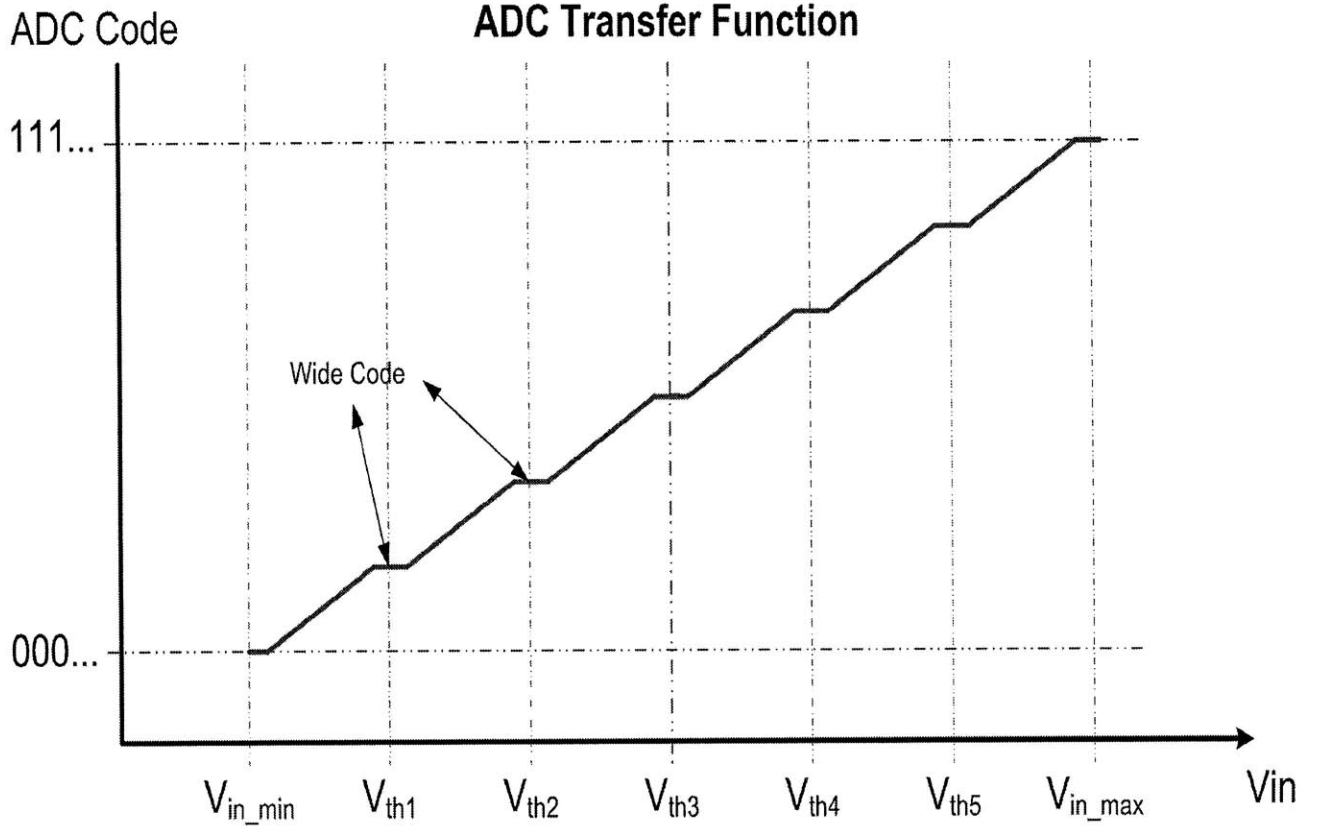
Figure 5-3: ADC transfer function when the gain of each stage is larger than the ideal gain.

5.2 Offset of the Zero-Crossing Detector

In new technology nodes, V_{th} variation increases as the supply voltage decreases. Random dopant fluctuation (RDF) increases V_{th} variation in new technology nodes [42]. The offset of zero-crossing detector is mainly due to variation in transistor threshold voltage (V_{th}), transistor width, and transistor length. In this section, the effect of the offset of zero-crossing detector on the system functionality is reviewed both in an ADC configuration and in a filter configuration.

5.3 Offset in an ADC Configuration

Simulation shows that the offset of the zero-crossing detector is in the range of 1mV to 15mV. As a result, it does not cause the output voltage to saturate (since the
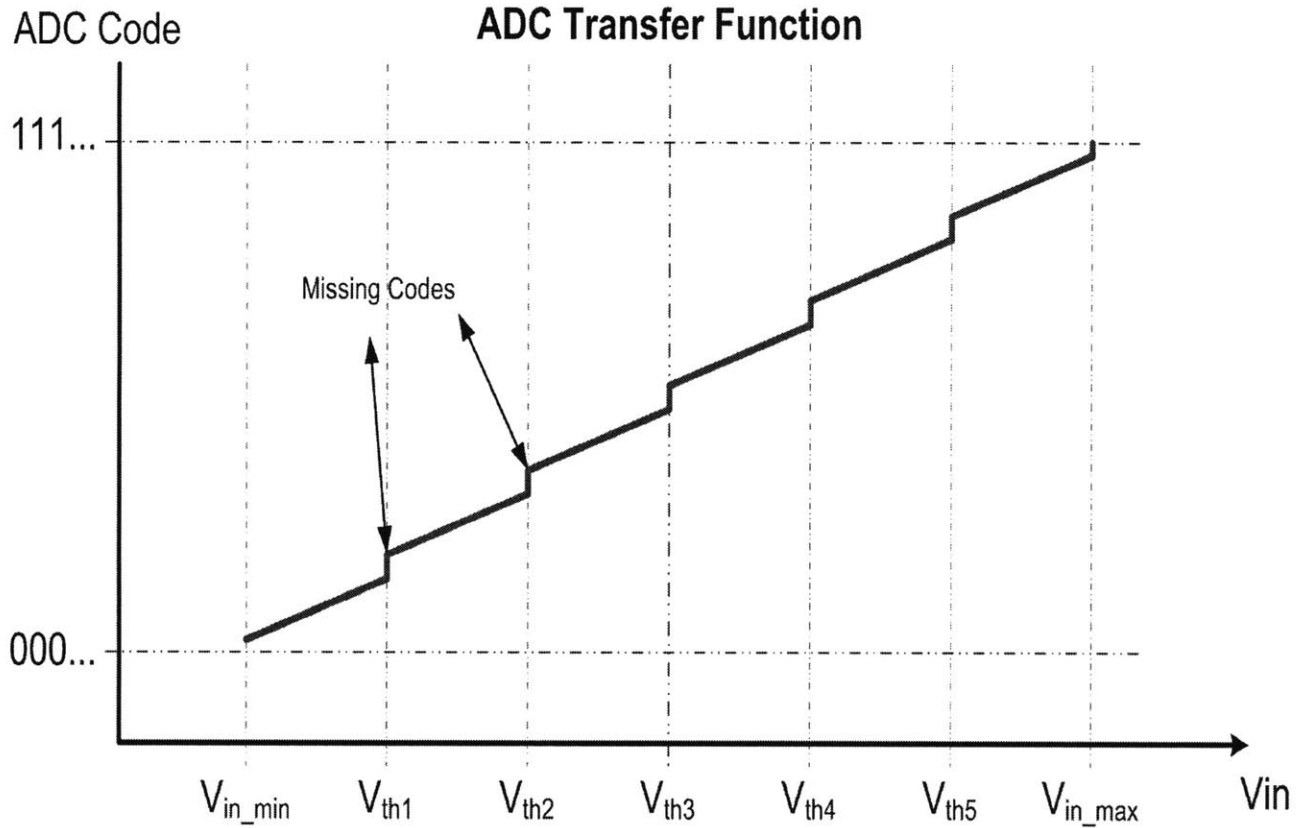
Figure 5-4: ADC transfer function when the gain of each stage is smaller than the ideal gain.

over-range protection allows the output to have the corresponding offset). The offset of each stage appears as the offset of the ADC. For most applications, this is not an important factor.

If the offset of the zero-crossing detector is larger than 15mV, it saturates the output. The output saturation increases the non-linearity of the system. In this system, the offset of zero-crossing detector can be adjusted by programming the active load of the preamplifier to reduce offset.

5.4 Offset in a filter Configuration

In a filter configuration, all stages are configured as integrators. At a first glance, an offset at the input of an integrator may seem troublesome since a small DC input may
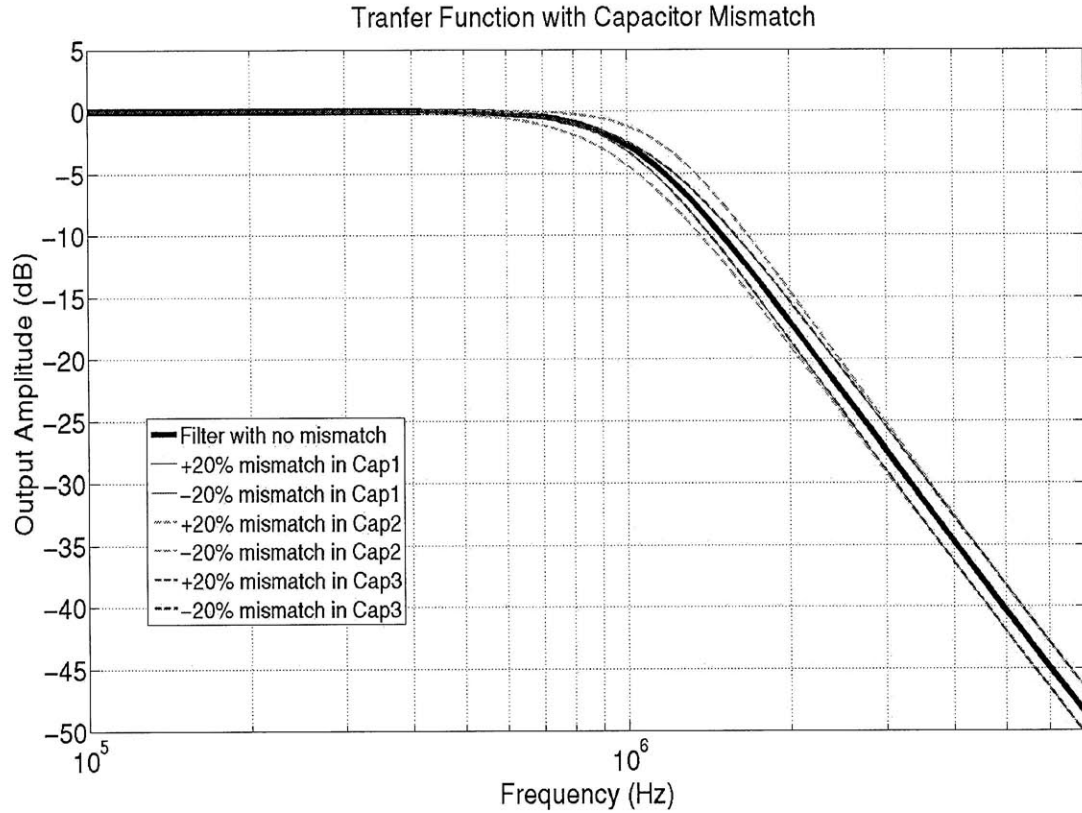
Figure 5-5: Transfer function of a third order butterworth filter with 20% mismatch on only one integrating capacitor.

saturate any integrator. However, there are local feedbacks that change the effects of the integrator for an offset. Figure 5-7 and Figure 5-8 show the passive and active implementation of a low-pass ladder filter. Figure 5-9 shows the block diagram of the active filter with the corresponding input referred offset of the integrators.

From the passive implementation, it can be expected that if a DC input is applied to the filter, each state variable (the voltage across a capacitor and the current through an inductor) has a constant DC value. The DC value of each stage can be calculated from the block diagram. Since in steady state, the DC voltages stay constant, the input of the integrators should have zero value. As a result, the sum of all input voltages of the integrator should be zero. If there is no offset, the following equations

92
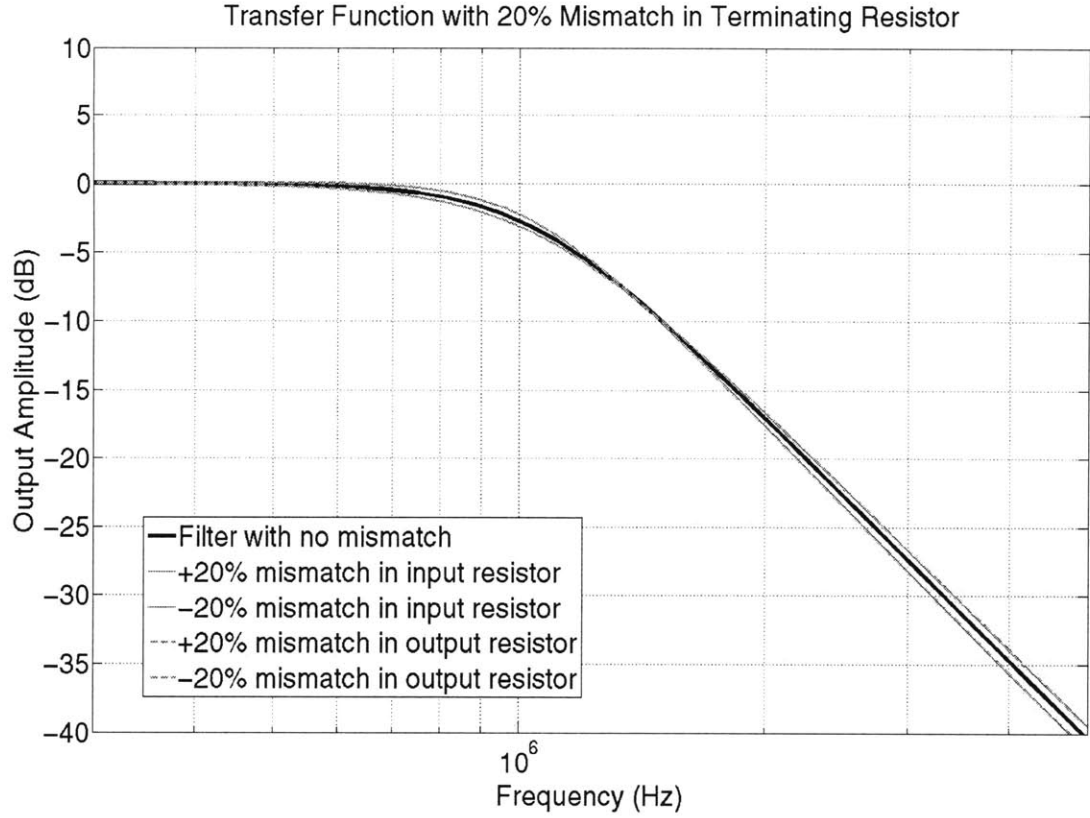
Figure 5-6: Transfer function of a third order butterworth filter with 20% mismatch on terminating resistors.

show the steady-state value of the system for a DC input.

$$First\ Integrator: V_{in} = V_1 + V_2 \tag{5.1}$$

$$Second\ Integrator: V_1 = V_3 \tag{5.2}$$

$$Third\ Integrator: V_2 = V_4 \tag{5.3}$$

$$Fourth\ Integrator: V_3 = V_{out} \tag{5.4}$$

$$Fifth\ Integrator: V_4 = V_{out} \tag{5.5}$$

Solving the system of the equations, it can be shown:

$$V_1 = V_2 = V_3 = V_4 = V_{out} = \frac{V_{in}}{2} \tag{5.6}$$

93
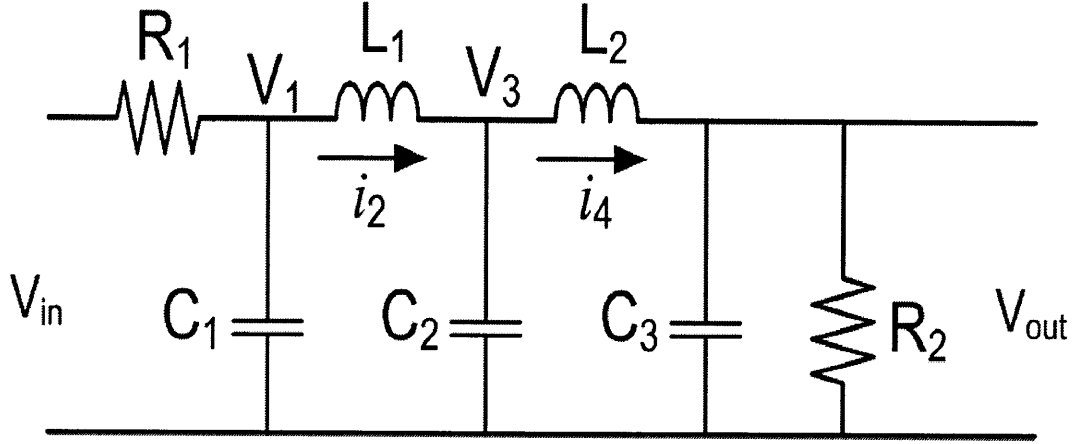
Figure 5-7: Passive implementation of a low-pass ladder filter.
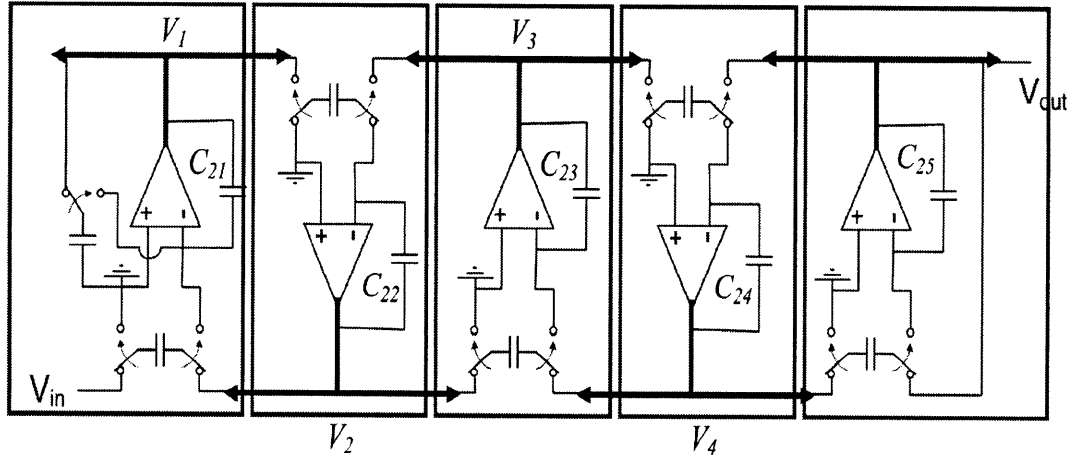
Figure 5-8: Active implementation of a low-pass ladder filter.

The offset can be included in the equations as well. For example, to find the effects of the offset of the third integrator on different voltages, Equation 5.3 can be rewritten as:

$$Third\ Integrator : V_2 + V_{off3} = V_4 \tag{5.7}$$

Solving the system of the equations, it can be shown:

$$V_1 = V_3 = V_4 = V_{out} = \frac{V_{in} - V_{off3}}{2} \tag{5.8}$$

$$V_2 = \frac{V_{in} + V_{off3}}{2} \tag{5.9}$$

94
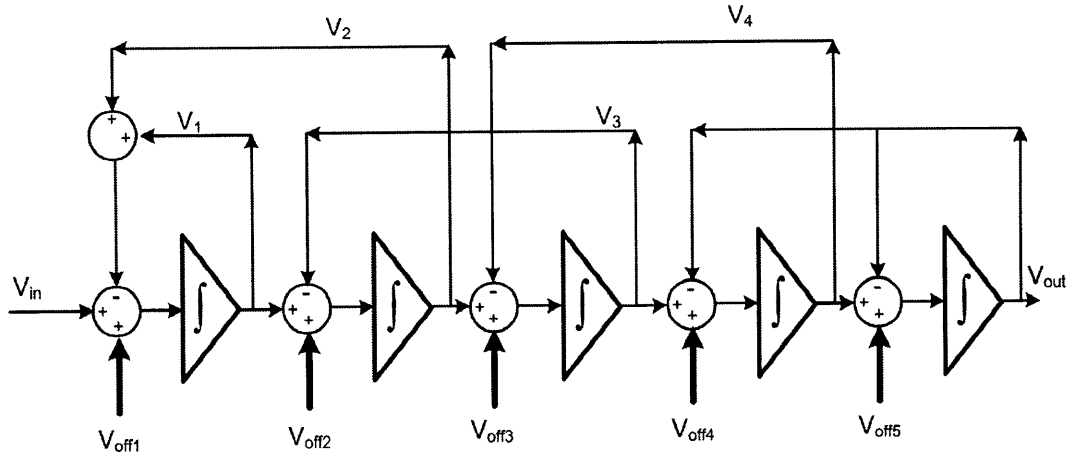
Figure 5-9: Block diagram of an active low-pass filter with the corresponding input referred offset of each integrator.

The offset in the third stage adds an offset to the output of all stages. This is the case for all stages. An offset in zero-crossing detector of any stage generates an offset at the output of all stages. When the input is grounded, the reference voltages of all stages are chosen to center the output of each stage at the middle of its dynamic range. An offset of any stage causes the output of all stages to move. As a result, the output dynamic range of each stage is reduced by the output offset. Similar to the ADC configuration, the offset can be cancelled with the programmable load in the first stage of the zero-crossing detector. However, for a small offset (less than 10mV), a simpler solution is to reduce the input range by the amount of the offset to compensate for the offset.

5.5   Conclusion

In an ADC configuration, capacitance mismatch causes a gain error of the ADC stage, consequently INL and DNL. In Filter configuration, capacitance mismatch does not introduce any non-linearity. However, it changes the filter characteristics.

A small offset does not affect the functionality of an ADC, but a large offset introduces non-linearity. In a filter reconfiguration, an offset in any stage causes the output of all stages to experience an offset. The offset also appears at the analog

95

output. An offset of each stage reduces the signal range at the input.

Chapter 6

Measurements of the Fabricated Chip

This chapter shows the measurement results of the fabricated chip and describes the significance of each measurement. Figure 6-1 shows the die photo of the chip fabricated in TSMC 65nm technology and Figure 6-3 shows the layout of each stage. The block diagram of the chip is shown in Figure 6-2. The core is 340um x 900um and consists of 8 identical stages (except for the sampling circuit of the first stage which has minor differences). Each stage can be programmed as an amplifier or an integrator with programmable coefficients. It can be used as a building block of a pipeline ADC or a low-pass filter. To demonstrate the configurability, the chip is configured as an ADC and filter for different sets of measurements (eight stages were sufficient to show these functionalities). In all measurements, the input is sampled at 50MSPS (unless specified). The clock has a 300ps non-overlapping period and reset pulses have 400ps pulse width. This corresponds to 1.4ns of the total clock period (the clock period of 50MSPS is 20ns). The reference voltage is provided externally and the power drawn from the external reference voltage is negligible.

97
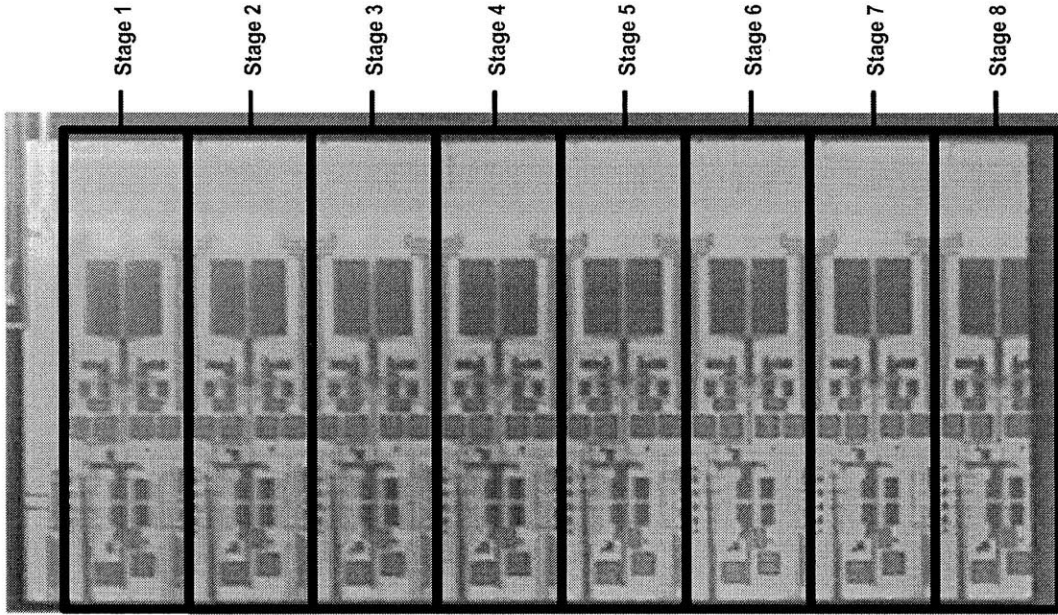
Figure 6-1: The die photo of the core that consists of eight stages.
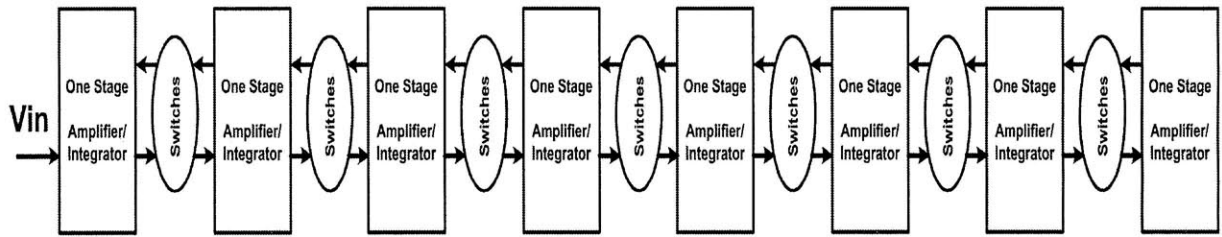
Figure 6-2: The block diagram of the fabricated chip.

6.1 ADC Measurement

In ADC configuration, stages 1 to 5 are used to implement a 10-bit ADC that operated at up to 50MSPS as shown in Figure 6-4. Figure 6-5 and Figure 6-6 show the dynamic performance of the ADC at 50 MSPS with a 1MHz and 24.7MHz sinusoidal input. The ENOB is measured to be 8.02bits. The performance of an ADC depends on its noise and its nonlinearities. An increase in the number of sampling points lowers the visual noise floor. This is because the total noise power does not depend on the number of sampling points. When the number of points increases, the noise in each frequency bin decreases. A lowered noise floor make it possible to distinguish between noise and harmonics (since only noise floor scales with number of sampling points
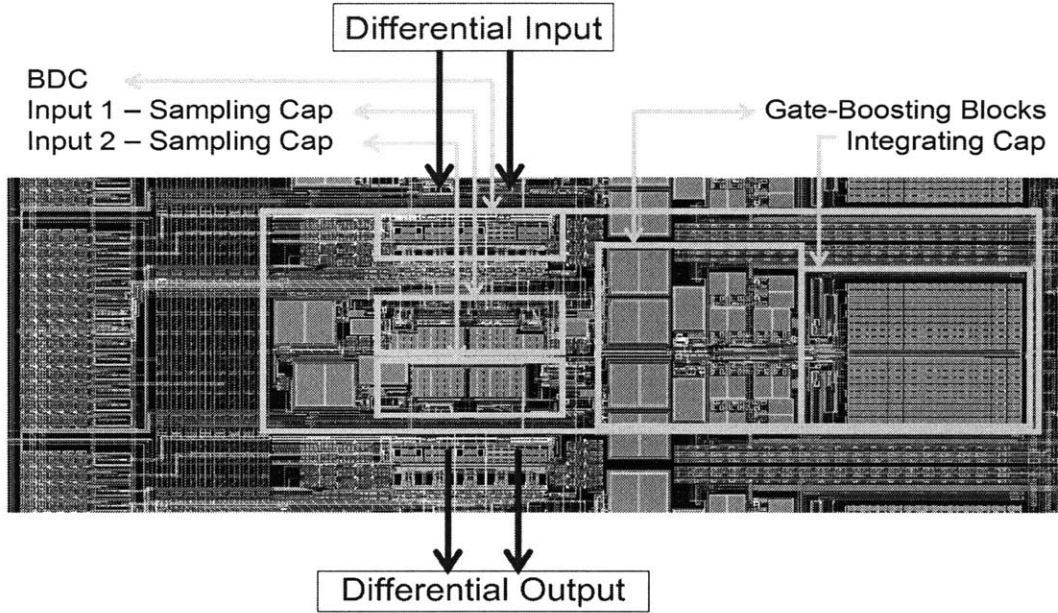
Figure 6-3: Layout of one stage.

and the amplitude of harmonics does not scale). The measurements show that the second and third harmonics are larger than others (Figure 6-5). The second harmonic was expected to be small because of differential implementation of the circuit. The second harmonic is mainly due to the mismatch between the positive and negative ramps which cause the common-mode voltage to vary with signal. Figure 6-5 also shows that high-order harmonics also have significant amplitudes. This corresponds to nonlinearities in one of the last stages. For example, if the offset of bit-decision comparators is larger than the over-range protection in stage four or five, high-order harmonics are introduced.

Integral nonlinearity (INL) of the ADC is measured by applying a low-frequency sinusoidal input, and performing a statistical analysis of the output codes as proposed in [33]. Figure 6-7 shows the INL of the 10-bit ADC which is +1.7/-1.8 bits. The pattern of the INL may hint the type and location of the nonlinearity [35]. For example, a sharp spike may indicate saturation of a block. In addition, the repetition of a pattern may indicate which stage is contributing to the nonlinearity. INL is most useful in diagnosis if there is only one or two dominant source(s) of nonlinearity since their effect may be identified more easily.
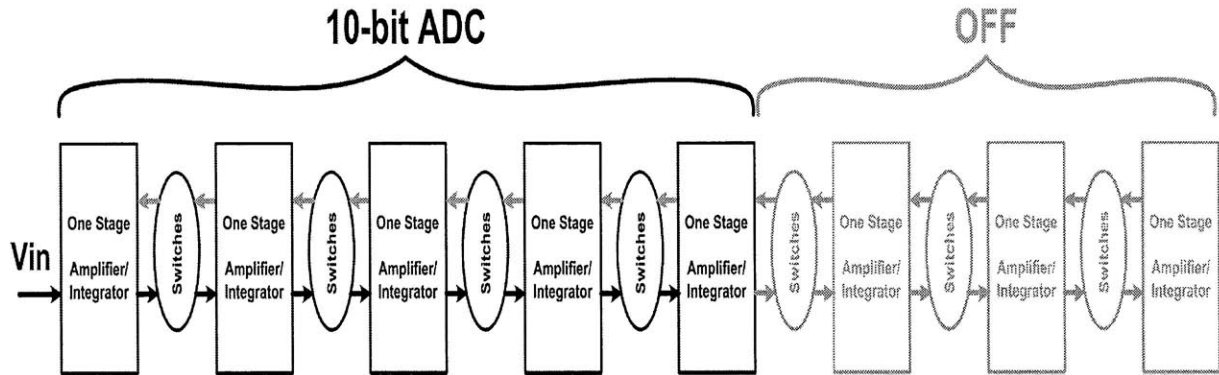
Figure 6-4: The chip configuration for test as an ADC.

Figure 6-8 shows the frequency response of the system when the differential input is grounded. Since no input signal is applied, the output contains no harmonics. This measurement is suitable to measure the internal noise of the system. The zero-input coincides with the threshold level of one of the bit-decision-comparators in the first stage. As a result, the noise of the bit-decision-comparator shows up in its decision in this measurement. Subsequent stages can recover the original analog signal because of the over-range protection. In ZCBCs, the outputs are reset at the beginning of each clock cycle. Therefore, when a zero input is applied, the internal nodes still have high activities. As a results, the coupling noise to the power supply and the reference voltages are still affected by the internal activities.

If a full signal tone (with no harmonics) is assumed to be present in the signal spectrum of Figure 6-8, an SNDR of 57.4873dB is obtained (which corresponds to an ENOB of 9.26 bits if the system has no harmonics). This measurement shows the noise of the system (including both random noise such as thermal noise and coupling noise).

Figure 6-9 shows the ENOB as the clock frequency changes. The measurement uses 100MSPS biasing at different sampling frequencies which means the ramp rate is the same in all cases and is fast enough to reach virtual ground condition for a clock as fast as 100MSPS. In opamp-based circuits, lowering the clock frequency provides more time for each stage to settle down more accurately to the final voltage. However, in ZCBCs, lowering the clock rate does not increase the accuracy of each
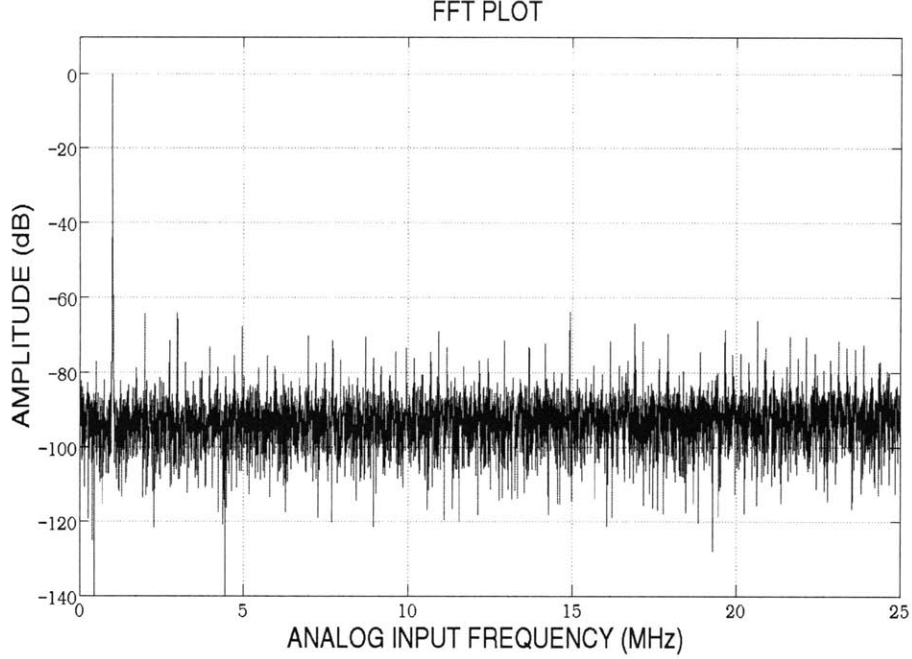
Figure 6-5: FFT plot of the ADC output with a 1MHz sinusoidal input.

stage if the ramp rate is kept the same. Figure 6-9 shows an ENOB of 8.4bits for low sampling frequencies (20MHz and 30MHz) which degrades as the sampling frequency increases, contradicting the expectation that the accuracy does not change since the ramp rate is kept the same in all measurements. One possibility is that the accuracy of each stage of the ADC does not change when the clock frequency changes, but the accuracy of the reference voltages does change. At lower clock frequency, each disturbance on the reference voltage has sufficient time to settle by the next clock. As the clock frequency increases, there is less time for the reference voltages to settle. The accuracy of the output signal directly depends on the accuracy of the reference voltages.

The ADC consumes 1.92mW at 50MSPS with an ENOB of 8.02bits and an FOM of 150fJ/conversion-step. The power consumption of digital blocks scales with frequency as shown by Equation 6.1.

$$P_{Digital} \propto C.V_{DD}^2.f_{Clk} \tag{6.1}$$

101
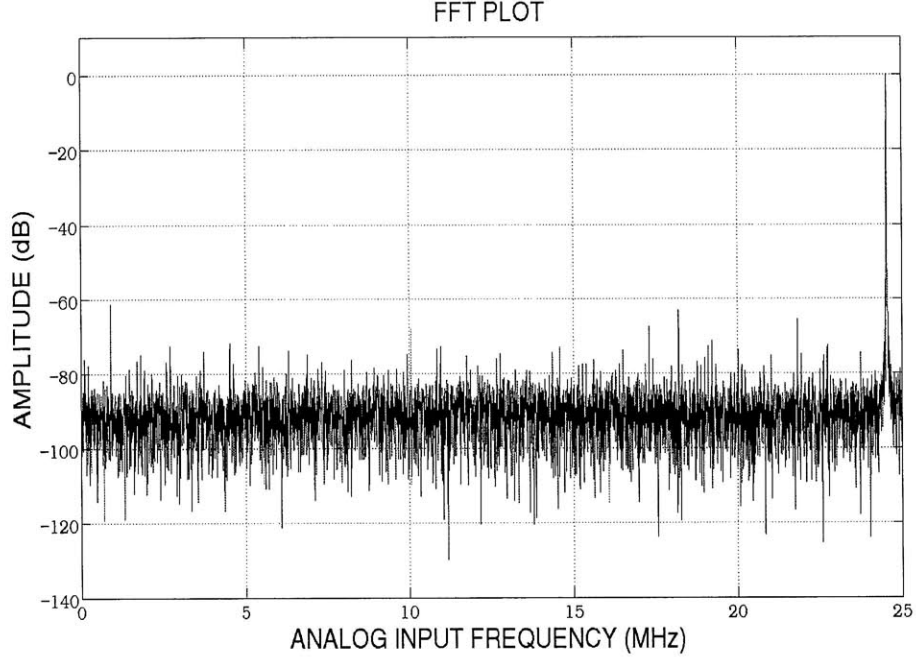
Figure 6-6: FFT plot of the ADC output at a near Nyquist rate.

The power consumption of bit-decision-comparators, control blocks, and switches fall in this category.

If analog circuits are biased with constant currents, their power consumption is constant regardless of the sampling frequency. In ZCBCs, power is consumed in two main circuits, one to drive the output ramps, and the other to bias the differential input of zero-crossing detector. The output ramp stops when the circuit reaches the virtual ground condition. As a result, the power consumption at the output is given by Equation 6.2 which scales with the sampling frequency.

$$P_{Output\ Ramp\_up} \propto C_{Load} \cdot V_{Output\ Swing} \cdot V_{dd} \cdot f_{Clk} \tag{6.2}$$

The zero-crossing detector turns on at the beginning of the amplification phase and turns off when the circuit reaches virtual ground condition. The power consumption of zero-crossing detector depends on its bias current and how long it stays on. If T_{On} denotes the average time that the comparator is on during one clock cycle, Equation 6.3 shows the power consumption of the ZCBC comparator.

102
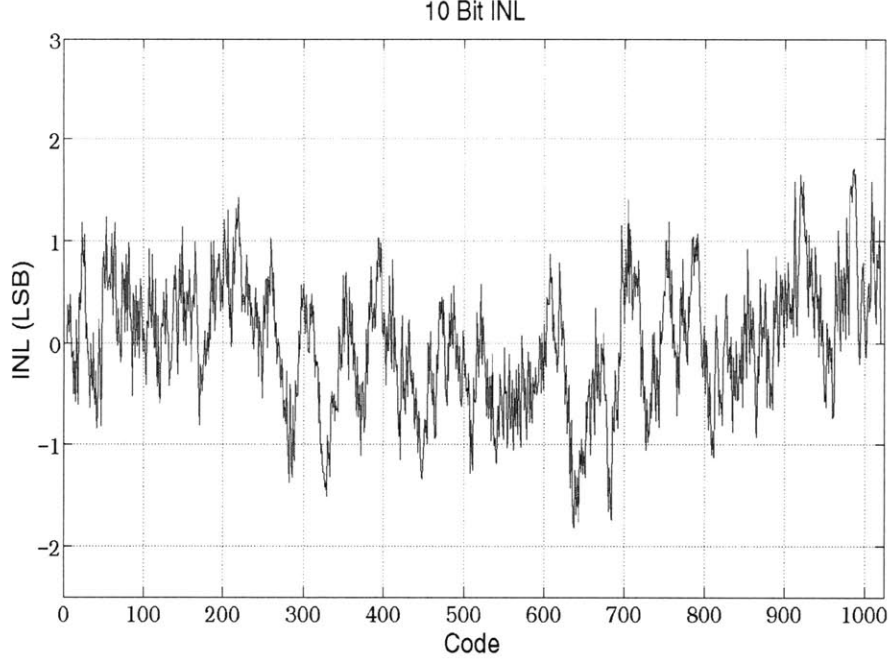
Figure 6-7: The INL of the ADC with 10-bit quantization levels.

$$P_{ZCBC\ Comp} \propto I_{Bias}.V_{DD}.T_{On}.f_{Clk} \qquad (6.3)$$

Since all different components of the power consumption scale linearly with the sampling frequency, the total power is expected to scale linearly with the sampling frequency as well. Figure 6-10 shows the measured power consumption as a function of the sampling frequency which scales linearly as expected. The FOM degrades, however, due to currents in the bias network, which do not scale with frequency. In opamp-based circuits, the power consumption can be scaled by changing the biasing current of the opamp. For example, [48] changes the opamp bias to optimize the power consumption of its ADCs while its sampling frequency changes. When the frequency changes by a factor of 100, its bias current (and hence its power consumption) changes by almost a factor of 400.

Changing the ramp rate changes the accuracy of ZCBC circuit. With the same comparator delay, slower ramp rate results in both smaller overshoot thus smaller overshoot variation. Figure 6-11 shows the ENOB of the ADC as the ramp rate

103
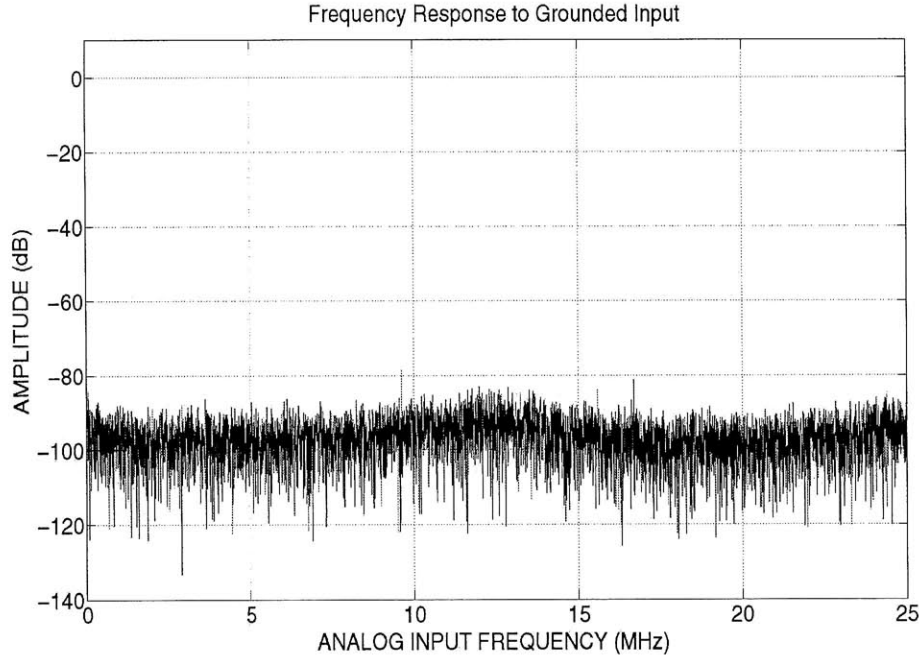
Figure 6-8: The FFT plot of the ADC output with grounded inputs.

changes where ramp rate of 1 corresponds to the ADC setting to operate at 100MSPS. Similarly, ramp rate of 0.7 corresponds to ramp rate suitable for 70MSPS and ramp rate of 1.2 corresponds to ramp rate suitable for 120MSPS. Figure 6-11 shows that slowing down the ramp rate does not improve ENOB. This indicates that the accuracy of the ADC is not limited by the accuracy of the zero-crossing detector or ramp linearity, because a lower ramp rate reduces the effects of non-idealities of zero-crossing detector and current sourced. For example, a lower ramp rate reduces the effects of the delay of zero-crossing detector and its delay variation. A lower ramp rate also means the output current is smaller; as a result, the output current variation is smaller too. In addition, increasing the ramp rate does not reduce the ENOB which implies the comparator is fast enough even with a faster ramp rates. As the ramp rate reduces to 0.6, ENOB reduces dramatically. This corresponds to the situation that the ramp does not have enough time to reach to the final value (or equivalently, the ZCBC circuit does not reach virtual ground condition). This threshold was expected to be at 0.5 since the chip is operating at 50MSPS. The difference is due to additional

104
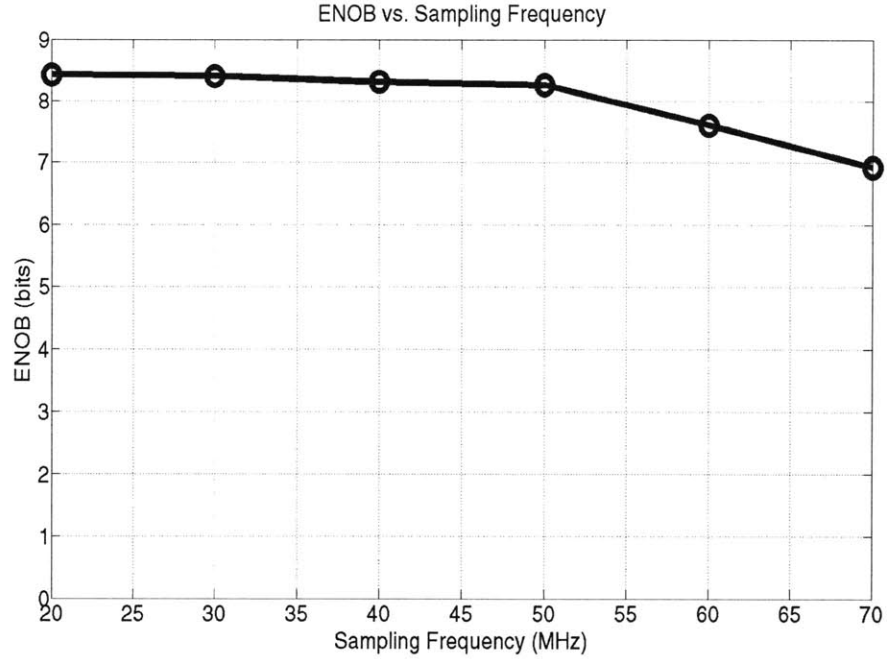
Figure 6-9: The ADC ENOB at different sampling rates.

parasitic capacitance at the output node.

The performance of an ADC may degrade as the frequency of the input signal approaches the Nyquist rate. The sampling circuit is designed to have a -3dB bandwidth of 60MHz. Figure 6-12 shows the measured ENOB of the ADC as a function of the frequency of the input signal. Note that since the output of each ZCBC stage is a ramp, it is not sensitive to the bandwidth of the input signal. The only stage which is sensitive to the bandwidth of the input signal is the sampling circuit of the first stage. Figure 6-12 shows that the ADC performs equally well at different input frequencies. For sampling rate of 50MSPS, the Nyquist rate is 25MHz. The ENOB does not degrade for the input frequency as high as 56MHz (where the ADC is sub-sampling).

Some wireless applications such as the receiver in wireless base transceiver stations require an ADC with high linearity [43],[44]. In these systems SFDR is a more important metric than SNDR or ENOB. Figure 6-13 shows the SFDR of the ADC at different input frequencies.
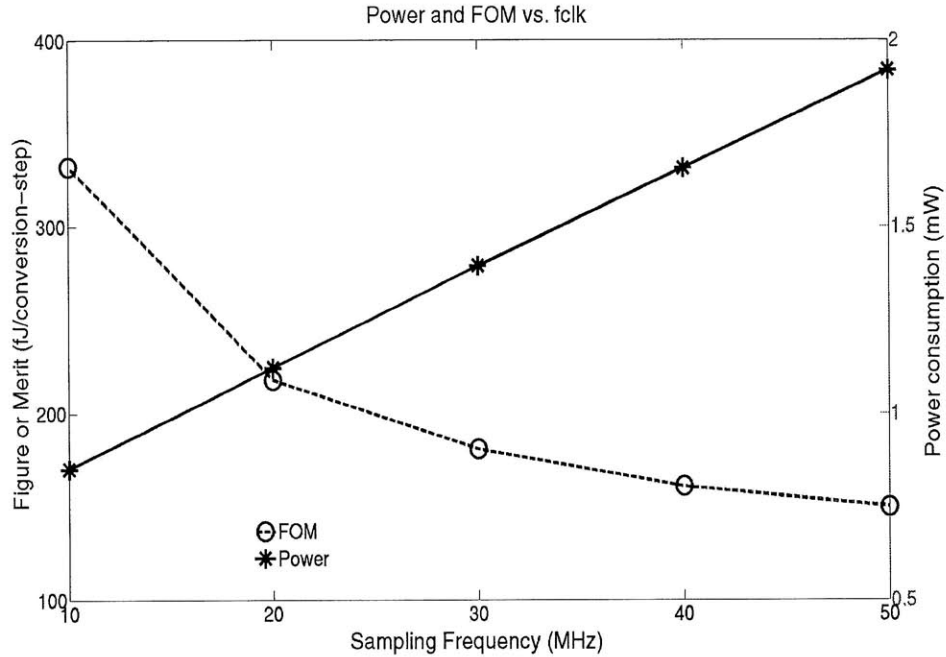
Figure 6-10: The power consumption and the FOM of the ADC as a function of the sampling frequency.

ENOB is maximum when the full input signal range is utilized. If the input signal is larger than the full range, the output saturates, which results large harmonic tones in the frequency response and reduces ENOB as shown in Figure 6-14. Applying a smaller input than the full range results in a lower signal to noise ratio and a lower ENOB. Figure 6-14 shows the measured ENOB of the ADC as a function of the input signal amplitude which reduces one bit for every 6dB reduction in the input amplitude.

Figure 6-15 compares the figure of merit (FOM) of the ADC with the state of the art non-reconfigurable pipeline ADCs that are recently published at ISSCC. As shown, the figure of merit of this chip is very competitive.

6.2   Filter Measurement

Filter functionality is verified with two different configurations. The first configuration is shown in Figure 6-16 where the first two stages of the chip are programmed as a
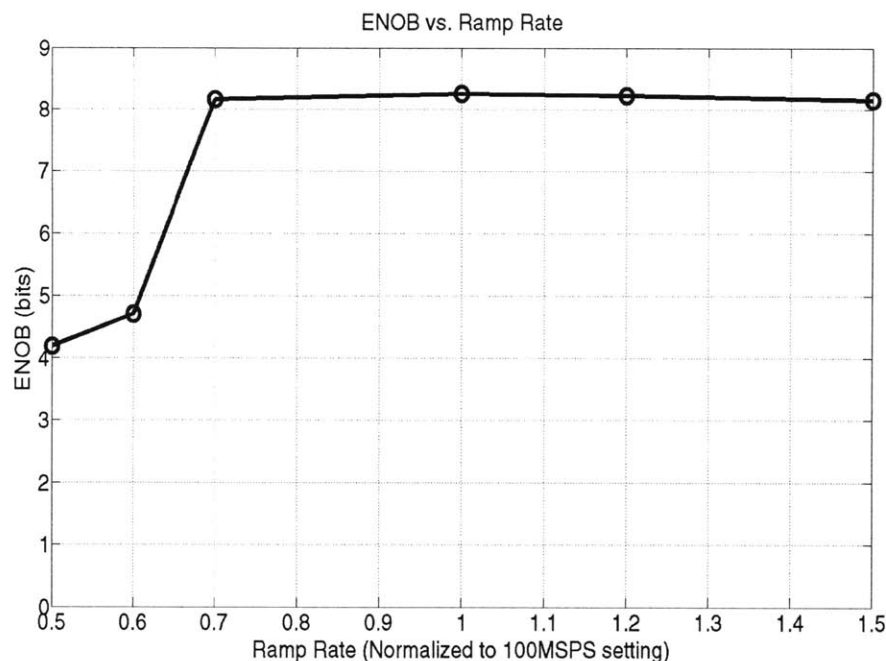
Figure 6-11: The ADC ENOB at different ramp rates.

second order Butterworth low-pass filter, the third stage as an amplifier, and the last five stages as a 10-bit ADC. Figure 6-17 shows both the measured and the ideal frequency response of the filter. This test is a very significant test since three different functionality of the stages are tested simultaneously and it is shown that the stages interact properly when configured for different functionalities.

The second configuration to test the filter functionality is shown in Figure 6-18 where the first three stages of the chip are programmed as a third order Butterworth filter with a cutoff frequency of 1MHz for the sampling rate of 50MSPS. Figure 6-19 shows both the measured and the ideal frequency response of the filter.

When the chip is configured as in Figure 6-18, the frequency components of the output is shown in Figure 6-20. Large harmonics are observed that are mainly due to non-linearity of the ADC. The bit-decision-comparators of the chip show large offset variation. Since the first three stages are more accessible to the input signal, the offset of bit-decision-comparators can be measured and adjusted by programming the capacitive load of bit-decision-comparators. However, the offset of bit-decision-
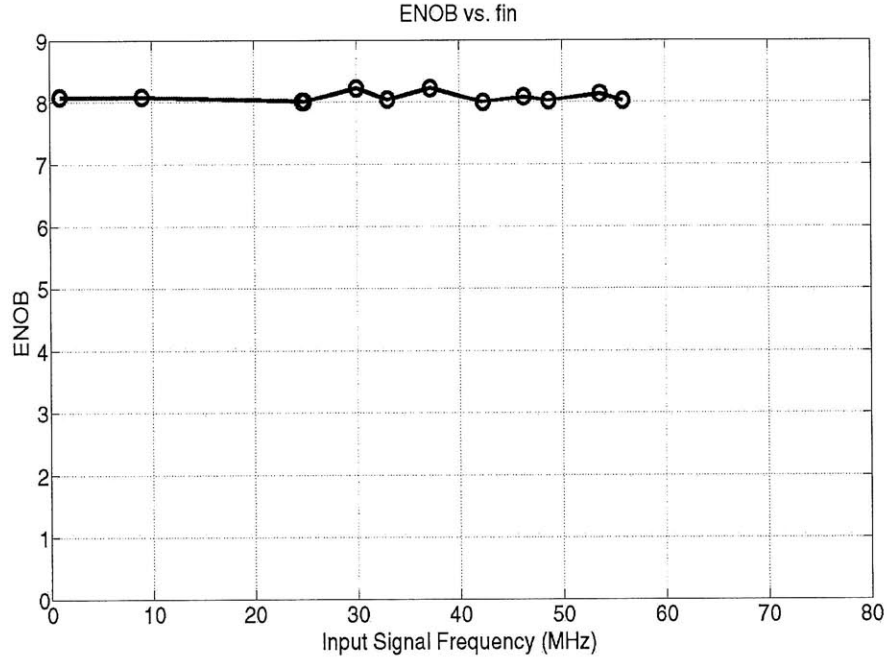
Figure 6-12: The ENOB as a function of the input signal frequency.

comparators in other stages is not adjusted.

6.3 Cost of Reconfigurability

Reconfigurability in the system is provided by additional programmable capacitors, switches, analog buffers, bootstrapping circuits, and an additional set of sampling capacitors. The additional components increase the total area of the chip and increase the length of wires that connect different stages. In addition, many signals need to connect more blocks as needed by the reconfigurability. This increases the parasitic capacitance of these signals and the coupling between different signals. The cost of reconfigurability is evaluated based on its effects on power consumption, speed, area, noise, and architectural limitation.
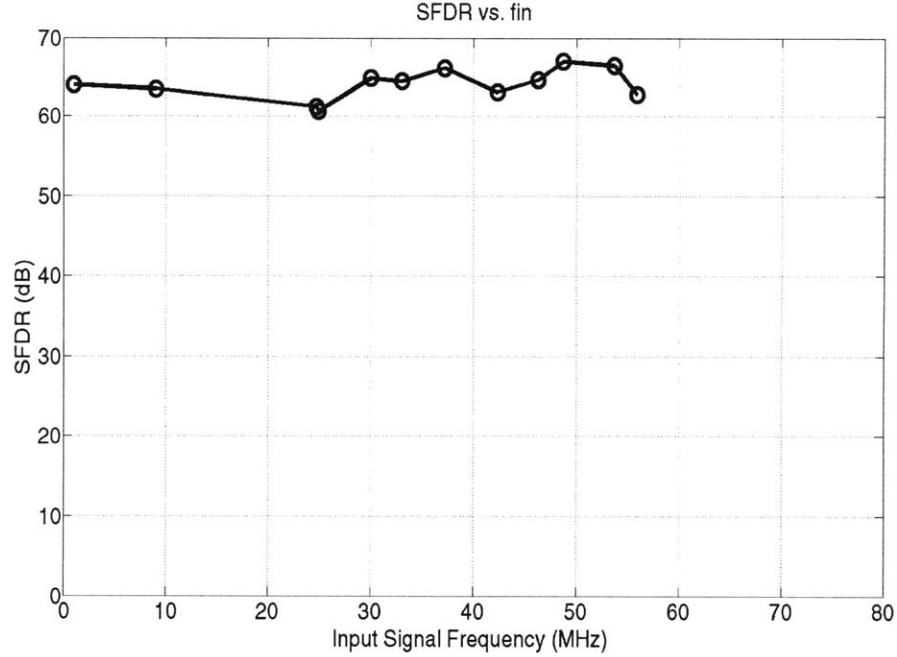
Figure 6-13: The SFDR as a function of the input signal frequency.

6.3.1 Power Consumption

Power consumption is affected by reconfigurability in several forms. In an ADC configuration, the additional components increase the length of wires, which increases the capacitive load of each stage by 38fF. Compared with total capacitive load of 225fF at the output of each stage, the output load increases by 17%. Since 21% of the power consumption in each stage is to drive the output load, the power consumption of each stage increases by 4% due to additional parasitic capacitance. Stage scaling can reduce power consumption. The input noise of the second stage is attenuated by a factor of 4^2 when referred to the input of the first stage since the gain of the first stage is 4. If we assume that the power consumption of each stage is 1 unit, the power consumption of 5 stages that are not scaled is 5 units. If only the second and third stages are scaled, and they are scaled only by a factor of two, the overall power consumption is 1+0.5+0.25+0.25+0.25=2.25 units. Without scaling, the noise

109
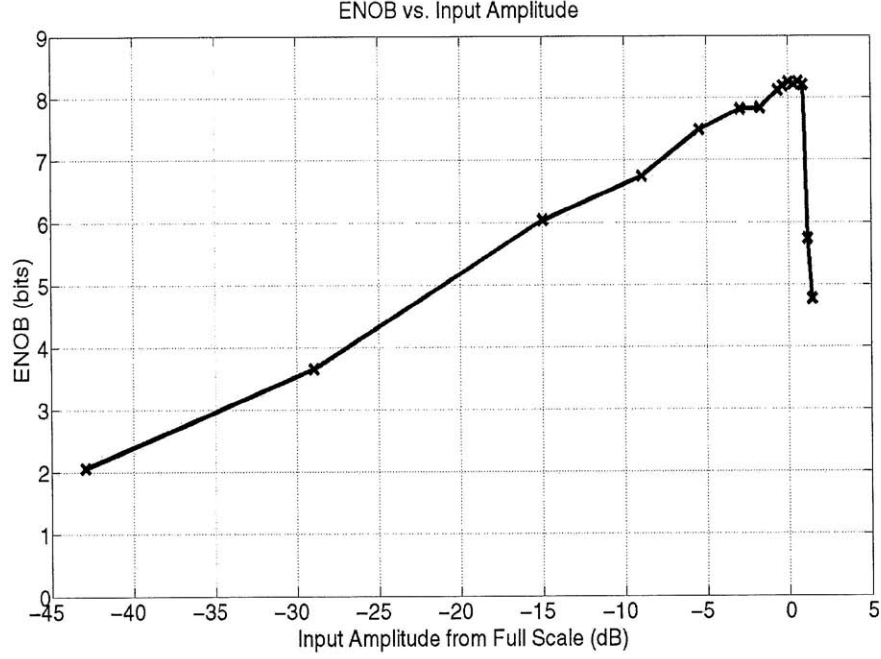
Figure 6-14: The ENOB as a function of the input signal amplitude.

is given by:

$$S_{ADC} = (1 + \frac{1}{4} + (\frac{1}{4})^2 + (\frac{1}{4})^3 + (\frac{1}{4})^4) * S_{stage} = 1.33 * S_{stage} \qquad (6.4)$$

With scaling, the noise can be calculated as:

$$S_{ADC} = (1 + \frac{1}{4} * 2 + (\frac{1}{4})^2 * 4 + (\frac{1}{4})^3 * 4 + (\frac{1}{4})^4 * 4) * S_{stage} = 1.82 * S_{stage} \qquad (6.5)$$

Therefore, the overall power consumption is reduced by a factor of $\frac{5}{2.25} = 2.22$ while the noise increases by 36%. In the reconfigurable system, it is not preferred to scale stages since it improves the power consumption in ADC configuration while exacerbates the total noise in filter configuration.

In a filter configuration, the additional power consumption for reconfigurability is mainly because of the parasitic capacitor of bootstrapping circuits that drive programmable switches. A non-reconfigurable filter does not require these components, and they can all be replaced with wires for a hardwired connection. The parasitic

110
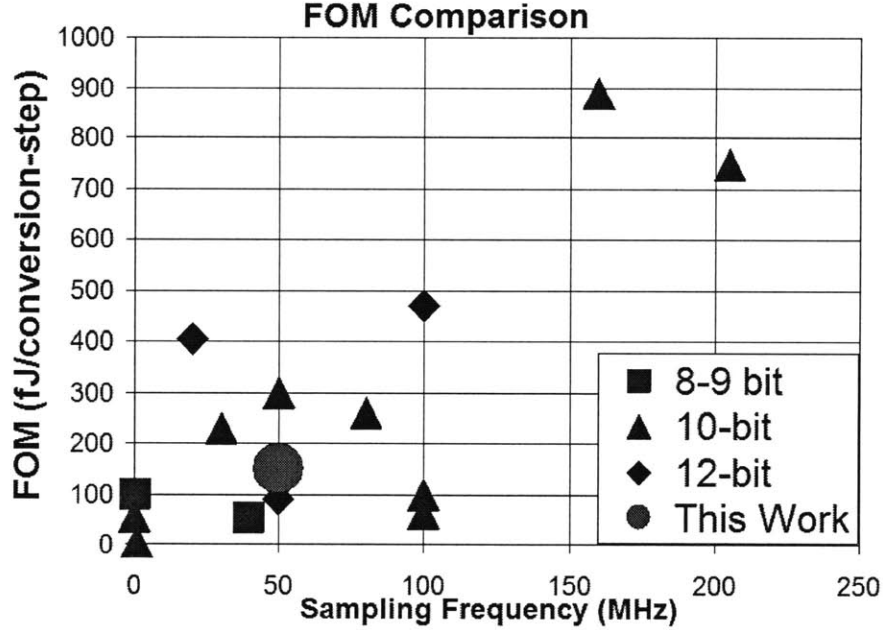
Figure 6-15: Comparison of state of the art non-reconfigurable ADCs (ISSCC 2007-2010) with this work. .

capacitance increases the load of each stage by 146fF. Compared with 360fF output load in filter configuration, the output load increases by 28%. Since the power consumption for driving the output capacitance is 21% of the power consumption of each stage, the power consumption of each stage increases by 6% due to additional parasitic capacitance. Stages can be scaled for power optimization. For example, since the last stage contributes the most to the noise, it can be scaled up, and other stages can scale down. In the reconfigurable system, however, the order of the filter (and therefore the last stage) is not known *a priori*. As a result, the stages scaling in a reconfigurable system is not practical even if only a filter functionality is desired.

6.3.2   Speed

Reconfigurability has minor effect on the maximum speed of the system. It increases the parasitic capacitance of different nodes. For analog signals, this is compensated by increasing the bias current of the circuit that drives those node. In ZCBC circuit,

111
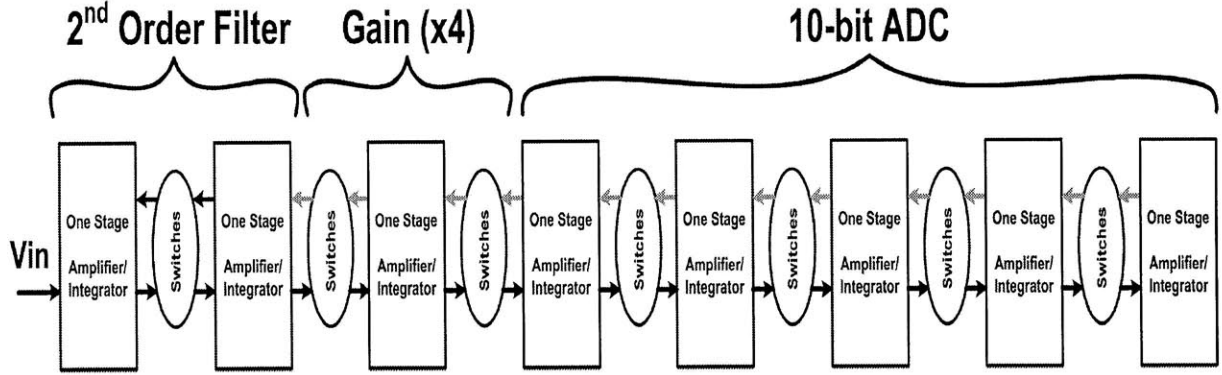
Figure 6-16: The chip configuration for test as a second order filter.

this corresponds to the increase of the output current sources the effect of which has been accounted for in the previous section (i.e. increase in power consumption). For digital circuits, the additional parasitic capacitors are driven by stronger buffers. This corresponds to one or two more additional buffers at the output of some digital signals. The additional delay of the buffers are negligible compared to a clock cycle. Therefore, the cost of reconfigurability on speed is negligible.

6.3.3 Area

The size of each stage is 340um x 114um. In an ADC configuration, the size of the required circuit blocks is 150um x 76um. As a result, the size of each stage is 3.4 times larger due to reconfigurability. In a filter configuration, the size of the required blocks is 266um x 91um. As a result, the size of each stage is 1.6 times larger due to reconfigurability assuming that all the reconfigurable capacitors are used.

If one core was designed only to implement an ADC and another core was designed only to implement a reconfigurable filter, the required area would be 90% of the current configuration. In other words, combining the two functionality in one core has 10% area penalty.

112
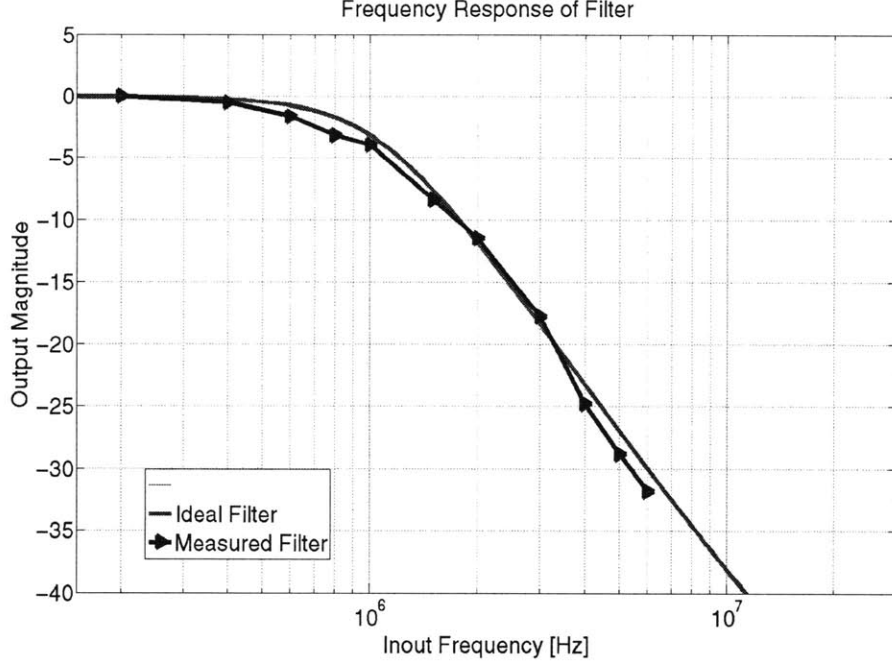
Figure 6-17: Ideal and measured filter transfer function for a second order butterworth filter.

6.3.4 Noise

In an ADC configuration, the reconfigurability increases the noise for several reasons. One reason is that in non-reconfigurable ADCs, the noise can be optimized by scaling the stages. For example, if the first stage is scaled up by a factor of 2 and stages 4 and 5 are scaled down by a factor of 2, the total power consumption remains the same, but the total mean-square noise is reduced almost by a factor of 2. Another reason that the noise increases in ADC configuration is the additional parasitic capacitance on the virtual ground node. Because of the reconfigurability, the virtual ground node is connected to many circuit blocks. As a result, an additional parasitic capacitance of 25fF is present on the node. The output referred noise of the zero-crossing detector is given by Equation 6.6 (Appendix D).

$$S_{n,output} = (\frac{180fF + 25fF}{60fF})^2 * 120nV^2 = 1400nV^2 \tag{6.6}$$

The input referred noise of zero-crossing detector is given by Equation 6.7.
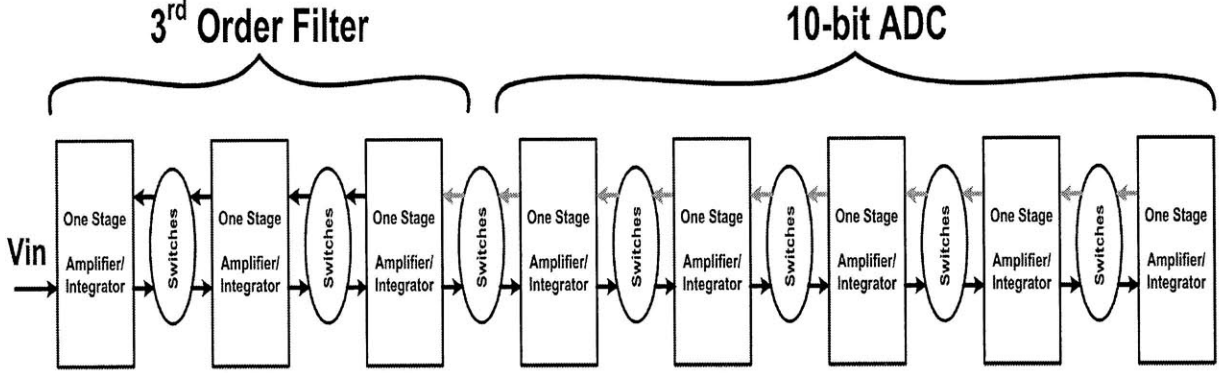
Figure 6-18: The chip configuration for test as a third order filter.

$$S_{n,input} = (\frac{1}{4})^2 * 1400nV^2 = 87nV^2 \qquad (6.7)$$

The noise is $67nV^2$ in the absence of the additional parasitic capacitance. The input referred noise of the zero-crossing detector increases by 29%. Considering sampling noise (kT/C) of $46nV^2$ in both cases, the total input referred mean-square noise of each stage increases by 18%.

In a filter reconfiguration, stages could scale to reduce the noise for the same power consumption. For example, in a third-order Butterworth filter, scaling up the last stage by a factor of 2 and reducing the size of the first two stages by a factor of 2 reduces the overall mean-square noise by almost a factor of 2.

During the noise analysis of an integrator, it was shown that the noise of a zero-crossing detector appears both at the input and at the output of the integrator. The noise at the output of the integrator does not depend on the value of any capacitor and is the dominant source of the noise in low-pass filters. As a result, the increase in the parasitic capacitance of the virtual-ground does not affect the overall noise of a low-pass filter.

6.3.5 Choice of Architecture

Reconfigurability limits the choice of the architecture significantly. The ADC or filter should have an architecture in which most components can be reused in different
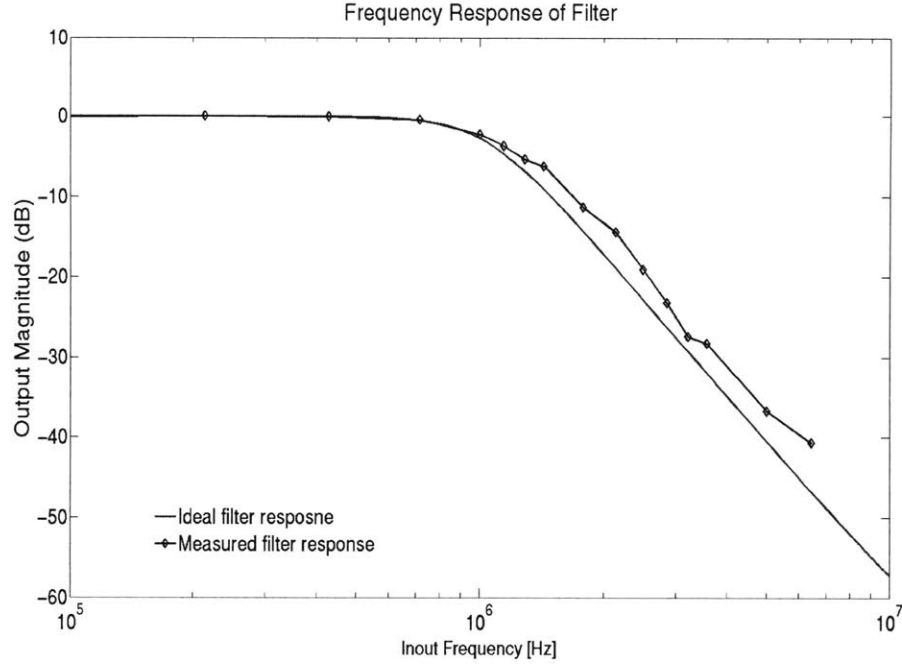
Figure 6-19: Ideal and measured filter transfer function for a third order butterworth filter.

configurations. For example, pipelining two successive-approximation-register (SAR) ADCs is proposed to improve the resolution and performance of an ADC [45] [46]. Since large SAR ADCs are not reusable for other functionalities, this method is not suitable for reconfigurable system. In general, it is difficult to quantify the effects of architectural limitation on the performance of the system. Table 6.1 summarizes the cost of reconfigurability.

6.4   Measurement Summary

The chip is tested as an ADC and two types of filters. In one test, one stage is also used as a gain stage. It is shown that the chip works properly in all configurations. In ADC configuration, the performance was limited by the offset of bit-decision-comparators and the settling time of reference voltages. The offset of bit-decision-comparators are adjusted for the first 2 stages. At 50MSPS reference voltages settle reasonably well. The FOM would improve if the target ENOB had been achieved. The chip is also

115
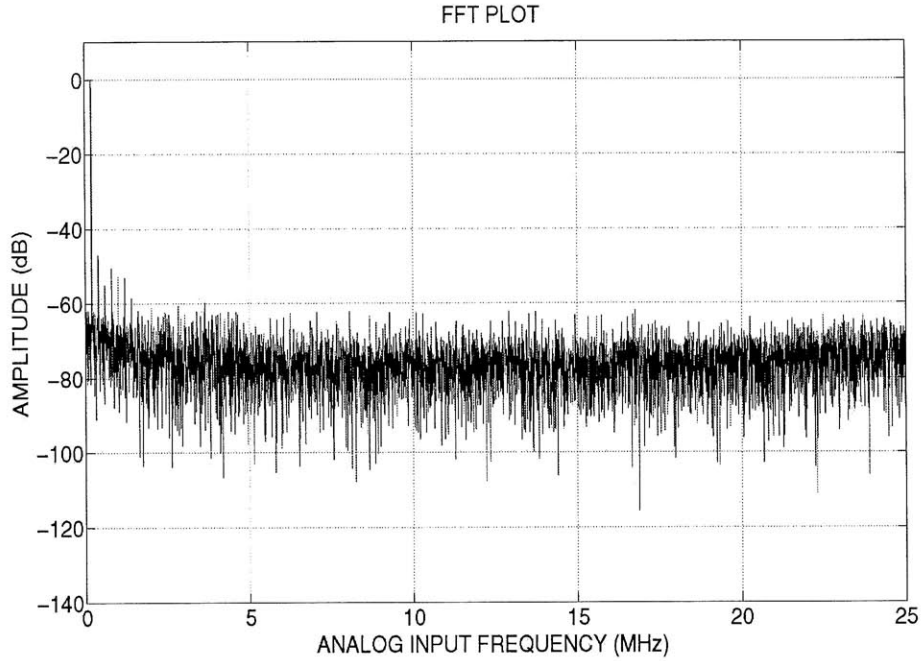
Figure 6-20: The main tone and its harmonic at the output of the ADC that measures the output of a third order low-pass filter.

tested with a ramp rate corresponding to 150MSPS resulting ENOB of 8bit.

In filter configurations, the filter characteristics are reasonably close to the expected one. The linearity of the filter also cannot be measured properly since the output non-linearity is dominated by the non-linearity of the on-chip ADC. The measurements are summarized in Table 6.2

116

Table 6.1: Cost of Reconfigurability.

Order of the filter	Noise Bandwidth
Power	ADC: 4% increase due to parasitics
	ADC: large increase due to scaling
	Filter: 6% increase due to parasitics
	Filter: large increase due to scaling
Area	ADC: 3.4x increase
	Filter: 1.6x increase
Noise	ADC: 18% increase due to parasitics
	Filter: No significant increase.
Speed	ADC: No significant increase.
	Filter: No significant increase.

Table 6.2: Summary of Measurements.

	General
Process	65nm Digital CMOS
Active Area	340um x 900um
Supply	1V
Functionalities	Pipeline ADC, Low-pass filter
	Pipeline ADC
Quantization Levels	10 bits
ENOB	8.02 bits
INL	+1.7/-1.8
SFDR	62dB
Power	1.92mW (Total)
FOM	150fJ/conversion-step
Input Signal Bandwidth	56MHz
Sampling Rate	50 MSPS
	Low-Pass Filter
Filter 1	Second order butterworth low-pass filter (switched capacitor)
Filter 2	Third order butterworth low-pass filter
Cut-off Frequency	1MHz
Sampling Frequency	50 MSPS

Chapter 7

Conclusions

A highly-configurable analog system is presented. A prototype chip is fabricated and an ADC and filter functionalities are demonstrated. The chip consists of eight identical programmable stages (except for the first stage that has minor differences in the sampling circuit). Each stage can either amplify or integrate its inputs. The output can be sent to the adjacent stages. The chip can be configured as a pipeline ADC, switched-capacitor filter, or a programmable gain amplifier (a gain of 4 is demonstrated).

In an ADC configuration, the first five stages are programmed to implement a 10-bit ADC. The ADC has ENOB of 8 bits at 50 MSPS. The ENOB improves to 8.5 bits if the sampling rate is lowered to 30MSPS. The ADC has an FOM of 150fJ/conversion-step, which is very competitive with the state of the art non-reconfigurable ADCs. The performance of the ADC is limited due to the offset of bit-decision-comparators, and the coupling noise and the ripples on the reference voltages. The offset of BDCs were adjusted for the first two stages. In addition 50MSPS sapling rate was used to allow enough time for the reference voltages to settle. Measurements show that if the ramp rate of the ZCBCs increases, the ENOB of the ADC does not change. This shows that the delay (or delay variation) of zero-crossing detector is not the bottleneck. It also shows that the output resistance of the current sources, and the resistance of the switches are not the bottleneck either (since their contribution to the ADC non-linearity is more at higher ramp rates). The first stage is responsible

119

for 75% of the input-referred mean square noise. Sampling noise is responsible for 40% of the total mean-square noise and the zero-crossing detector is responsible for 60%. As a result, optimizing the mean-square noise of the zero-crossing detector of the first stage is the most effective way in reducing the overall noise of the chip in the ADC configuration.

In the filter configuration, several input stages are programmed as a filter and the next stages are programmed as an ADC. The chip is tested in two different filter configurations. In one set of tests, the first two stages of the chip are configured as a second order Butterworth filter and the third stage is configured as an amplifier. The remaining stages are programmed as an ADC. It was demonstrated that the desired filter functionality is properly achieved in this configuration. In another test, the first three stages of the chip are programmed as a third-order Butterworth filter and the next stages are programmed as an ADC. The desired filter functionality is also demonstrated in the configuration.

The noise of the system in a filter configuration is also analyzed. It is shown that in a third order Butterworth filter, more than 90% of the noise is due to the zero-crossing detector of the last stage. This is mainly due to the fact that the noise of earlier stages is filtered with the filter transfer function in a similar way that the input signal is filtered. The last stage of the filter contributes the most to the total noise power since its noise is not filtered.

The ZCBC architecture has been used to avoid the stability problems of opamp-based circuits and scale power consumption for a wide range of sampling frequencies. It is shown that the power consumption of the chip scales linearly with the sampling frequency.

A new technique is introduced to implement the terminating resistors in a ladder filter. This technique is very compatible with the reconfigurable architecture and does not have any area or power overhead. As a result, any stage can be programmed to be the first stage or the last stage of a filter. The technique saves the area and reduces the complexity of implementing the terminating resistors in a filter.

An asymmetric differential signaling is also introduced. This method improves the

dynamic range of the output signals which is particularly important in new technology nodes with low supply voltage.

7.1 Future Work

The signal-to-noise ratio of the current chip was limited due to the coupling and the ripples on the reference voltages. In particular, the bond-wire inductance introduces oscillations of the reference voltage. An on-chip reference voltage can improve the performance significantly and should be integrated in the future revisions of the chip.

Dual ramp-rate has been proposed for stand-alone ADCs [23]. The linearity of the system improves with dual ramp rates. This technique should be considered for the future revisions of the chip.

In this chip, only the feedback capacitors are reconfigurable and provide reconfigurability for integration. In the future work, the sampling capacitors can also be reconfigurable, which has two advantages. One advantage is that the sampling noise of each stage can be changed based on the requirement. In addition, the gain of each stage can be reconfigured as well to implement programmable gain amplifier. Alternatively, several rows of reconfigurable stages can be implemented where the size of all stages are the same in one row and scale from one row to another row. If a larger (or smaller) stage is needed, the current stage can be connected to a stage in a different row.

The connectivity of the stages in the current chip is limited to the adjacent stages for the ADC and filter functionality. In the next revision of the chip, the research can focus to provide more programmability for the switches.

The current chip architecture has most of the building blocks of a sigma-delta ADC such as integrators, bit-decision-comparators, and adders. More connectivity is required between different stages to implement a sigma-delta ADC. The future work can examine how to extend the functionalities of the chip to sigma-delta ADC. Similarly, the current architecture of the chip has most of the building blocks for a time-interleaved ADC. In future research, such functionality can be added to the

system.

Finally, there are two more techniques that can be used to improve the functionality of reconfigurable analog systems as described next. However, each technique has some challenges. In future work, these techniques can be researched more.

7.1.1 Pulse-Width Modulated Signals

Figure 7-1 shows a block diagram of two stages of the system that are configured to amplify the signal. There are two signals that connect the two stages. One signal is V_{out1} which is the analog output of the first stage. The other signal is $V_{control}$ which is the digital signal that controls the current sources of the next stage. Figure 7-1 shows the shape of signals in the time domain. As shown the pulse width of $V_{control}$ increases linearly with the amplitude of V_{out}. In fact, V_{out} can be reproduced in stage 2 using $V_{control}$ (if the ramp rate of the two stages are adjusted to be the same). Since it is much easier to have a reconfigurable connection between different stages for digital signals, $V_{control}$ can be used as the output of each stage. This method has several challenges. One challenge is that the ramp rate of the two stages should match very well. Another challenge is that the jitter of the control signal increases the noise significantly. In future work, this method can be researched more since it provides better connectivity between different stages, but the matching of the ramp rates and the jitter of $V_{control}$ should be addressed. Alternatively, this method can provide connection between stages that don't require a large signal-to-noise ratio.

7.1.2 Programmable Feedback Ratio Using Programmable Current Sources

Figure 7-3 shows a ZCBCs with a programmable capacitor in the feedback. Ideally, the current source that drives the output node provides a constant current I_1. The current that passes through C_2 and C_3 depends on their relative values. Once C_3 is programmed, its value stays the same for the rest of the operation. As a result, I_2 and I_3 also remain constant whenever I_1 is on. Since I_3 is constant, it can be replaced with
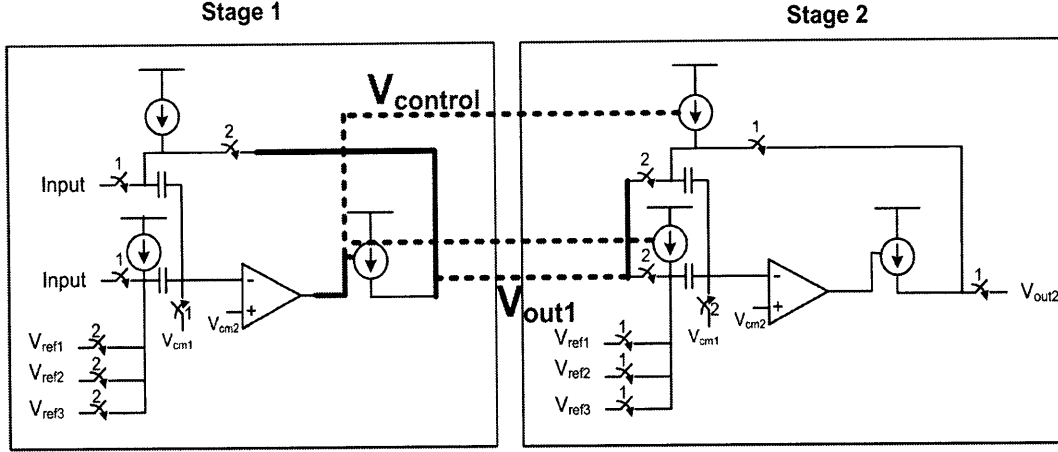
Figure 7-1: Two stages of ZCBCs with the corresponding signals.

a current source as shown in Figure 7-4. If the value of C_3 is changed, the ratio of I_2 and I_3 changes. Since the output ramp rate is preferred to stay constant (regardless of the value of the feedback capacitors), it is desired to keep I_2 constant regardless of the value of the feedback capacitors. As a result, when C_3 is programmed, I_1 should be programmed as well to keep I_2 constant. This means, for each value of C_3, I_3 should change so that $I_3 = \frac{I_2 \cdot C_3}{C_2}$. If the circuit is implemented by replacing C_3 with a current source, adjusting I_3 has the same effect as adjusting C_3.

This implementation can be optimized more as shown in Figure 7-5. The current of capacitor C_1 and C_2 in Figure 7-5 is the same as those in Figure 7-4. As a result, the voltage at the virtual ground node and at the output is the same in the two figures. It is easier to implement current sources when one side of the current source is connected to either ground or V_{dd}. Therefore, Figure 7-5 is simpler for implementation.

The advantage of this method is that programmable current sources are easier to implement compared to programmable capacitors since they are smaller and their parasitic capacitors are smaller as well. However, this method has two main challenges. One challenge is that the output resistance of the current sources is limited and the output current is voltage dependent. Since the ratio of the currents changes with the output voltage, nonlinearity is introduced. Another challenge is that the programmable current source is a proper replacement for the programmable capac-
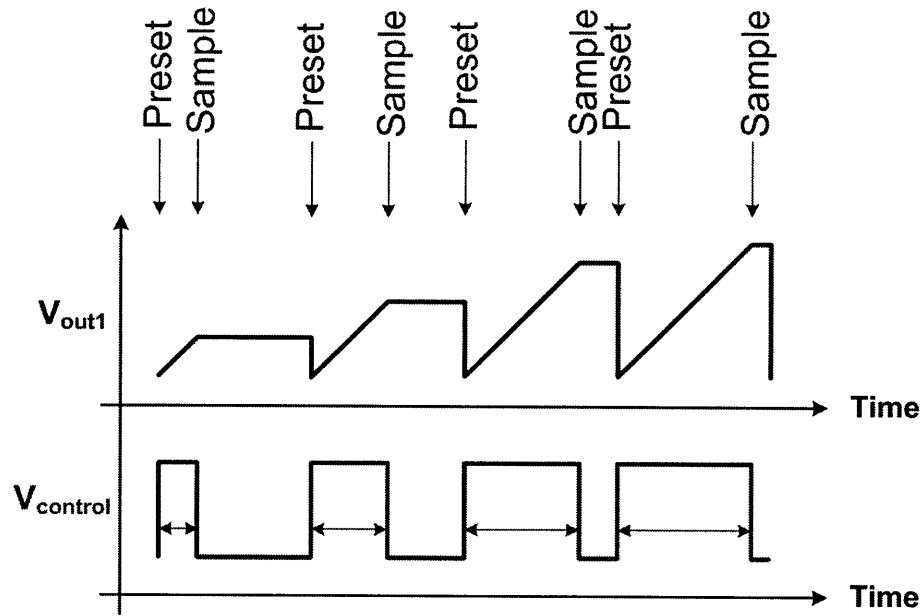
Figure 7-2: Time-domain representation of V_{out} and $V_{control}$ that send an analog signal from one stage to the next stage.

itor only during the output ramp. During the preset (or pre-charge) of the output node, the current through the programmable capacitor is not constant. As a result, the current source is not a proper substitute for the programmable capacitor during the preset. This can be fixed if the output is not preset. Instead, another ramp is used to ramp the output in the reverse direction any possible output. The combination of two ramps in opposite directions can drive the output voltage so that the virtual ground condition is met. This method can significantly increase the range of programmability since current sources are by far smaller than capacitors.
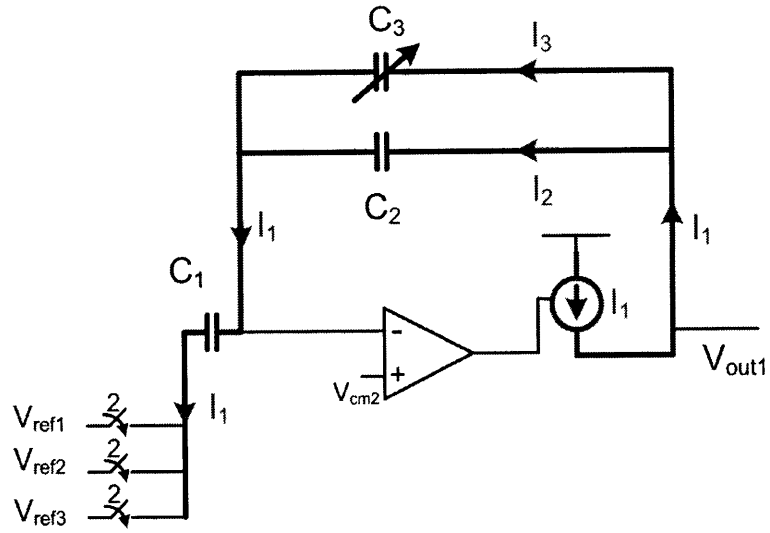
Figure 7-3: Programmable capacitor in the feedback of a ZCBC circuit.
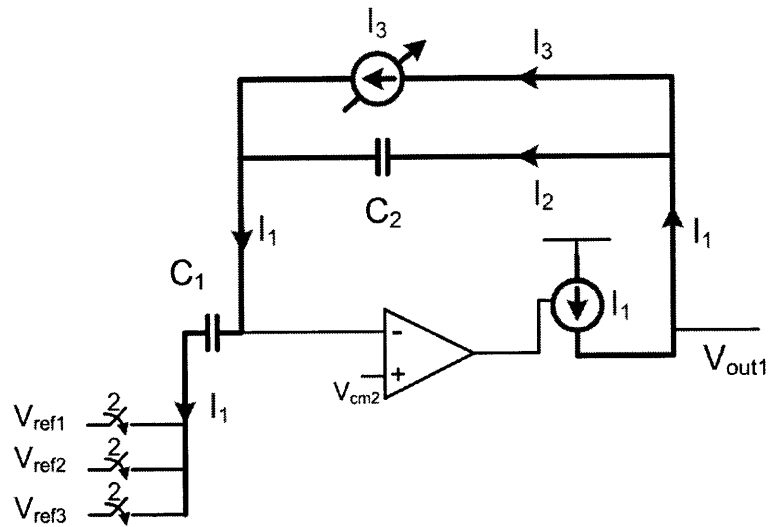
Figure 7-4: Alternate method to implement a programmable capacitor in the feedback of a ZCBC circuit.
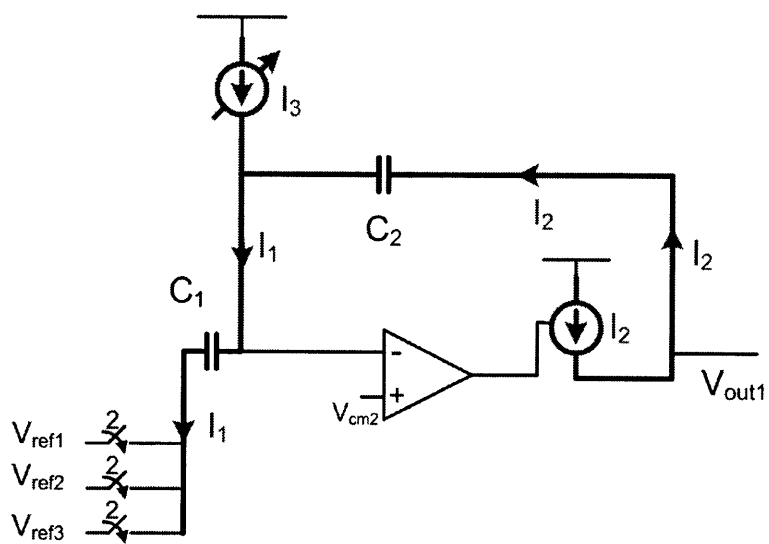
Figure 7-5: Simplified method to implement a programmable capacitor in the feedback of a ZCBC circuit.

Appendix A

The Script to Program the Chip

A scan chain is used to program the chip. Since all stages are identical, their scan chain is also identical. Tektronix pattern generator (TLA 7012) is used to send the bit-stream to the chip. The following script is used to generate a bit-stream. The output of this script can be directly loaded into the Tektronix pattern generator.

```perl
#!/opt/mtl/bin/perl
  if ( $ARGV[0] eq "" )  {$Output_file = "ANALOG_FPGA_ADC_CONF.txt";}
  else                   {$Output_file = $ARGV[1] ;}
  $Output_file2 = $Output_file.".HELP";
  print "\n\n\n\n\nOutput file: $Output_file\n";
  print "\nOutput file for Help: $Output_file2\n";

open(Output_file,  ">$Output_file");
open(Output_file2, ">$Output_file2");

$line_number=0;
$line_number++;
print Output_file   "[vectors]\n";
print Output_file2  "[vectors]\n";
print Output_file   "Siample[]\tDin_conf[0:0]\tClk_conf[0:0]\tWrite_conf[0:0]\tRead_conf[0:0]\tTimestamp[]\n";
print Output_file2  "Siample[]\tDin_conf[0:0]\tClk_conf[0:0]\tWrite_conf[0:0]\tRead_conf[0:0]\tTimestamp[]\n";
print Output_file   "0\t0\t0\t0\t0\n";
print Output_file2  "0\t0\t0\t0\t0\n";


$Timestamp="10.0000000 us";

#------------------- Setup Voltages ----
$VDD= "0.989";
#$VcasP      = &BITsR($VDD,"0","6","0.325") ;    #  S1 ... S6
#$VcasN      = &BITsR($VDD,"0","6","0.74") ;     #  S1 ... S6
# $Vcm       = &BITsR($VDD,"0","6","0.530") ;    #  S1 ... S6

$VcasP      = &BITsR($VDD,"0","6","0.305") ;     #  S1 ... S6
$VcasN      = &BITsR($VDD,"0","6","0.764") ;     #  S1 ... S6
$Vcm        = &BITsR($VDD,"0","6","0.518") ;     #  S1 ... S6



#------------------- Setup Currents
# All values in uA
# $Iref  = 93 ;      #  93*5=465
#         BDC:   C1P  C2P  C2N  C1N
$BDCS1 = "4"."0001"."0000"."0000"."0000"."0100";
@BDCS  = split(//,$BDCS1);

$BDCSetup1 = $BDCS[18].$BDCS[16].$BDCS[15].$BDCS[14].$BDCS[11].$BDCS[13].$BDCS[17].$BDCS[20].$BDCS[19].$BDCS[12];
$BDCSetup01 = $BDCSetup1.$BDCS[3].$BDCS[1].$BDCS[4].$BDCS[8].$BDCS[9].$BDCS[10].$BDCS[7].$BDCS[6].$BDCS[5].$BDCS[2];

print "BDC setup: $BDCS1\n";

$BDCS2 = "4"."0000"."0000"."0000"."0100"."0000";
@BDCS  = split(//,$BDCS2);
```

Figure A-1: The script to program the chip Part 1.

```
$BDCSetup2 = $BDCS[18].$BDCS[16].$BDCS[15].$BDCS[14].$BDCS[11].$BDCS[13].$BDCS[17].$BDCS[20].$BDCS[19].$BDCS[12];
$BDCSetup02 = $BDCSetup2.$BDCS[3].$BDCS[1].$BDCS[4].$BDCS[8].$BDCS[9].$BDCS[10].$BDCS[7].$BDCS[6].$BDCS[5].$BDCS[2];

print "BDC setup: $BDCS2\n";

$BDCS3 = "4"."0000"."0000"."0000"."0000"."0000";
@BDCS  = split(//,$BDCS3);

$BDCSetup3 = $BDCS[18].$BDCS[16].$BDCS[15].$BDCS[14].$BDCS[11].$BDCS[13].$BDCS[17].$BDCS[20].$BDCS[19].$BDCS[12];
$BDCSetup03 = $BDCSetup3.$BDCS[3].$BDCS[1].$BDCS[4].$BDCS[8].$BDCS[9].$BDCS[10].$BDCS[7].$BDCS[6].$BDCS[5].$BDCS[2];

print "BDC setup: $BDCS3\n";

$BDCS4 = "4"."0000"."0000"."0001"."0000"."0000";
#$BDCS4 = "4"."0000"."0000"."0000"."0000"."0000";
@BDCS  = split(//,$BDCS4);

$BDCSetup4 = $BDCS[18].$BDCS[16].$BDCS[15].$BDCS[14].$BDCS[11].$BDCS[13].$BDCS[17].$BDCS[20].$BDCS[19].$BDCS[12];
$BDCSetup04 = $BDCSetup4.$BDCS[3].$BDCS[1].$BDCS[4].$BDCS[8].$BDCS[9].$BDCS[10].$BDCS[7].$BDCS[6].$BDCS[5].$BDCS[2];

print "BDC setup: $BDCS4\n";

$compload  = "101101";   # P N          N3 N2 N1 P1 P2 P3
$compload1 = $compload ;
$compload2 = $compload ;
$compload3 = $compload ;
$compload4 = $compload ;

 $compload1 =  "010010";
 $compload2 =  "010010";
 $compload3 =  "100001";
 $compload4 =  "010010";

# $compload1 =  "110100";
# $compload2 =  "110100";
# $compload3 =  "110100";
# $compload4 =  "100100";

# Current sources
$RR = 1;          #Ramp Rate (slope of the ramp)
$Iref  = 93*2.0 ;    # 93*5=300
$IP_GND_BDC  = &BITsBarR($Iref  ,"0","5","25") ;
$IN_VDD_BDC  = &BITsR($Iref     ,"0","5","25") ;

$IN_VDD_GB   = &BITsR($Iref     ,"0","5","18") ;
$IP_GND_GB   = &BITsBarR($Iref  ,"0","5","18") ;
```

Figure A-2: The script to program the chip Part 2.

```
$IN_VDD        = &BITsR($Iref      ,"0","5","20") ;
$IP_GND        = &BITsBarR($Iref   ,"0","5","20") ;

$IN_VDD_Vin    = &BITsR($Iref      ,"0","5","25") ;
$IP_GND_Vin    = &BITsBarR($Iref   ,"0","5","25") ;

$IP_Comp       = &BITsBarR($Iref   ,"0","5","20") ;

$IP_CompS1     = &BITsBarR($Iref   ,"0","5","60") ;
$IP_CompS2     = &BITsBarR($Iref   ,"0","5","60") ;
$IP_CompS3     = &BITsBarR($Iref   ,"0","5","60") ;
$IP_CompS4     = &BITsBarR($Iref   ,"0","5","60") ;
$IP_CompS5     = &BITsBarR($Iref   ,"0","5","60") ;
$IP_CompS5     = &BITsBarR($Iref   ,"0","5","0") ;

$IN_VDD_GBi2   = &BITsR($Iref      ,"0","5","0") ;
$IP_GND_GBi2   = &BITsBarR($Iref   ,"0","5","0") ;

$IN_VDD_Vini2  = &BITsR($Iref      ,"0","5","0") ;
$IP_GND_Vini2  = &BITsBarR($Iref   ,"0","5","0") ;


$IN_Analog_Buf_P       = &BITsR($Iref      ,"0","5","0") ;
$IN_Output_Trace_P     = &BITsR($Iref      ,"0","5","0") ;
$IN_Integrate_Out_VDD  = &BITsR($Iref      ,"0","5","0") ;
$IP_Integrate_Out_GND  = &BITsBarR($Iref   ,"0","5","0") ;
$IP_Output_Trace_N     = &BITsBarR($Iref   ,"0","5","0") ;
$IP_Analog_Buf_N       = &BITsBarR($Iref   ,"0","5","0") ;


#-------------------- Setup CLK
# All values in ps

# CLK_Delay = 100ps + 100ps * S1 + 200ps * S2      S2 S1
$CLK_Delay      = &BITs("400" ,"100","2", "300")   ; print "CLK Delay   : 200ps \n";

# Pulse Width = 100ps + 100ps * S1 + 200ps * S2 + 400ps S3      S1 S2 S3
$Pulse_Width    = &BITsR("800" ,"100","3","400") ; print "Pulse width : 200p \n";



#------------------------------------------------------------------------------
#------------------ Vref ------------------

WriteConf("Vcm  "    ,"6",$Vcm);        # S1 ... S6
WriteConf("VcasN"    ,"6",$VcasN);      # S1 ... S6
WriteConf("VcasP"    ,"6",$VcasP);      # S1 ... S6
```

Figure A-3: The script to program the chip Part 3.

```
#------------------- Vref -----------------
#----------------------------------------------------------------------------

for ($StageNumber= 1;  $StageNumber <9; ++$StageNumber)
{
#----------------------------------------------------------------------------
#------------------- Stage 1-8 ----------------

WriteConf("Integrating_Cap P 1...7" ,"7","0000000"  );       # Cap1...Cap7
WriteConf("Analog Buf_En"   ,"1","0"  );

WriteConf("IP_Analog_Buf_N"      ,"5",$IP_Analog_Buf_N     );        # S1 ... S5
WriteConf("IP_Output_Trace_N"    ,"5",$IP_Output_Trace_N   );        # S1 ... S5
WriteConf("IP_Integrate_Out_GND" ,"5",$IP_Integrate_Out_GND );       # S1 ... S5
WriteConf("IN_Integrate_Out_VDD" ,"5",$IN_Integrate_Out_VDD );       # S1 ... S5
WriteConf("IN_Output_Trace_P"    ,"5",$IN_Output_Trace_P     );      # S1 ... S5
WriteConf("IN_Analog_Buf_P"      ,"5",$IN_Analog_Buf_P       );      # S1 ... S5

WriteConf("Terminating Resistor"   ,"1","0"  );
WriteConf("Integrating Cap Output En " ,"1","0"  );
WriteConf("Integrating_Cap 1...7 " ,"7","0000000"  );       # Cap1...Cap7

#------------------- Stage 1-8 ----------------
#----------------------------------------------------------------------------
}

for ($StageNumber= 8;  $StageNumber >6; --$StageNumber)
{
#----------------------------------------------------------------------------
#------------------- Stage 7-8 ----------------

WriteConf("In2 On " ,"1","0"  );       #

WriteConf("Vin En " ,"1","1"  );       #
WriteConf("Comparator Offset " ,"6","010010"  );     #
WriteConf("Sample on Feedback Cap " ,"1","1"  );     #

# WriteConf("BDC_offset " ,"20","$BDCSetup"  );
WriteConf("BDC_offset " ,"4","0000"  );     #
WriteConf("BDC_offset " ,"4","0000"  );     #
WriteConf("BDC_offset " ,"4","0000"  );     #
WriteConf("BDC_offset " ,"4","0000"  );     #
WriteConf("BDC_offset " ,"4","0000"  );     #

WriteConf("Conf_BDC_en " ,"1","1"  );
WriteConf("Conf_BDC " ,"5","00000"  );    # D .... D
```

Figure A-4: The script to program the chip Part 4.

```
WriteConf("S2_Out  " ,"1","0"  );          # 0: D       1:GND
WriteConf("S1_Out  " ,"1","0"  );          # 0: Clean   1:RZ

WriteConf("IP_GND_GBi2  " ,"5","00000"    );        #  S1 ... S5
WriteConf("IP_GND_Vini2 " ,"5","00000"    );        #  S1 ... S5
WriteConf("IN_VDD_Vini2 " ,"5","00000"    );        #  S1 ... S5
WriteConf("IN_VDD_GBi2  " ,"5","00000"    );        #  S1 ... S5
WriteConf("IP_Comp      " ,"5","00000"    );        #  S1 ... S5
WriteConf("IP_GND_GB    " ,"5","00000"    );        #  S1 ... S5
WriteConf("IP_GND       " ,"5","00000"    );        #  S1 ... S5
WriteConf("IP_GND_Vin   " ,"5","00000"    );        #  S1 ... S5
WriteConf("IN_VDD_Vin   " ,"5","00000"    );        #  S1 ... S5
WriteConf("IN_VDD       " ,"5","00000"    );        #  S1 ... S5
WriteConf("IN_VDD_GB    " ,"5","00000"    );        #  S1 ... S5
WriteConf("IN_VDD_BDC   " ,"5","00000"    );        #  S1 ... S5
WriteConf("IP_GND_BDC   " ,"5","00000"    );        #  S1 ... S5


#------------------ Stage 7-8  ------------------
#----------------------------------------------------------------------------


}


#----------------------------------------------------------------------------
#------------------ Stage 6  ------------------

WriteConf("In2 On  " ,"1","0"  );      #

WriteConf("Vin En  " ,"1","0"  );      #
WriteConf("Comparator Offset " ,"6","010010"  );      #
WriteConf("Sample of Feedback Cap  " ,"1","1"  );      #

WriteConf("BDC_offset  " ,"4","0000"  );      #
WriteConf("BDC_offset  " ,"4","0000"  );      #
WriteConf("BDC_offset  " ,"4","0000"  );      #
WriteConf("BDC_offset  " ,"4","0000"  );      #
WriteConf("BDC_offset  " ,"4","0000"  );      #

WriteConf("Conf_BDC_en  " ,"1","0"  );
WriteConf("Conf_BDC  " ,"5","00000"  );    # D1 .... D5
```

Figure A-5: The script to program the chip Part 5.

```
WriteConf("S2_Out  ","1","0"  );          # 0: D       1:GND           #Seems to work
WriteConf("S1_Out  ","1","0"  );          # 0: Clean   1:RZ            #Seems to work
WriteConf("IP_GND_GBi2 ","5","00000"    );        #  S1 ... S5
WriteConf("IP_GND_Vini2 ","5","00000"   );        #  S1 ... S5
WriteConf("IN_VDD_Vini2 ","5","00000"   );        #  S1 ... S5
WriteConf("IN_VDD_GBi2 ","5","00000"    );        #  S1 ... S5
WriteConf("IP_Comp    ","5","00000"     );        #  S1 ... S5
WriteConf("IP_GND_GB  ","5","00000"     );        #  S1 ... S5
WriteConf("IP_GND     ","5","00000"     );        #  S1 ... S5
WriteConf("IP_GND_Vin ","5","00000"     );        #  S1 ... S5
WriteConf("IN_VDD_Vin ","5","00000"     );        #  S1 ... S5
WriteConf("IN_VDD     ","5","00000"     );        #  S1 ... S5
WriteConf("IN_VDD_GB  ","5","00000"     );        #  S1 ... S5
WriteConf("IN_VDD_BDC ","5","00000"     );        #  S1 ... S5
WriteConf("IP_GND_BDC ","5","00000"     );        #  S1 ... S5
#------------------- Stage 6 ------------------
#------------------------------------------------------------------------------
#------------------------------------------------------------------------------
#------------------- Stage 5 ------------------
WriteConf("In2 On  ","1","0"  );          #
WriteConf("Vin En  ","1","1"  );          #
WriteConf("Comparator Offset ","6","010010"  );        #
WriteConf("Sample of Feedback Cap ","1","1"  );        #
WriteConf("BDC_offset  ","4","0000"  );        #
WriteConf("BDC_offset  ","4","0000"  );        #
WriteConf("BDC_offset  ","4","0000"  );        #
WriteConf("BDC_offset  ","4","0000"  );        #
WriteConf("BDC_offset  ","4","0000"  );        #
WriteConf("Conf_BDC_en  ","1","1"  );
WriteConf("Conf_BDC  ","5","00000"  );    # D1 .... D5
WriteConf("S2_Out  ","1","0"  );          # 0: D       1:GND           #Seems to work
WriteConf("S1_Out  ","1","0"  );          # 0: Clean   1:RZ            #Seems to work
WriteConf("IP_GND_GBi2 ","5","00000"    );        #  S1 ... S5
WriteConf("IP_GND_Vini2 ","5","00000"   );        #  S1 ... S5
WriteConf("IN_VDD_Vini2 ","5","00000"   );        #  S1 ... S5
WriteConf("IN_VDD_GBi2 ","5","00000"    );        #  S1 ... S5
WriteConf("IP_CompS5   ","5",$IP_CompS5 );        #  S1 ... S5
WriteConf("IP_GND_GB   ","5",$IP_GND_GB );        #  S1 ... S5
WriteConf("IP_GND      ","5",$IP_GND    );        #  S1 ... S5
WriteConf("IP_GND_Vin  ","5",$IP_GND_Vin );       #  S1 ... S5
WriteConf("IN_VDD_Vin  ","5",$IN_VDD_Vin );       #  S1 ... S5
WriteConf("IN_VDD      ","5",$IN_VDD    );        #  S1 ... S5
WriteConf("IN_VDD_GB   ","5",$IN_VDD_GB );        #  S1 ... S5
WriteConf("IN_VDD_BDC  ","5",$IN_VDD_BDC );       #  S1 ... S5
WriteConf("IP_GND_BDC  ","5",$IP_GND_BDC );       #  S1 ... S5
#------------------- Stage 5 ------------------
#------------------------------------------------------------------------------
```

Figure A-6: The script to program the chip Part 6.

```
#------------------- Stage 04 -------------------
WriteConf("In2 On  ","1","0"  );      #
WriteConf("Vin En  ","1","1"  );      #
WriteConf("Comparator Offset " ,"6",$compload4  );      #
WriteConf("Sample of Feedback Cap " ,"1","1"  );      #
WriteConf("BDC_offset  ","20",$BDCSetup04"  );
WriteConf("Conf_BDC_en  ","1","1"  );
WriteConf("Conf_BDC  ","5","00000"  );      # D1 .... D5
WriteConf("S2_Out  ","1","0"  );          # 0: D        1:GND          #Works
WriteConf("S1_Out  ","1","0"  );          # 0: Clean    1:RZ           #Works
WriteConf("IP_GND_GBi2  ","5",$IP_GND_GBi2  );      # S1 ... S5
WriteConf("IP_GND_Vini2 ","5",$IP_GND_Vini2 );      # S1 ... S5
WriteConf("IN_VDD_Vini2 ","5",$IN_VDD_Vini2 );      # S1 ... S5
WriteConf("IN_VDD_GBi2  ","5",$IN_VDD_GBi2  );      # S1 ... S5
WriteConf("IP_CompS4   ","5",$IP_CompS4   );      # S1 ... S5
WriteConf("IP_GND_GB   ","5",$IP_GND_GB   );      # S1 ... S5
WriteConf("IP_GND     ","5",$IP_GND     );      # S1 ... S5
WriteConf("IP_GND_Vin  ","5",$IP_GND_Vin  );      # S1 ... S5
WriteConf("IN_VDD_Vin  ","5",$IN_VDD_Vin  );      # S1 ... S5
WriteConf("IN_VDD     ","5",$IN_VDD     );      # S1 ... S5
WriteConf("IN_VDD_GB   ","5",$IN_VDD_GB   );      # S1 ... S5
WriteConf("IN_VDD_BDC  ","5",$IN_VDD_BDC  );      # S1 ... S5
WriteConf("IP_GND_BDC  ","5",$IP_GND_BDC  );      # S1 ... S5
#------------------- Stage 04 -------------------
#--------------------------------------------------------------------------
#------------------- Stage 03 -------------------
WriteConf("In2 On  ","1","0"  );      #
WriteConf("Vin En  ","1","1"  );      #
WriteConf("Comparator Offset " ,"6",$compload3  );      #
WriteConf("Sample of Feedback Cap " ,"1","1"  );      #
WriteConf("BDC_offset  ","20",$BDCSetup03"  );
WriteConf("Conf_BDC_en  ","1","1"  );
WriteConf("Conf_BDC  ","5","00000"  );      # D1 .... D5
WriteConf("S2_Out  ","1","0"  );          # 0: D        1:GND          #Works
WriteConf("S1_Out  ","1","0"  );          # 0: Clean    1:RZ           #Works
WriteConf("IP_GND_GBi2  ","5",$IP_GND_GBi2  );      # S1 ... S5
WriteConf("IP_GND_Vini2 ","5",$IP_GND_Vini2 );      # S1 ... S5
WriteConf("IN_VDD_Vini2 ","5",$IN_VDD_Vini2 );      # S1 ... S5
WriteConf("IN_VDD_GBi2  ","5",$IN_VDD_GBi2  );      # S1 ... S5
WriteConf("IP_CompS3   ","5",$IP_CompS3   );      # S1 ... S5
WriteConf("IP_GND_GB   ","5",$IP_GND_GB   );      # S1 ... S5
WriteConf("IP_GND     ","5",$IP_GND     );      # S1 ... S5
WriteConf("IP_GND_Vin  ","5",$IP_GND_Vin  );      # S1 ... S5
WriteConf("IN_VDD_Vin  ","5",$IN_VDD_Vin  );      # S1 ... S5
WriteConf("IN_VDD     ","5",$IN_VDD     );      # S1 ... S5
WriteConf("IN_VDD_GB   ","5",$IN_VDD_GB   );      # S1 ... S5
WriteConf("IN_VDD_BDC  ","5",$IN_VDD_BDC  );      # S1 ... S5
WriteConf("IP_GND_BDC  ","5",$IP_GND_BDC  );      # S1 ... S5
#------------------- Stage 03 -------------------
```

Figure A-7: The script to program the chip Part 7.

```
#------------------- Stage 02 ----------------
WriteConf("In2 On  ","1","0"  );       #
WriteConf("Vin En  ","1","1"  );       #
WriteConf("Comparator Offset " ,"6", $compload2 );      #
WriteConf("Sample of Feedback Cap  " ,"1","1"  );      #
WriteConf("BDC_offset  ","20","$BDCSetup02"  );
WriteConf("Conf_BDC_en  ","1","1"  );
WriteConf("Conf_BDC  " ,"5","00000"  );     # D1 .... D5
WriteConf("S2_Out  ","1","0"  );             # 0: D        1:GND          #Seems to work
WriteConf("S1_Out  ","1","0"  );             # 0: Clean    1:RZ           #Seems to work
WriteConf("IP_GND_GBi2  ","5",$IP_GND_GBi2 );     # S1 ... S5
WriteConf("IP_GND_Vini2 ","5",$IP_GND_Vini2 );    # S1 ... S5
WriteConf("IN_VDD_Vini2 " ,"5",$IN_VDD_Vini2 );   # S1 ... S5
WriteConf("IN_VDD_GBi2  " ,"5",$IN_VDD_GBi2  );   # S1 ... S5
WriteConf("IP_CompS2     " ,"5",$IP_CompS2    );  # S1 ... S5
WriteConf("IP_GND_GB    " ,"5",$IP_GND_GB    );   # S1 ... S5
WriteConf("IP_GND       " ,"5",$IP_GND       );   # S1 ... S5
WriteConf("IP_GND_Vin   " ,"5",$IP_GND_Vin   );   # S1 ... S5
WriteConf("IN_VDD_Vin   " ,"5",$IN_VDD_Vin   );   # S1 ... S5
WriteConf("IN_VDD       ","5",$IN_VDD        );   # S1 ... S5
WriteConf("IN_VDD_GB    " ,"5",$IN_VDD_GB    );   # S1 ... S5
WriteConf("IN_VDD_BDC   " ,"5",$IN_VDD_BDC   );   # S1 ... S5
WriteConf("IP_GND_BDC   " ,"5",$IP_GND_BDC   );   # S1 ... S5
#------------------- Stage 02 ----------------
#------------------------------------------------------------------------------
#------------------- Stage 01 ----------------
WriteConf("In2 On  ","1","0"  );       #
WriteConf("Vin En  ","1","1"  );       #
WriteConf("Comparator Offset " ,"6", $compload1 );      #
WriteConf("Sample of Feedback Cap  " ,"1","1"  );      #
WriteConf("BDC_offset  ","20","$BDCSetup01"  );
WriteConf("Conf_BDC_en  ","1","1"  );
WriteConf("Conf_BDC  " ,"5","00000"  );     # D1 .... D5
WriteConf("S2_Out  ","1","0"  );             # 0: D        1:GND          #Seems to work
WriteConf("S1_Out  ","1","0"  );             # 0: Clean    1:RZ           #Seems to work
WriteConf("IP_GND_GBi2  ","5",$IP_GND_GBi2 );     # S1 ... S5
WriteConf("IP_GND_Vini2 ","5",$IP_GND_Vini2 );    # S1 ... S5
WriteConf("IN_VDD_Vini2 " ,"5",$IN_VDD_Vini2 );   # S1 ... S5
WriteConf("IN_VDD_GBi2  " ,"5",$IN_VDD_GBi2  );   # S1 ... S5
WriteConf("IP_CompS1     " ,"5",$IP_CompS1    );  # S1 ... S5
WriteConf("IP_GND_GB    " ,"5",$IP_GND_GB    );   # S1 ... S5
WriteConf("IP_GND       " ,"5",$IP_GND       );   # S1 ... S5
WriteConf("IP_GND_Vin   " ,"5",$IP_GND_Vin   );   # S1 ... S5
WriteConf("IN_VDD_Vin   " ,"5",$IN_VDD_Vin   );   # S1 ... S5
WriteConf("IN_VDD       " ,"5",$IN_VDD       );   # S1 ... S5
WriteConf("IN_VDD_GB    " ,"5",$IN_VDD_GB    );   # S1 ... S5
WriteConf("IN_VDD_BDC   " ,"5",$IN_VDD_BDC   );   # S1 ... S5
WriteConf("IP_GND_BDC   " ,"5",$IP_GND_BDC   );   # S1 ... S5
#------------------- Stage 01 ----------------
```

Figure A-8: The script to program the chip Part 8.

```
#----------------- Clock/Pulse Gen -----------------

WriteConf("Pulse Width"   ,"3",$Pulse_Width);        # = 100ps + 100ps * S1 + 200ps * S2 + 400ps S3     S1 S2 S3
WriteConf("CLK Enable S8" ,"1","0");
WriteConf("CLK Enable S7" ,"1","0");
WriteConf("CLK Enable S6" ,"1","0");
WriteConf("CLK Enable S5" ,"1","1");
WriteConf("CLK Enable S4" ,"1","1");
WriteConf("CLK Enable S3" ,"1","1");
WriteConf("CLK Enable S2" ,"1","1");
WriteConf("CLK Enable S1" ,"1","1");                 # Seems to work
WriteConf("NOne Overlapping CLK delay" ,"2",$CLK_Delay);     # = 100ps + 100ps * S1 + 200ps * S2     S2 S1
#----------------- Clock/Pulse Gen -----------------
#-----------------------------------------------------------------------------------
WriteConf("S1-S3"         ,"1","1");     #S4-S8=0  S1-S5=1          #works
#--------------- END of Analog FPGA #2 ---------------
#-----------------------------------------------------------------------------------------------
close (Output_file);
close (Output_file2);
print "Configuration file created.\n\n";
system "date";
print "\n";
print "  ------------------------  Completed   ----------------------------\n\n\n\n\n";
sub WriteConf
{
  # Name of configuration bits
  # Number of bits
  # Value of bits
  $Comment = $_[0];
  $NofBits = $_[1];
  $BitValues = $_[2];
  @BitVal = split(//,$BitValues);
  for ($temp = $NofBits-1; $temp > -1; --$temp)
  {
    print Output_file  "$line_number\t $BitVal[$temp]\t 0\t 0\t 0\t $Timestamp\n";
    if ($NofBits>1)
    { print Output_file2 "$line_number\t $BitVal[$temp]\t 0\t 0\t 0\t $Timestamp\t\t$Comment\t\tb$temp\n"; }
    else
    { print Output_file2 "$line_number\t $BitVal[$temp]\t 0\t 0\t 0\t $Timestamp\t\t$Comment\n";  }
    $line_number++;
    print Output_file  "$line_number\t $BitVal[$temp]\t 1\t 0\t 0\t $Timestamp\n";
    print Output_file2 "$line_number\t $BitVal[$temp]\t 1\t 0\t 0\t $Timestamp\n";
    $line_number++;
  }
}
```

Figure A-9: The script to program the chip Part 9.

```
sub BITs
{
  #Full Scale_Max
  #Full Scale_Min
  #Number of Bits
  #Input Signal

  $B_Full_Max = $_[0];
  $B_Full_Min = $_[1];
  $B_Bits     = $_[2];
  $B_Input    = $_[3];
  $B_Full_Max = $B_Full_Max - $B_Full_Min;
  $B_Input    = $B_Input    - $B_Full_Min;
  $Output     = "";
  for($temp_B=1; $temp_B<$B_Bits+1; ++$temp_B)
  {
    $B_Full_Max = $B_Full_Max/2;
    if ($B_Input <$B_Full_Max)
    {
      $Output = $Output."0";
    }
    else
    {
      $B_Input = $B_Input - $B_Full_Max;
      $Output  = $Output."1";
    }
  }
  $Output;
}
```

Figure A-10: The script to program the chip Part 10.

```perl
sub BITsR
{
  # The output of BITsR is in the reverse order of BITs

  #Full Scale_Max
  #Full Scale_Min
  #Number of Bits
  #Input Signal

  $B_Full_Max = $_[0];
  $B_Full_Min = $_[1];
  $B_Bits     = $_[2];
  $B_Input    = $_[3];
  $B_Full_Max = $B_Full_Max - $B_Full_Min;
  $B_Input    = $B_Input    - $B_Full_Min;
  $Output     = "";
  for($temp_B=1; $temp_B<$B_Bits+1; ++$temp_B)
  {
    $B_Full_Max = $B_Full_Max/2;
    if ($B_Input <$B_Full_Max)
    {
      $Output = "0".$Output;
    }
    else
    {
      $B_Input = $B_Input - $B_Full_Max;
      $Output  = "1".$Output;
    }
  }
  $Output;
}
```

Figure A-11: The script to program the chip Part 11.

```
sub BITsBar
{
    #Full Scale_Max
    #Full Scale_Min
    #Number of Bits
    #Input Signal

    $B_Full_Max = $_[0];
    $B_Full_Min = $_[1];
    $B_Bits     = $_[2];
    $B_Input    = $_[3];
    $B_Full_Max = $B_Full_Max - $B_Full_Min;
    $B_Input    = $B_Input    - $B_Full_Min;
    $Output     = "";
    for($temp_B=1; $temp_B<$B_Bits+1; ++$temp_B)
    {
        $B_Full_Max = $B_Full_Max/2;
        if ($B_Input <$B_Full_Max)
        {
            $Output = $Output."1";
        }
        else
        {
            $B_Input = $B_Input - $B_Full_Max;
            $Output  = $Output."0";
        }
    }
    $Output;
}
```

Figure A-12: The script to program the chip Part 12.

```
sub BITsBarR
{
  #Full Scale_Max
  #Full Scale_Min
  #Number of Bits
  #Input Signal

  $B_Full_Max = $_[0];
  $B_Full_Min = $_[1];
  $B_Bits     = $_[2];
  $B_Input    = $_[3];
  $B_Full_Max = $B_Full_Max - $B_Full_Min;
  $B_Input    = $B_Input    - $B_Full_Min;
  $Output     = "";
  for($temp_B=1; $temp_B<$B_Bits+1; ++$temp_B)
  {
    $B_Full_Max = $B_Full_Max/2;
    if ($B_Input <$B_Full_Max)
    {
      $Output = "1".$Output;
    }
    else
    {
      $B_Input = $B_Input - $B_Full_Max;
      $Output  = "0".$Output;
    }
  }
  $Output;
}
```

Figure A-13: The script to program the chip Part 13.

Appendix B

Noise Bandwidth Calculation

The noise bandwidth calculation is shown in Figure B-1. In this calculation, the poles are located at $f_p = \frac{1}{2\pi}$. The results is multiplied by 2π if the pole is located at 1Hz, and multiplied by $2\pi f_{pole}$ if the poles are located at f_{pole}. The results are summarized in Table B.1

Table B.1: Noise bandwidth of low-pass filters when all poles are located at the same frequency.

Order of the filter	NBW-Poles at $\frac{1}{2\pi}$	NBW-Poles at 1Hz	NBW-Poles at f_{pole}
First order	1/4	$\pi/2$	$1.57 f_{pole}$
Second order	1/8	$\pi/4$	$0.78 f_{pole}$
Third order	3/32	$3\pi/16$	$0.58 f_{pole}$
Forth order	5/64	$5\pi/32$	$0.49 f_{pole}$
Fifth order	35/512	$35\pi/256$	$0.43 f_{pole}$

```
In[1]:= H1[f_] := 1 / (1 + 2 * Pi * I * f)

     Integrate[(Abs[H1[f]])^2, {f, 0, ∞}]

            1
Out[2]=    ---
            4

In[4]:= H2[f_] := (1 / (1 + 2 * Pi * I * f))^2

In[5]:= Integrate[(Abs[H2[f]])^2, {f, 0, ∞}]

            1
Out[5]=    ---
            8

In[6]:= H3[f_] := (1 / (1 + 2 * Pi * I * f))^3

In[7]:=
     Integrate[(Abs[H3[f]])^2, {f, 0, ∞}]

            3
Out[7]=    ----
            32

In[8]:= H4[f_] := (1 / (1 + 2 * Pi * I * f))^4

In[9]:= Integrate[(Abs[H4[f]])^2, {f, 0, ∞}]

            5
Out[9]=    ----
            64

In[10]:= H5[f_] := (1 / (1 + 2 * Pi * I * f))^5

In[11]:= Integrate[(Abs[H5[f]])^2, {f, 0, ∞}]

            35
Out[11]=   -----
            512
```

Figure B-1: Integral calculation by mathematica

Appendix C

Transfer Function of Noise from Different Sources

In the block diagram of Figure C-1, Mason rule [49] [50] can be used to derive the transfer function of different inputs to the output as follows:

$$H_{Vn11}(s) = \frac{1}{(C1 + C3 + L2) * S + (C1 * L2 + C3 * L2) * S^2 + C1 * C3 * L2 * S^3 + 2}$$

$$\text{(C.1)}$$

$$H_{Vn12}(s) = \frac{C1 * S}{(C1 + C3 + L2) * S + (C1 * L2 + C3 * L2) * S^2 + C1 * C3 * L2 * S^3 + 2}$$

$$\text{(C.2)}$$

$$H_{Vn21}(s) = \frac{1 + C1 * S}{(C1 + C3 + L2) * S + (C1 * L2 + C3 * L2) * S^2 + C1 * C3 * L2 * S^3 + 2}$$

$$\text{(C.3)}$$

$$H_{Vn22}(s) = \frac{C1 * L2 * S^2 + L2 * S}{(C1 + C3 + L2) * S + (C1 * L2 + C3 * L2) * S^2 + C1 * C3 * L2 * S^3 + 2}$$

$$\text{(C.4)}$$

$$H_{Vn31}(s) = \frac{C1 * L2 * S^2 + L2 * S + 1}{(C1 + C3 + L2) * S + (C1 * L2 + C3 * L2) * S^2 + C1 * C3 * L2 * S^3 + 2}$$

$$(C.5)$$

$$H_{Vn32}(s) = \frac{C1 * C3 * L2 * S^3 + C3 * L2 * S^2 + C3 * S}{(C1 + C3 + L2) * S + (C1 * L2 + C3 * L2) * S^2 + C1 * C3 * L2 * S^3 + 2}$$

$$(C.6)$$

$$H_{vin}(s) = \frac{1}{2 + (C3 + L2 + C1) * S + (L2 * C1 + C3 * L2) * S^2 + C3 * L2 * C1 * S^3}$$

$$(C.7)$$

For a corner frequency is 1MHz, the following values are used

R1 = 1

C1 = 1.59155e-07 F

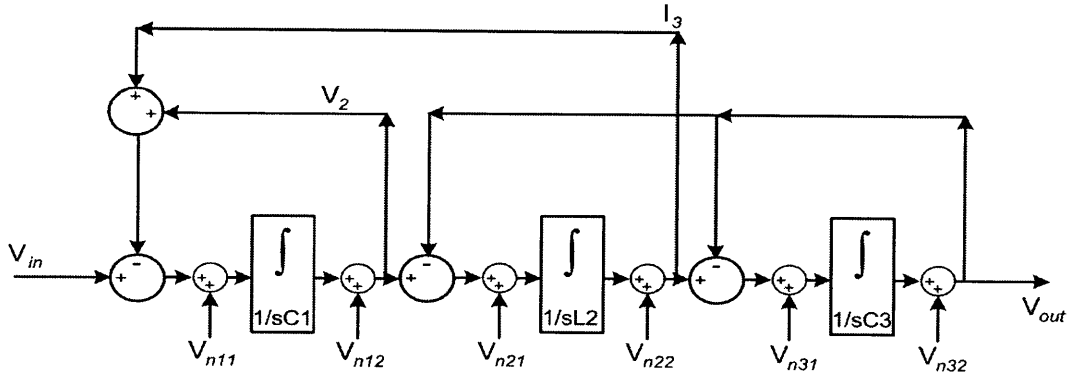L2 = 3.1831e-07 H

C3 = 1.59155e-07 F

R5 = 1

Figure C-1: Block diagram of a third order low-pass filter with sources of noise.

Appendix D

Noise of an Amplifier with Parasitic Capacitance on Virtual Ground Node

Figure D-1 shows an amplifier. During the phase 1, V_{in} is sampled across the 180fF and 60fF capacitors. The charge across each capacitor is:

$$Q_1 = V_{in} * 180fF \tag{D.1}$$

$$Q_2 = V_{in} * 60fF \tag{D.2}$$

During phase 2, the charge on the 180fF capacitor transfers to the 60fF capacitor. In the absence of V_n (V_n=0), the output voltage at the end of phase 2 is:

$$V_{out} = \frac{180fF + 60fF}{60fF} V_{in} = 4V_{in} \tag{D.3}$$

Figure D-2 shows the circuit in phase 2. If the 25fF parasitic capacitor is ignored, the contribution of the V_n at the output can be calculated as:

$$V_{out} = \frac{180fF}{60fF} V_n = 3V_n \tag{D.4}$$

Adding the parasitic capacitor, the output noise is:

$$V_{out} = \frac{180fF + 25fF}{60fF} V_n \tag{D.5}$$

As a result:

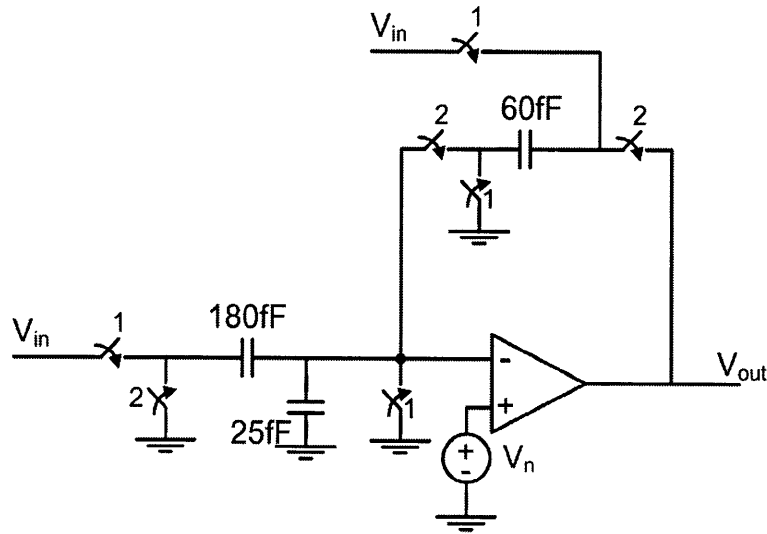$$\overline{V_{out}^2} = (\frac{180fF + 25fF}{60fF})^2 * \overline{V_n^2} \tag{D.6}$$

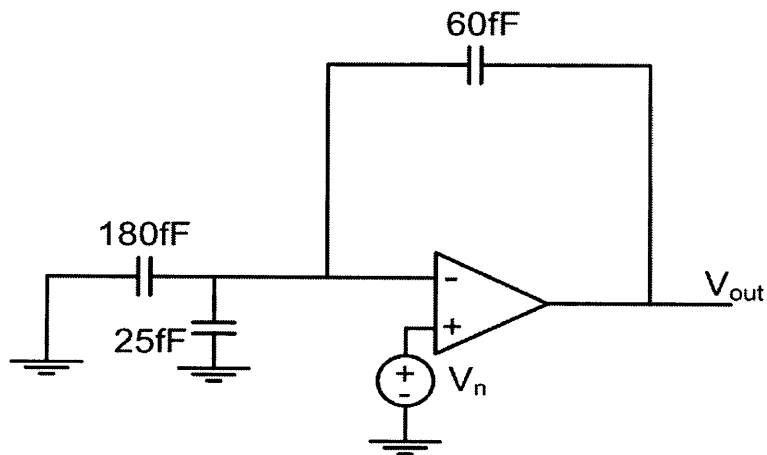Figure D-1: Schematic of an amplifier.

Figure D-2: Phase 2 of the amplifier.

Bibliography

[1] J. Becker, F. Henrici, et al., "A Continuous-Time Hexagonal Field-Programmable Analog Array in 0.13um CMOS with 186MHz GBW," *ISSCC Dig. Tech. Papers*, pp.70-71, Feb.,2008.

[2] B. Pankiewicz, M. Wojcikowski, S. Szczepanski, Y. Sun, "A Field Programmable Analog Array for CMOS Continuous-Time OTA-C Filter Applications," *IEEE J. Solid-State Circuits*, vol. 37, pp. 125-136 Feb. 2002.

[3] K. Gulati, H.-S Lee, "A low-power reconfigurable analog-to-digital converter," ISSCC Dig. Tech. Papers, pp.54-55, Feb.,2001.

[4] D.C. Daly, A.P. Chandrakasan, "A 6b 0.2-to-0.9V Highly Digital Flash ADC with Comparator Redundancy," in *IEEE International Solid-State Circuits Conference Digest of Technical Papers*, San Francisco, CA, Feb. 2008, pp.554-555.

[5] S. Park, Y. Palaskas, M.P. Flynn, "A 4GSs 4b Flash ADC in 0.18spl mum CMOS," in *IEEE International Solid-State Circuits Conference Digest of Technical Papers*, San Francisco, CA, Feb. 2006, pp.2330-2339.

[6] B. Verbruggen, J. Craninckx, M. Kuijk, P. Wambacq, G. Van der Plas, "A 2.2mW 5b 1.75GSs Folding Flash ADC in 90nm Digital CMOS ," in *IEEE International Solid-State Circuits Conference Digest of Technical Papers*, San Francisco, CA, Feb. 2008, pp.252-253.

[7] M. Yoshioka, K. Ishikawa, T. Takayama, "A 10b 50MSs 820uW SAR ADC with On-Chip Digital Calibration," in *IEEE International Solid-State Circuits Conference Digest of Technical Papers*, San Francisco, CA, Feb. 2010, pp.384-385.

[8] B.P. Ginsberg "Energy-Efficient Analog-to-Digital Conversion for Ultra-Wideband Radio," PhD Thesis, Massachusetts Institute of Technology, 2007.

[9] I. Ahmed, "Pipelined ADC Design and Enhancement Techniques," Springer Science + Business Media B.V. 2010.

[10] B. Murmann, B.E. Boser, "Digitally Assisted Pipeline ADCs: Theory and Implementation," Kluwer Academic Publisher, 2004.

[11] R. Schreier, G.C. Temes, "Understanding Delta-Sigma Data Converters," Wiley-IEEE Press, Inc. 2004.

[12] L.Y. Nathawad, R. Urata, B.A. Wooley, D.A.B. Miller, "A 20 GHz bandwidth, 4 b photoconductive-sampling time-interleaved CMOS ADC," in *IEEE International Solid-State Circuits Conference Digest of Technical Papers*, San Francisco, CA, Feb. 2003, pp.320-321.

[13] S. Limotyrakis, S.D. Kulchycki, D. Su, B.A. Wooley, " A 150MSs 8b 71mW time-interleaved ADC in 0.18m CMOS," in *IEEE International Solid-State Circuits Conference Digest of Technical Papers*, San Francisco, CA, Feb. 2004, pp.258-259.

[14] W. Kester, "Which ADC Architecture is Right for Your Application," http://bbs.ednchina.com/Upload/Blog/2008/12/12/31e83bac-500f-4182-acca-4d360295fd9c.pdf, Analog Devices, Analog Dialogue 39-06, June 2005.

[15] D. A. Johns, K. Martin "Analog Integrated Circuit Design," John Wiley & Sons, Inc. 1997.

[16] D.J. Allstot, R. W. Brodersen, P.R. Gray, "MOS Switched Capacitor Ladder Filters," *IEEE J. Solid-State Circuits*, vol. sc-13, no. 6, pp. 806-814, December 1978.

[17] H. Y-F. Lam, "Analog and Digital Filters, Design and Realization," Prentice-Hall, 1979.

[18] L.P. Huelsman, "Active and Passive Analog Filter Design, an Introduction," McGraw-Hill, 1993.

[19] LC Filter Design, online tool to design passive ladder filters, http://www-users.cs.york.ac.uk/ fisher/lcfilter/

[20] T. Sepke, J. Fiorenza, C.G. Sodini, P. Holloway, and H.-S Lee, "Comparator-based switched-capacitor circuits for scaled CMOS technologies," in *IEEE International Solid-State Circuits Conference Digest of Technical Papers*, San Francisco, CA, Feb. 2006, pp.220-221.

[21] T. Sepke. "Comparator Design and Analysis for Comparator-Based Switched-Capacitor Circuits," PhD Thesis, Massachusetts Institute of Technology, 2006.

[22] T. Sepke, P. Holloway, C.G. Sodini, H.-S. Lee, "Noise Analysis for Comparator-Based Circuits," *IEEE Transactions on Circuits and Systems*, vol. 56, no. 3, pp. 541-553, March 2009.

[23] J.K. Fiorenza "A comparator-Based Switched Capacitor Pipelined Analog-to-Digital Converter," PhD Thesis, Massachusetts Institute of Technology, 2007.

[24] L. Brooks "Circuits and Algorithms for Pipelined ADCs in Scaled CMOS Technologies," PhD Thesis, Massachusetts Institute of Technology, 2008.

[25] W. Yu, B. Leung, "Distorion and noise performance of bottom-plate-sampling mixers," *IEEE International Symposium on Circuits and Systems*, vol. 4, pp. 401-404, 1998.

[26] B. Razavi "Design of Analog CMOS Integrated Circuits," McGraw-Hill, Inc. 2001.

[27] A.M. Abo and P.R. Gray, "A 1.5-V, 10-bit, 14.3-MS/s CMOS Pipeline Analog-to-Digital Converter," it *IEEE J. Solid-State Circuits*, vol. 34, no. 5, pp. 599-606 May 1999.

[28] J.M. Rabaey, A. Chandrakasan, B. Nikolic "Digital Integrated Circuits," Prentice Hall, Inc. 2003.

[29] B. Goll, H. Zimmermann, "A clocked, regenerative comparator in 0.12m CMOS with tunable sensitivity," in *IEEE European Solid-State Circuits Conference*, 2007, pp.408-411.

[30] R. Wang, K. Li, J. Zhang, B. Nie, "A High-Speed High-Resolution Latch Comparator for Pipeline Analog-to-Digital Converters," in *IEEE International Workshop on Anti-counterfeiting, Security, Identification*, 2007, pp.28-31.

[31] P. Nuzzo, F. Bernardinis, P. Terreni, and G. Plas, "Noise Analysis of Regenerative Comparators for Reconfigurable ADC Architectures ," *IEEE TRANSACTIONS ON CIRCUITS AND SYSTEMS*, VOL.55, NO. 6, pp.1441-1454, July 2008.

[32] L. Brooks and H.-S Lee, "A zero-crossing-based 8b 200MS/S pipeline ADC," in *IEEE International Solid-State Circuits Conference Digest of Technical Papers*, San Francisco, CA, Feb. 2007, pp.460-461.

[33] J. Doernberg, H-S. Lee, D. A. Hodges "Full-Speed Testing of A/D Converters," *IEEE J. Solid-State Circuits*, vol. sc-19, no. 6, pp. 820-827, December 1984.

[34] M.C. Guyton "A Low-Voltage Zero-Crossing-Based Delta-Sigma Analog-to-Digital Converter," PhD Thesis, Massachusetts Institute of Technology, 2010.

[35] B. Murmann, Course Handouts of EE315 at Stanford University, VLSI Data Conversion Circuits, https://ccnet.stanford.edu/cgi-bin/course.cgi?cc=ee315&action=handout_menu

[36] R.H. Walden, "Analog-to-digital converter technology comparison," *IEEE GaAs IC Symposium, Technical Digest*, pages 217-219, October 1994.

[37] R.H. Walden, "Analog-to-digital converter survey and analysis," *IEEE Journal on Selected Areas in Communication*, pp. 539-550, April 1999.

[38] A.V. Oppenheim, A.S. Willsky, S.H. Nawab "Signals & Systems," Prentice Hall, Second edition 1997.

[39] R. Schreier, J. Silva, J. Steensgaard, G.C. Temes, "Design-Oriented Estimation of Thermal Noise in Switched-Capacitor Circuits," in *IEEE Transactions on Circuits and Systems*, Nov. 2005, pp.2358-2368.

[40] J.H. Fischer, "Noise Sources and Calculation Techniques for Switched Capacitor Filters," *IEEE J. Solid-State Circuits*, vol. sc-13, no. 6, pp. 806-814, December 1978.

[41] S.-W. Sun, and P.G.Y. Tsui, "Limitation of CMOS supply voltage scaling by MOSFET threshold-voltage variation," in *IEEE J. Solid-State Circuits*, vol. 30, no. 8, pp. 947-949 May 1995.

[42] H. Mahmoodi, S. Mukhopadhyay, and K. Roy, "Estimation of delay variations due to random-dopant fluctuations in nanoscale CMOS circuits," in *IEEE J. Solid-State Circuits*, vol. 40, no. 9, pp. 1787-1796 May 2005.

[43] A.M.A. Ali, A. Morgan, C. Dillon, G. Patterson, S. Puckett, M. Hensley, R. Stop, P. Bhoraskar, S. Bardsley, D. Lattimore, J. Bray, C. Speir, R. Sneed, "A 16b 250MSs IF-Sampling Pipelined AD Converter with Background Calibration," in *IEEE International Solid-State Circuits Conference Digest of Technical Papers*, San Francisco, CA, Feb. 2010, pp.292-293.

[44] R. Payne, M. Corsi, D. Smith, S. Kaylor, D. Hsieh, "A 16b 100-to-160MSs SiGe BiCMOS Pipelined ADC with 100dBFS SFDR," in *IEEE International Solid-State Circuits Conference Digest of Technical Papers*, San Francisco, CA, Feb. 2010, pp.294-295.

[45] C. P. Hurrell, C. Lyden, D. Laing, D. Hummerston, M. Vickery "An 18b 12.5MHz ADC with 93dB SNR," in *IEEE International Solid-State Circuits Conference Digest of Technical Papers*, San Francisco, CA, Feb. 2010, pp.378-379.

[46] M. Furuta, M. Nozawa, T. Itakura "A 0.06mm8.9b ENOB 40MS/s Pipelined SAR ADC in 65nm CMOS," in *IEEE International Solid-State Circuits Conference Digest of Technical Papers*, San Francisco, CA, Feb. 2010, pp.382-383.

[47] E. Kusse, J. Rabaey, "Low-Energy Embedded FPGA Structure", *International Symposium on Low Power Electronics and Design*, pp.155-160, Aug. 1996.

[48] K. Gulati, H.-S. Lee "A Low-Power Reconfigurable Analog-to-Digital Converter," in *IEEE J. Solid-State Circuits*, vol. 36, no. 12, pp. 1900-1911, December 2001.

[49] http://en.wikipedia.org/wiki/Mason

[50] R.C. Dorf, R.H. Bishop "Modern Control Systems," Prentice Hall. 2008.